12-2018

Forestry and Arboriculture Applications Using High-Resolution Imagery from Unmanned Aerial Vehicles (UAV)

Brian A. Ritter
Clemson University, britter@g.clemson.edu

FORESTRY AND ARBORICULTURE APPLICATIONS USING HIGH-RESOLUTION IMAGERY FROM UNMANNED AERIAL VEHICLES (UAV)

A Dissertation
Presented to
the Graduate School of
Clemson University

In Partial Fulfillment
of the Requirements for the Degree
Doctor of Philosophy
Forest Resources

---

by
Brian A. Ritter
December 2018

Accepted by:
Dr. Christopher J. Post, Committee Chair
Dr. Elena Mikhailova
Dr. William Bridges
Dr. Mark A. Schlautman

ABSTRACT

Forests cover over one-third of the planet and provide unmeasurable benefits to the ecosystem. Forest managers have collected and processed countless amounts of data for use in studying, planning, and management of these forests. Data collection has evolved from completely manual operations to the incorporation of technology that has increased the efficiency of data collection and decreased overall costs. Many technological advances have been made that can be incorporated into natural resources disciplines. Laser measuring devices, handheld data collectors and more recently, unmanned aerial vehicles, are just a few items that are playing a major role in the way data is managed and collected. Field hardware has also been aided with new and improved mobile and computer software. Over the course of this study, field technology along with computer advancements have been utilized to aid in forestry and arboricultural applications. Three-dimensional point cloud data that represent tree shape and height were extracted and examined for accuracy. Traditional fieldwork collection (tree height, tree diameter and canopy metrics) was derived from remotely sensed data by using new modeling techniques which will result in time and cost savings. Using high resolution aerial photography, individual tree species are classified to support tree inventory development. Point clouds were used to create digital elevation models (DEM) which can further be used in hydrology analysis, slope, aspect, and hillshades. Digital terrain models (DTM) are in geographic information system (GIS), and along with DEMs, used to create canopy height models (CHM). The results of this study can enhance how the

data are utilized and prompt further research and new initiatives that will improve and garner new insight for the use of remotely sensed data in forest management.

DEDICATION

Success is measured by those around us that support who we are and what we are doing. When success is measured, it cannot fully quantify the value provided by those that selfishly provide patience, encouragement, support and love. This study is dedicated to the two people whom have exceeded in providing beyond measure the success needed to not only fulfill but to exceed the requirements needed to complete my degree at Clemson University. Those two people are my wife Laurie and son Zachary. Thanks for being there and sharing in this experience.

ACKNOWLEDGMENTS

I wish to thank my committee: Dr. Christopher Post, Committee Chairman, Dr. Elena Mikhailova, Dr. William Bridges and Dr. Mark A. Schlautman for their help and support during development and completion of this study. Thanks to Clemson University Facilities Services for providing funding, and to Paul Minerva, Clemson University Arborist. I wish to acknowledge and thank Russell Buchanan, GIS Specialist, who early on provided field data collection, photogrammetry, and key coding assistance. I want to thank Clemson University for my graduate opportunity and teaching assistantship. Along my academic path I meet many who have assisted in different ways; Dr. Greg Yarrow, Jennifer Hooper, all my lab students during the years who keep me on my toes, peer graduate students and classroom professors who challenged me, to you I want to say thanks. Acknowledgements go out to my employer Pickens County Government and supervisor Jimmy Threatt who provided me the time to pursue my degree. I also want to thank Dr. Lawrence Gering and Dr. Patrick Hiesl for their contribution to this study.

TABLE OF CONTENTS

Table of Contents (Continued) Page

CHAPTER ONE

Introduction: Effective management of natural resources requires access to dependable geospatial information for decision making. This information is often in the form of remotely sensed data which shows the location and condition of the environment at a specific point in time. Data collected by remote devices such as aerial photography, satellite imagery, and Light Detection and Ranging (LiDAR) is critical information for effective decision making. Remotely sensed data provides information that is up-to-date and temporally repeatable (Lachowski, 1998). Remotely sensed data products provide some basic advantages over ground observations. These birds-eye views cover larger areas and provide a better understanding of the objects of interest. The moment a remote sensing device acquires information, the existing conditions are captured to provide a static view of a dynamic world. Another advantage is the ability of some sensors to capture data that the human eye cannot see because they can collect reflectance information over a broader spectral range. An example is the near infrared portion of the spectrum which is often used for vegetative monitoring. Remotely sensed data can also provide, with ground references, measurements related to the area, distances, elevation, volumes, slope, and location (Lillesand, et al., 2015). In 1960, Evelyn L. Pruitt presented the use of 'remote sensing' which came 100^{+} years after the first aerial photograph. The term 'remote sensing' historically followed aerial photography on to airplanes then

eventually the term became established after satellites became effective in viewing surface conditions on Earth (Baumann, 2014).

Aerial photography is the oldest form of remote sensing and began with the use of balloons carrying cameras to map topographical features (Arjomandi, 2007, Baumann, 2014). Aerial photography was a film-based data collection technique throughout most of its history. However, digital camera technology replaced film during the 1990s (Lillesand, et al., 2015). Additionally, aerial imagery can be used through stereoscopic stereo pairing to extract 3D data (Colomina, 2014, Mueller, 2014, Penn State, 2017). This advancement has enabled more efficient and timely extraction of objects and in many cases replaced manual methods (Mueller, 2014).

Light Detection and Ranging (LiDAR) is a form of remote sensing that uses active sensors to measure returned pulses of light to accurately measure characteristics of objects on the earth's surface (Dubayah, 2000, NOAA, 2018). The use of LiDAR has increased dramatically in recent years with the technology utilized currently by many disciplines for a wide variety of applications. For example, it is used for ground topography mapping (Cook, 2016), measurements of 3D structure of vegetation (Lefsky et al., 2002), forest structure (Mohan et al., 2017, Jayathunga et al., 2018), forest biomass (Ma et al., 2018) and other ecological measurements (Hoffman, et al., 2018, Carr et al., 2018, Zhang et al. 2016). Many of these applications can be performed with surveying and photogrammetric techniques which are typically much more time consuming than LiDAR acquisition and processing. LiDAR applications are only limited by high costs and data availability (Lefsky et al., 2002).

The unmanned aerial vehicle (UAV) has been part of remote sensing since the first aerial photograph was taken. The UAV was identified thirty years ago as having great prospect and contribution to remote sensing and photogrammetry. In recent years, technological advances have increased UAV use and applications, and it is rapidly becoming a standard tool for natural resources management (Colomina, 2014). The UAV is considered a low-cost repeatable alternative to modern-day aerial imagery and its use is being driven by the civilian market (Nex, 2014, Tang, 2015). Different onboard sensors can be carried on the UAV to meet the objectives of multiple natural resource applications (Johnston et al., 2003, Hunt et al., 2010, Rudol and Doherty, 2008, Wallace, 2012). The UAV can improve the temporal and resolution of remotely sensed data. For example, the spatial resolution on satellite imagery does not contain enough detail for forest planning (Holmgren, 2008). The UAV is a tool that can be flexible, inexpensive and efficient to fill in these temporal gaps (Tang, 2015).

This research examines the use of a UAV to capture ultra-high resolution imagery and computer techniques to extract information that can be utilized in traditional forestry and arboriculture applications. The organization of this dissertation is within three main chapters:

- Chapter two contrasts and compares different types of point clouds (LiDAR and Photogrammetry based on UAV Imagery). Chapter two takes a spatial and comparative look to determine the accuracy and potential of UAV photogrammetry derived 3D point cloud and its feasibility to be used during

temporal LiDAR gaps. This chapter key point is to provide information that will allow for individual decisions related to the comparison debate.

- Chapter three focuses on extracting forest metrics. Tree height, canopy metrics (volume, shape, and radius) and diameter at breast height (DBH) are measurements describing characteristics of the forest. These measurements are essential in the planning and management of a forest. Utilizing UAV platforms along with algorithms for structure from motion and photogrammetric processing contributes to forest inventory and management (Puliti et al., 2017). Traditional ground-based operations are time and labor intensive and constitute a large amount of human effort. Using techniques developed in this chapter, landscape-level data can be derived reducing overall inventory costs. This chapter's main focus will provide logistics and models to extract forest metrics from a 3D point cloud.
- Chapter four examines the relevancy of using ultra-high detail imagery from the UAV for species classification. Traditional classification models do exist but were developed using remotely sensed data at coarser resolutions. The existing models are deficient in their ability to extract individual tree species and cannot handle the detail offered by UAV imagery. The chapter will result in a model that can absorb high-resolution imagery and use an improved supervised classification scheme that can classify individual trees down to the species level.

Across all three main chapters, this study looks at ancillary data that can be derived from 3D point clouds. Digital elevation models (DEM), digital terrain models (DTM) and

canopy height models (CHM) can be generated with practical contributions to forestry. From these layers, others can be derived from analysis to produce slope, aspect, contours, and terrain models among others. Also, the utilization of third-party software aimed at the consumption of LiDAR point clouds, are examined in these chapters to determine their applicability to for photogrammetrically derived 3D point clouds.

REFERENCES

Arjomandi, M. 2007. *Classification of Unmanned Aerial Vehicles*. The University of Adelaide, Australia.

Baumann, Paul R., 2014. History of Remote Sensing, Aerial Photography. Retrieved from: https://www.oneonta.edu/faculty/baumanpr/geosat2/RS%20History%20I/RS-History-Part-1.htm on September 5, 2018.

Carr Andres, Matt R. K. Zeale, Andrew Weatherall, Jeremy S. P. Froidavaux, Gareth Jones, 2018. Ground-based and LiDAR-derived measurements reveal scale-dependent selection of roost characteristics by the rare tree dwelling bat *Barbastella barbastellus*. *Forest Ecology and Management*, Vol. 417, May 15, 2018, pp. 237-246.

Colomina, I, P. Molina, 2014. Unmanned aerial systems for photogrammetry and remote sensing: A review. *ISPRS Journal of Photogrammetry and Remote Sensing.* Vol. 92, June 2014, pg. 79-97.

Cook, Kristen L., 2016. An evaluation of the effectiveness of low-cost UAVs and structure from motion for geomorphic change detection. *Geomorphology*, 278, November 15, 2016, pp. 195-208.

Holmgren, Peter, Thomas Thuresson, 2008. Satellite remote sensing for forestry planning- A review. *Scandinavian Journal of Forest Research*, Vol. 13, Issue 1-4, December 15, 2008, pp. 90-110.

Hoffman, Kira M., Andrew J. Trant, Wiebe Niijland, Brian M. Starzomski, 2018. Ecological legacies of fire detected using plot-level measurements and LiDAR in an old growth coastal temperate rainforest. *Forest Ecology and Management*, Vol. 424, September 15, 2018, pp. 11-20.

Jayathunga, Sadeepa, Toshiaki Owari, Satoshi Tsuyuki, 2018. Evaluating the Performance of Photogrammetric Products Using Fixed-Wing UAV Imagery over a Mixed Conifer-Broadleaf Forest: Comparison with Airborne Laser Scanning. *Remote Sensing*, Vol. 10, 187, January 27, 2018, pp 1-24.

Lachowski, Henry, M. 1998. Remote Sensing Applied to Resource Management. USDA Forest Service Gen. Tech. Rep. PSW-GTR-166.

Lefsky, Michael A., Warren B. Cohen, Geoffrey G. Parker, David J. Harding, 2002. Lidar Remote Sensing for Ecosystem Studies: Lidar, an emerging remote sensing technology that directly measures the three dimensional distribution of plant canopies, can accurately estimate vegetation structural attributes and should be of particular interest to forest, landscape, and global ecologists. *BioScience*, Vol. 52, Issue 1, January 1, 2002, pp. 19-30.

Lillesand, Thomas, Ralph W. Kiefer, Jonathan Chipman, 2015. *Remote Sensing and Image Interpretation*. Whiley Global Education, February 13, 2015, pages 768.

Ma Wu, Grant Michael Domke, Anthony D'Amato, Christopher w. Woodall, Brian Walters, Ram Deo, 2018. Using matrix models to estimate above ground forest biomass dynamics in the Eastern USA through various combinations of LiDAR, Landsat, and Forest Inventory Data. *Environmental Research Letters*, October 23, 2018. Retrieved from: http://iopscience.iop.org/article/10.1088/17489326/aaeaa3/meta.

Mohan, Midhun, Carlos Alberto Silva, Carine Klauberg, Prahlad Jat, Glenn Catts, Adrian Cardil, Andrew Thomas Hudak, Mahendra Dia, 2017. Individual Tree Detection From Unmanned Aerial Vehicle (UAV) Derived Canopy Height Model in an Open Canopy Mixed Conifer Forest. *Forests*, Vol. 8, 340, September 11, 2017, pp. 1-17.

Mueller, Amanda R., 2014. Lidar and Image Point Cloud Comparison. Thesis for Master of Science in Remote Sensing Intelligence. Naval Post Graduate School, September 2014. Retrieved from: https://calhoun.nps.edu/handle/10945/43960.

Nex, Francesco, Fabio Remondino, 2014. UAV for 3D Mapping Applications: A Review. *Applied Geomatics*, Vol 6, Issue 1, March 2014, pp. 1-15.

NOAA, 2018. What is LiDAR?. Retrieved from: https://oceanservice.noaa.gov/facts/lidar.html on September 7, 2018.

Penn State, 2017. Geometry of the Aerial Photograph. GEOG 480 Exploring Imagery and Elevation Data in GIS Applications Course. Retrieved from: https://www.e-education.psu.edu/geog480/node/452.

Puliti, Stefano, Liviu Theodor Ene, Terje Gobakken, Erik Naesset, 2017. Use of partial coverage UAV data in sampling for large scale forest inventories. *Remote Sensing of Environment*, Vol. 194, March 30, 2017, pp. 115-126.

Tang, Lina, Guofan Shao, 2015. Drone remote sensing for forestry research and practices. *Journal of Forestry Research*, Vol. 26, Issue 4, December 2015, pp. 791-797.

Zhang, Jian, Jianbo Hu, Juyu Lian, Zongji Fan, Xuejun Ouyang, Wanhui Ye, 2016. Seeing the forest from drones: Testing the potential of lightweight drones as a tool for long-term forest monitoring. *Biological Conservation*, Vol. 198, April 18, 2016, pp. 60-69.

CHAPTER TWO

Comparison of LiDAR- and UAV Photogrammetry-Based Point Clouds

Abstract: Both photogrammetry based and Light Detection and Ranging (LiDAR) derived point clouds are commonly used to represent x, y, and z measurements of objects on the surface of the earth but it is unclear if they produce comparable results. In recent years, computer vision software has been developed to extract 3D point clouds from aerial images of the earth. When coupled with ultra-high-resolution imagery from unmanned aerial vehicles (UAV), computer vision software can extract point clouds from imagery that becomes an alternative to LiDAR. A comparison of point clouds (LiDAR, UAV-derived leaf off and leaf on) was performed in this study to determine if the different technologies produce a similar result. The x, y, z values were compared, and spatial differences were examined using the near analysis tool in ArcMap 10.5.1. Point stratification was conducted to compare different classification groups. Similar spatial proximities of LiDAR and UAV-derived point clouds were observed in and between classifications with an exception of building points. Building extraction was best with LiDAR however was not precise across all point clouds. These results may be from points being miss-classified during the classification process into other classifications. Elevation differences determined by digital elevation models (DEMs) derived by both types of point clouds were found to be within 58 cm of each other. Comparison of DEMs to survey grade elevations revealed that point cloud elevations were close to one another

(> 95.8 %). Results of this study indicate that point clouds generated from high-resolution UAV imagery can be comparable to LiDAR data. Based on these results, 3D point clouds can be used when LiDAR is not available (due to either time- or spatial-constraints).

Keywords: aerial photography, GIS, LiDAR, point cloud, UAV

1. Introduction

Light Detection and Ranging (LiDAR), an optical remote sensing technique, generates point cloud data that contains highly accurate x, y, z measurements of objects on the surface of the earth (Dubayah, 2000; ESRI, 2018). Many disciplines use LiDAR technology, including flood plain mapping, forest inventory, landscape ecology, and geomorphology. LiDAR generates highly accurate data but is often not repeated on a regular basis due to its high cost (Chen, 2007). LiDAR is a laser system that emits light and measures its reflection as it travels back to the sensor (Song et al., 2002; Cao et al., 2011) (Figure 1). LiDAR samples the earth's surface (up to 150,000+ measurements per second), in contrast to a passive sensor that relies upon the reflective energy of the sun. Laser-light energy can penetrate forest canopies and identify objects missed by passive sensors. In many cases, the light is reflected multiple times off of objects before it is reflected off of the ground. For example, in a forest, the emitted light signal can strike a tree in different locations resulting in return of one to three light reflections until the final ground reflection returns (Figure 2). LiDAR can analyze locations photogrammetry cannot.

LiDAR has many potential uses within traditional and urban forestry. Individual trees (Jeronimo et al. 2018) as well as stand level classifications (Fedrigo et al., 2018) can be detected across diverse landscapes. Above ground carbon (Asner et al., 2018, Hughes et al., 2018) and biomass (Ma et al., 2018) measurements can be measured from LiDAR. Forest structure measurements such as tree height, tree densities (Mielcarek et al., 2018)

and canopy metrics (Estornell et al. 2018) can be generated from LiDAR point clouds. Across diverse forests, vertical structure measurements in most cases can be reconstructed using LiDAR point clouds (Silva et al. 2018). Species classification at the stand (Fedringo et al., 2018) and individual tree (Wang et al., 2018, Shi, et al., 2018) levels can be achieved. LiDAR applications within forestry are being used across many locations and forest types to identify forest characteristics with high levels of accuracy (Lim et al, 2003, Lefsky, et al., 2002, Hodgson and Bresnahan, 2004, Caccamo et al. 2018, Harikumar et al., 2018, Giannoulas et al., 2018).

Colonel Aime Laussedat was considered to be the "Father of Photogrammetry". In 1851, he developed a model based on photographs he took that replaced labor intensive methods used to create topographic maps (Mueller, 2014). Technology has improved dramatically since balloons were used to take the first aerial photographs. When an observer looks at aerial imagery, depth and heights of objects are visually observed through a process called stereoscopic vision. This manual photogrammetric processing of images extracts information and–like other photogrammetry applications–has benefited from technological advances.

Today, unmanned aerial vehicles (UAVs) represent a low-cost option for acquiring ultra-high-resolution imagery (< 5 cm) (Merino et al., 2006; Tang, 2015). The UAV, with its ease of use, flexibility, and applicability has the capacity to acquire imagery at high spatial and temporal resolutions (Fraser and Congalton, 2018). The UAV can alleviate issues related to temporal and economic limitations for obtaining aerial photography (Giannoulas et al., 2018). In addition to these positive characteristics, the

UAV is capable of capturing imagery and with photogrammetric techniques can provide three-dimensional (3D) detailed canopy surfaces across forest landscapes (Jayathunga et al., 2018).

Computer vision techniques have been developed that facilitate imagery analysis and point cloud extraction (Colomina, 2014; Mueller, 2014). The objective and goal of computer vision and photogrammetry is to make logical conclusions about observed objects. Object recognition can be accurately constructed from aerial imagery using advanced computer vision techniques (Seo, 2003). Structure from Motion (SfM) is a relatively new technique that follows stereoscopic photogrammetry principles. Using offset/overlapping images, 3D models can be developed. This process utilizes a bundle adjustment technique that is iteratively extracted from multiple overlapping images. Originating from computer vision and automatic feature matching algorithms, SfM has evolved and utilized for automatic 3D point cloud extraction (Westoby et al., 2012). Within forestry applications, SfM can be utilized as a low cost alternative to airborne laser scanning (ALS or LiDAR). SfM does have some accuracy limitations (when compared to ALS) within dense forest canopies however it still provides adequate vertical forest structure results (Wallace et al., 2016). LiDAR is the best technique to obtain forest structure, but it has temporal and economic limitations which increased the popularity of SfM as a low-cost alternative to obtain forest structure from two-dimensional imagery (Frey et al., 2018).

In recent years, utilization of LiDAR has surpassed aerial imagery within many traditional applications. Documentation of this trend can be found in many technical and

scientific publications (Leberl et al., 2010). According to Wang et al. (2009), photogrammetric methods are being rapidly replaced by LiDAR. Photogrammetry was developed before LiDAR and its application has recently increased drive by UAV technologies (Mueller, 2014). With the technological advancements in computer vision, both point clouds (LiDAR and 3D) are being used in a range of applications (Frey et al., 2018). SfM point clouds (3D point clouds) have higher point density and increased spatial characteristics with similar correlations when compared to LiDAR (Malambo et al., 2018). Leberl et al. (2010) verified that both LiDAR and 3D point clouds are comparable and no significant conclusions can be made as to which method is better.

The use of UAVs allows for low-cost acquisition of high-resolution imagery for numerous applications. Utilization of UAVs by natural resource disciplines has increased, which provides these disciplines with remotely sensed products for decision making. In contrast, LiDAR is often not repeated because of the high cost of acquisition (Chen, 2007). Computer vision techniques combined with UAV imagery derived point clouds may be an alternative to LiDAR. The objectives of this comparative study using aerial LiDAR and 3D point clouds are to: A) determine the degree of accuracy of both types of point clouds and B) determine if 3D point clouds can serve as an effective substitute for LiDAR point clouds.

2. Materials and Methods

2.1. Study Area

The area of study in this work was the main campus of Clemson University (located in Clemson, South Carolina; Figure 3). Clemson University was founded in 1893 on land gifted by Thomas Clemson. Clemson University is located in the southwestern portion of Pickens County in South Carolina and encompasses 566 ha of urban forest. Research, teaching, and support facilities host a student population of 23,406. In addition to the core campus, an additional 12,949 ha are utilized for research and teaching within agriculture and forest settings. (Clemson, 2014)

2.2. UAV Aerial Imagery

The UAV model used in this study to collect ultra-high resolution true color imagery was the eBee plus (Figure 4; senseFly, Cheseaux-sur-Lausanne, Switzerland). Images were captured along planned flight lines with lateral and longitudinal overlap (70% and 60%, respectively). Flight parameters were managed by a portable ground control station via radio link to the UAV autopilot. Differential global positioning system (GPS) was used for navigation and target ground sample distance (GSD) was 2.85 cm/pixel. The UAV was managed and flown by autopilot settings that controlled the onboard camera (senseFly S.O.D.A., 20 megapixel, red (660 nm), green (520 nm), blue (450 nm)) and sensor activation (12.75 x 8.5 mm (1-inch); F 2.8-11; ground resolution of 2.9 cm at 122 m). Image resolutions of 2.4-3.5 cm were obtained while the UAV

maintained an altitude of 120.9 m. These parameters and image resolutions were based on a previous forest canopy and landscape diversity study (Anderson and Gaston, 2013). Open landing zones (minimum 10 m x 15 m) for autonomous take off/landings were used. UAV and ground control communication were managed using a 2.4 GHz radio universal serial bus (USB) link.

Two separate flights were conducted: on July 8, 2017 (Leaf On) and on March 4, 2018 (Leaf Off). Multiple missions were flown between the hours of 10 AM and 3 PM. (Table 1). Pre-flight planning was conducted to determine forward observer positions, designate landing/take off zones, and to identify topographic and photographic requirements. Prior to flight, ground control points (GCPs) were established across the study area using a mapping grade global positioning system (GPS) (Trimble 7x, Accuracy: horizontal = 25 cm, vertical = 50 cm), Trimble Inc., Sunnyvale, California). There were 102 GCPs (established objects that could be directly observed in the resulting images) spatially dispersed throughout the study area. These GCPs were used as horizontal controls during post-orthorectification processing.

2.3. Imagery Processing

Upon completion of each UAV flight, the secure digital card (SD), onboard the UAV, containing captured images was removed. The SD card was placed in a computer where the images were transferred for storage and processing. Post-processing began with geotagging camera and spatial information to each image's exchangeable image file (EXIF) header. Parameters for orthorectification were designated within Agisoft

PhotoScan Professional Edition Ver. 1.3 (64-bit) (Agisoft, St. Petersburg, Russia). Within Agisoft, six steps were needed for orthorectification and product generation, including: alignment, building geometries, georeference (GCP inclusion), mesh, texture, mosaic, seamless image export, and point cloud extraction. To utilize GCP during processing, ArcMap 10.5.1 was used to generate a text file formatted for the Agisoft schema. Agisoft uses GCP to calculate accurate image locations. Following selection of a GCP, the corresponding images (ones that have the GCP present) would appear in the console. After selecting an image, the GCP and its relationship to the corresponding position on the image was shown. Alignment of the GCP relies on the computer mouse to move the GCP to match the correct location on the image. After all images are manually aligned for a specified GCP, the process is repeated for all GCPs. The result of processing the imagery within Agisoft, is a seamless orthorectified image created for each flight using established GCPs for horizontal control. Upon completion of orthorectification, a 3D point cloud was extracted using structure from motion (SfM) processing within Agisoft. After 3D point clouds are created from each flight they were exported in LASer (LAS) format.

2.4. LiDAR

Aerial LiDAR data were collected by Towill Inc. (Colorado Springs, Colorado) during the spring of 2011 under a contract from the South Carolina Department of Natural Resources (SCDNR). An Optech Orion M-200 sensor was used for data acquisition, which flew at 1,500 meters with a scan half angle of 20 degrees at a 38-hertz

rate with a plane speed of 150 knots utilizing 50% overlap. Airborne GPS and inertial measurement unit (IMU) were used during flight. GPS data logging was conducted by active Continuing Operating Reference Stations (CORS) (South Carolina Geodetic Survey). All flights initiated at the Rock Hill Airport in South Carolina.

Post-processing of LiDAR data was performed by Dewberry (Fairfax, Virginia). Dewberry uses various software packages for classification and processing (Point Accuracy @ 95% Confidence Level: Vertical RMSE = 18.5 cm, Horizontal RMSE = 1m). The data were tiled to match map tiles (3,048 m x 3,048 m) from the geographic information system (GIS) of Pickens County, South Carolina. The data were classified into the following classes using LAS 1.2 format: Class 1 - unclassified (including, but not limited to, vegetation, buildings, and noise); Class 2 - ground; Class 7 - noise; Class 8 - model key points; Class 9 - water; and Class 10 - ignored ground (SCDNR, 2011). LiDAR data (LAS Files) were obtained from Pickens County South Carolina GIS Mapping Department. Processed LiDAR products for South Carolina (by county): terrain, hydrolines, intensity images, digital elevation model and two-foot contours are freely available on South Carolina's Department of Natural Resources web site: http://www.dnr.sc.gov/GIS/lidarstatus.html. LiDAR LAS point clouds can be obtained freely from: https://viewer.nationalmap.gov/basic/.

2.5. ArcGIS Processing

ArcGIS version 10.5.1 (Environmental Systems Research Institute (ESRI), Redlands, California) was used for processing and comparing 3D and LiDAR point

clouds and their respective elevation models. The LASTools Toolbox (rapidlasso GmbH, Gilching, Germany), is an assortment of tools utilized for processing point clouds, primarily LiDAR. Each point cloud used in this study was processed by LASTools using a similar process so associations between points and ground counterparts could be designated. LASTools can be used in one of four methods: standalone, graphical user interface (GUI), command line, or as a toolbox in ArcGIS. LASTools (individual tools) and LASTools Production (batch processing tools) were added to ArcToolbox in ArcMap 10.5.1. Classification of each point cloud (leaf off, leaf on, and LiDAR) was completed using a series of tools, which included las2las (project), lastilePro, lasgroundPro, lasheightPro, and lasclassifyPro. Las2las (project) was used to convert the native coordinate system (WGS 1984) of the 3D point clouds to UTM WGS 84 17N and LiDAR points from Lambert Conformal Conic 2SP to UTM NAD 1983 17N. To increase efficiency (maximum number of points: 15-million per tile), lastile was used to divide the 3D points into manageable tiles. Lastile was not needed for the LiDAR point cloud since tiling was performed by the vendor that resulted in eight tiles needed to cover the study area. Following tiling, ground points were identified using lasgroundPro. Tiles were individually processed until batch processing was complete. LASheightPro used similar batch processing to calculate the heights of points in which lasgroundPro results were used as input. Batch processing of lasheightPro results was performed that classified each point as either unclassified, building, or high vegetation (ground classification was completed in previous step).

Following point cloud processing, ArcCatalog was used to create a LasDataset for displaying and processing point clouds in ArcMap. LAS datasets were generated for each point cloud and processed point files (LAS format) were imported. After importing tiled points, the statistics tool was used to prepare the data for display in ArcMap 10.5.1. Using the LAS dataset to raster tool in ArcMap 10.5.1, a digital elevation (DEM), digital terrain (DTM), and canopy height (CHM) models were generated for each point cloud (leaf off, leaf on, and LiDAR). For DEM and DTM creation, the LASDataset was filtered by point classification, ground and high vegetation points to generate each model respectively. A CHM model was generated by subtracting the DEM from DTM using the Minus tool in ArcMap 10.5.1. Each LASDataset was converted to a Multipoint file in ArcMap 10.5.1. The Multipoint file will reference one set of attributes of a feature that has more than one physical part (ESRI, 2018). This conversion allows the mass points of point clouds to be processed by other ArcMap tools for further comparisons. A multipoint file was created from each point cloud LASDataset representing all points, ground points, building points, and high vegetation points. The LASDataset to polygon tool was used to determine the spatial extent of each point cloud (Figure 5). The area of these polygons was compared and the smallest (Leaf On) was used as processing extent for all comparison analysis. The Leaf On boundary was also used in the Clip tool to remove outlier points from the Multiple Point feature classes.

Comparisons of point clouds (leaf off vs. leaf on, leaf off vs. LiDAR, and leaf on vs. LiDAR) were conducted using near analysis, which calculated the distance from each point to its closest neighbor for spatial correlation. Near analysis was conducted for each

multipoint file that represented: all, ground, building and high vegetation points. Each stratified multipoint layer (all points, ground points, building points, high vegetation points), new attributes were created. These attributes included x, y, z, Min z, and Max z parameters. Using the Calculate Geometry tool in ArcMap, each attribute was populated and descriptive statistics (mean, standard deviation, and number (N)) were transferred into a table to facilitate comparisons.

The LASBoundary tool was used to differentiate buildings from the multipoint feature class(s). A polygon feature class resulted in building footprints created from points classified as buildings. The resulting feature classes of each point cloud (LiDAR, Leaf On, and Leaf Off) were compared to an existing digitized building footprint feature class, which was generated from aerial imagery in 2016 and was provided by Pickens County, South Carolina GIS Department.

A random point feature class (Figure 6) was generated in ArcMap that resulted in distribution of 206 points across the spatial extent of the Leaf on LASDataset. The Extract Values by Point tool was used to interpolate the value of each DEM and DTM. The corresponding values were then added to the attribute table and were used to determine statistical significance and to assist in point cloud validation. A separate random point feature class was created with points spatially distributed across the study area. These points were used as locations to collect survey-grade GPS (Trimble R8, RTK Accuracy: horizontal = 8 mm vertical = 15 mm, Trimble Inc., Sunnyvale, California) data. Both vertical and horizontal positions of the 30 random points were utilized to further evaluate surface model accuracy.

ArcMap 10.5.1 was used to produce a third point feature class containing 30 points distributed randomly across the study area. Upon creation, a square box (2m x 2m) was constructed around each point. Each box will represent areas for point to point comparison analysis. Using the clip tool in ArcMap, each Multipoint file (total of 12) was clipped to provide residual points inside each square box. The resulting clipped Multipoint file was then converted to single points using the Multipart to Single Part tool in ArcMap 10.5.1. Using the output from the Multipart to Single Part tool, paired points (selected one point from each comparison group closest to each other) were selected within each box (Figure 7) and using tools in ArcMap each points x, y, z, Min z and Max z values will be extracted and placed in a table to compute statistical comparisons.

2.6. Statistical Analysis

Mean absolute percentage error (MAPE) was used for point to point and total point (mean) comparisons (Van der Zane et al., 2011). ArcMap 10.5.1 was used to evaluate a point to point comparison. Using a random grid (2 m x 2 m) generated in ArcMap 10.5.1, comparison point files (LiDAR vs. Leaf Off, LiDAR vs. Leaf On and Leaf Off vs. Leaf On) were activated revealing points inside each grid. Using the select tool in ArcMap 10.5.1, two points (one point from each comparison) closest to one another and their respective values were extracted to an excel table. This process was repeated until sufficient samples of points were obtained. In Microsoft Excel, these values were examined using MAPE calculations to determine how close each 3D point (Observed) was to its adjacent LiDAR (Actual) point. Comparison was also made

between 3D point clouds (Leaf Off = Actual, Leaf On = Observed) using MAPE. In addition, the mean values of points (all, ground, building and high vegetation) were also compared (LiDAR vs. Leaf Off, LiDAR vs. Leaf On, and Leaf Off vs. Leaf on) and evaluated using MAPE. Surface model accuracy was evaluated by determining the MAPE of each survey-grade GPS measured elevation (Actual) and each point cloud surface model elevation (Observed).

3. Results and Discussion

3.1. UAV Aerial Imagery

Two separate time periods were identified to capture images during leaf off and leaf on conditions. Ultra-high-resolution true color images were captured by the eBee, a fixed wing UAV. The UAV collected a total of 1,392 images on July 8, 2017 and 1,686 images on March 4, 2018 (Table 1). Although all flights were designed to follow the same pattern, exact flight lines were not maintained, and spatial irregularities occurred during the leaf off missions (due to logistical variables), resulting in a slightly larger area of coverage for these particular missions. Compared to traditional image capture, the UAV was economical and effective with no issues encountered during the missions.

3.2. Imagery Processing

Agisoft PhotoScan provided very good results with opportunity by the user to choose and fine tune processing parameters. Processing time for all steps was between 3-4 days (continuous operation) depending on number of photos, GCPs and computer resources. The inclusion of GCPs during photogrammetric processing improved the horizontal accuracy (< 15 cm) of the final mosaic which is important when comparing on-ground objects. The procedure with GCPs was performed on both mission days, which generated seamless orthomosaic images (Figures 8 and 9) that contain four-bands and a resolution of 4.1 cm. SfM processing allowed for the extraction of point clouds for

both leaf off and leaf on conditions resulting in las point files with 54.26 and 53.59 points/m^2 respectively (Table 2).

3.3. ArcGIS Processing

Processing of point clouds using LASTools was a seamless operation and adequate user defined parameters were available to ensure desired outcomes. The use of Lastile resulted in a total of 66 tiles for leaf on and 72 tiles for leaf off that were then used as inputs for batch processing with other tools. LAStool was found to process 3D point clouds as if they were LiDAR data. Although no errors or issues occurred during processing, a large amount of points (Table 2) were listed as unclassified (Leaf On = 34.35 %, Leaf off = 50.86%) when compared to LiDAR (10.04%). Further research is needed but it is surmised that the detection algorithms and or tool parameters for LasGroundPro and LasClassifyPro need to be refined which may utilize more of the unclassified points within the 3D point cloud. Too is the question in regard to how many points are actually needed within classes for point cloud applications. If a lesser/larger number of points are needed, this could result in changes to flight parameters as well as reduced file sizes increasing processing efficiencies.

Spatial proximity between point clouds was determined using the Near Tool (Table 3), which showed that point clouds had spatial consistency, except for building classification. Further research is needed to explain this discrepancy with building classification, but it is possible that points were misclassified by the classification process. Points belonging to buildings were sometimes incorrectly classified as

unclassified, ground, or high vegetation. It is also possible that points classified as buildings should have been classified as unclassified, ground, or high vegetation.

Visual interpretation of these comparative results (Figure 10) revealed discrepancies between the point clouds generated in this work and the building feature class from 2016. Inconstancies of building identification, shape, and size were apparent (Table 4). These results suggest that building extraction from 3D point clouds does not yield accurate results. This conclusion is in agreement with the results of building point near analysis. Collectively, these results indicate that point cloud processing (point classification) is not accurate. Further research is needed to understand why point cloud-misclassification occurred. Resolution of this issue with classification parameters could improve the accuracy of point cloud building extractions. Of the three point clouds (LiDAR leaf off, leaf on) LiDAR buildings are more similar to Pickens County GIS building footprints.

3.4. Statistical Analysis

Statistical analysis was performed to compare and validate point clouds which will also be used to determine if the point clouds (LiDAR and 3D) are equal. If statistically similar, it could be surmised that a one-point cloud could be used in place of the other technology (Photogrammetry or LiDAR). Following generation of multipoint feature classes and calculation of the X, Y, Z, Min Z and Max Z attributes in ArcGIS, points were stratified (all, ground, building, and high vegetation) and descriptive statistics (mean, range, and standard deviation) generated. The means for each comparison

(LiDAR vs. Leaf Off, LiDAR vs. Leaf On and Leaf Off vs. Leaf On) were transferred to an excel spreadsheet and compared using Mean Absolute Percentage Error (MAPE). MAPE is a measure of the amount of error between observed and actual values in terms of a percentage. Smaller MAPE values indicate that observed and actual values are relatively closer (MAPE, 2000). The results (Table 5) indicate that the point clouds are correlated to one another when observing all points and points stratified by point classifications (ground, building and high vegetation). To further evaluate and compare, a point to point comparison was completed using MAPE. Rather than looking at all the points as a whole (mean vs. mean) individual points (point vs. point) were evaluated. The results (Table 6) are in similar fashion to the MAPE mean comparison.

Surface model elevations generated for each point cloud were compared to survey-grade GPS elevations. These results (Table 7) show that the mean elevation of each DEM is close to one another (< 0.66 m). MAPE was used to compare DEM elevations (observed) to survey elevations (actual). MAPE results indicate that LiDAR generated elevations were closer to survey elevations as compared to Leaf Off and Leaf On elevations (0.21%, 0.34% and 4.20%, respectively) (Table 8). Although Leaf On MAPE was higher than the other point clouds, all three are relatively close to the actual values (survey-grade), indicating that all three point cloud DEMs are accurate.

4. Conclusions

Utilization of the UAV to collect ultra-high-resolution imagery proved to be an efficient and low-cost alternative to traditional methods. No problems were encountered during post-processing of the images and the inclusion of GCPs in the process increased horizontal accuracy. This study showed spatial consistency between LiDAR and 3D point clouds. Horizontal (X, Y) positioning of both point clouds were within proximity to one another and along with Z values statistical analysis reflect correlation with LiDAR points. All points were consistent even when stratified by point classification (ground, high vegetation, and buildings). Point extraction for the creation of surface models was effective and results showed high degree of elevation accuracy (> 95.8%) when compared to survey grade measurements. The results of this study also indicate that extracting buildings from point clouds may be inconsistent or not applicable. Additional research is needed, but either the classification parameters need modification, or the detection algorithms were not efficient at distinguishing building points. In particular, this study indicated that 3D point clouds can serve as a replacement for LiDAR. 3D point clouds can cover temporal periods when LiDAR is not available and landscape modifications need to be captured. This study contributes to previous works where comparisons between point clouds were made and confirms that 3D point clouds are accurate.

REFERENCES

Anderson, Karen, Kevin J. Gaston, 2013. Lightweight unmanned aerial vehicles will revolutionize spatial ecology. *Frontiers in Ecology and the Environment.* Vol. 11, Issue 3, April 2013, pg. 138-146.

Asner Gregory, P, Philip G. Brodrick, Chritopher Philipson, Nicolas R. Vaughn, Roberta E. Martin, David E. Knapp, Joseph Heckler, Luke J. Evans, Tommaso Jucker, Benoit Goossens, Danica J. Stark, Glen Reynolds, Robert Ong, Nathan Renneboog, Fred Kugan, David A. Commes, 2018. Mapped aboveground carbon stocks to advance forest conservation and recovery in Malaysian Borneo. *Biological Conservation*, Vol. 217, January 2018, pp. 289-310.

Caccamo, G., Iqbal, I.A., Osborn, J., Bi, H., Arkley, K., Melville, G., Aurik, D. and Stone, C., 2018. Comparing yield estimates derived from LiDAR and aerial photogrammetric point-cloud data with cut-to-length harvester data in a Pinus radiata plantation in Tasmania. *Australian Forestry*, pp.1-11.

Chen, Qi, 2007. Airborne Lidar Data Processing and Information Extraction. *Photogrammetric Engineering & Remote Sensing*, 73(2):109-112 February 2007.

Cao, Y., Zhao, H., Li, N., & Wei, H., 2011. Land-cover classification by airborne LIDAR data fused with aerial optical images. In *Multi-Platform/Multi-Sensor Remote Sensing and Mapping (M2RSM), 2011 International Workshop on* (pp. 1-6). IEEE.

Clemson, 2014. Clemson University Website History Page; http://www.clemson.edu/about/history/ About the Clemson University Land Use Property Page; http://www.clemson.edu/administration/public-affairs/landuse/about.html Graduate School Information page; http://www.grad.clemson.edu/GeneralInformation.php.

Colomina, I, P. Molina, 2014. Unmanned aerial systems for photogrammetry and remote sensing: A review. *ISPRS Journal of Photogrammetry and Remote Sensing.* Vol. 92, June 2014, pg. 79-97.

Dubayah, Ralph, Jason B. Drake, 2000. Lidar Remote Sensing for Forestry. *Journal of Forestry.* Vol. 98, No. 6, June 2000, pg. 44-46.

Environmental Systems Resource Institute (ESRI), 2018. Online ArcGIS Resource Center. Help Desk ArcGIS Pro. Available online at app/help/data/las-dataset/what-is-lidar-.htm.

Estornell, Javier, Borja Velazquez-Marti, Alfonso Fernandez-Sarria, jesus Marti, 2018. LiDAR methods for measurement of trees in urban forests. *Journal of Applied Remote Sensing*, Vol. 12(4), October 23, 2018, 046009.

Fedrigo, Melissa, Glenn J. Newnham, Nicholas C. Coops, Darius S. Culvenor, Douglas K. Bolton, Craig R. Nitschke, 2018. Predicting temperate forest stand types using only structural profiles from discrete return airborne LiDAR. *ISPRS Journal of Photogrammetry and Remote Sensing*, Vol. 136, February, 2018, pp. 106-119.

Fraser, B. and Congalton, R., 2018. Issues in Unmanned Aerial Systems (UAS) Data Collection of Complex Forest Environments. *Remote Sensing*, 10(6), June 8, 2018, June 9, 2018, p.908.

Frey, J., Kovach, K., Stemmler, S. and Koch, B., 2018. UAV Photogrammetry of Forests as a Vulnerable Process. A Sensitivity Analysis for a Structure from Motion RGB-Image Pipeline. *Remote Sensing*, *10*(6), p.912.

Giannoulas, V.J., Mosxopoulou, H. and Drosos, V.C., 2018, August. The contribution of unmanned systems to updating forest maps. In *Sixth International Conference on Remote Sensing and Geoinformation of the Environment (RSCy2018)*(Vol. 10773, p. 107731I). International Society for Optics and Photonics, August 6, 2018. Retrieved from: https://www.spiedigitallibrary.org/conference-proceedings-of-spie/10773/107731I/The-contribution-of-unmanned-systems-to-updating-forest-maps/10.1117/12.2506929.full?casa_token=7Pr2OTJp5jYAAAAA%3azfD9-d7UUs1Q5-fbBQ1t988AY9pGLFvLv6dsx7iDOe5PiwlJ0FOyjSq9hzwd5K6WLzYsBYo.

Harikumar, A., Bovolo, F. and Bruzzone, L., 2018. A Local Projection-Based Approach to Individual Tree Detection and 3-D Crown Delineation in Multistoried Coniferous Forests Using High-Density Airborne LiDAR Data. *IEEE Transactions on Geoscience and Remote Sensing*, (99), September 10, 2018, pp.1-15.

Hodgson, M.E. and Bresnahan, P., 2004. Accuracy of airborne LiDAR-derived elevation. *Photogrammetric Engineering & Remote Sensing*, 70(3), March 2004, pp.331-339.

Hughes Flint, R., Gregory P. Asnet, James A. Baldwin, Joseph Mascaro, Lori K. K. Bufil, David E. Knapp, 2018. Estimating aboveground carbon density across forest landscapes of Hawaii: Combining FIA plot-derived estimates and airborne LiDAR. *Forest Ecology and Management*, Vol. 424, September 15, 2018, pp. 323-337.

Jayathunga, S., Owari, T. and Tsuyuki, S., 2018. Evaluating the Performance of Photogrammetric Products Using Fixed-Wing UAV Imagery over a Mixed Conifer–Broadleaf Forest:Comparison with Airborne Laser Scanning. *Remote Sensing*, 10(2), January 27, 2018, p.187.

Jeronimo Sean M. A., Van R. Kane, Derek J. Churchill, Robert J. McGaughey, Jerry F. Franklin, 2018. *Journal of Forestry*, Vol. 116, Issue 4, June 29, 2018, pp. 336-346.

Leberl, F., A. Irschara, T. Pock, P. Meixner, M. Gruber, S. Scholz, A. Wiechert, 2010. Point Clouds: Lidar versus 3D Vision. *Photogrammetric Engineering & Remote Sensing*. Vol. 76, No. 10, October 2010, pp.1123-1134.

Lefsky, M.A., Cohen, W.B., Parker, G.G. and Harding, D.J., 2002. Lidar remote sensing for ecosystem studies: Lidar, an emerging remote sensing technology that directly measures the three-dimensional distribution of plant canopies, can accurately estimate vegetation structural attributes and should be of particular interest to forest, landscape, and global ecologists. *AIBS Bulletin*, 52(1), January 1. 2002, pp.19-30.

Lim Kevin, Paul Treiltz, Michael Wulder, Benoit St-Onge, Martin Flood, 2003. LiDAR remote sensing of forest structure. *Progress in Physical Geography*, Vol. 27(1), March 1, 2003, pp. 88-106.

Ma Wu, Grant Michael Domke, Anthony D'Amato, Christopher w. Woodall, Brian Walters, Ram Deo, 2018. Using matrix models to estimate above ground forest biomass dynamics in the Eastern USA through various combinations of LiDAR, Landsat, and Forest Inventory Data. *Environmental Research Letters*, October 23, 2018. Retrieved from: http://iopscience.iop.org/article/10.1088/17489326/aaeaa3/meta.

Mean Absolute Percentage Error (MAPE), 2000. In: Swamidass P.M. (eds) Encyclopedia of Production and Manufacturing Management. Springer, Boston, MA. Retrieved from: https://link.springer.com/referenceworkentry/10.1007%2F1-4020-0612-8_580.

Merino, L., Caballero, F., Martinez-de Dios, J. R., Ferruz, J., Ollero, A. 2006. A cooperative perception system for multiple UAVs: Application to automatic detection of forest fires. *Journal of Field Robotics*, Vol. 23, Iss. 3-4, March-April 2006 pp. 165-184, Available online at http://www3.interscience.wiley.com/cgi-bin/jhome/111090262 Wiley Periodicals Inc.

Mielcarek, Milosz, Krzyszlof Sterericzak, Anahita Khosravipour, 2018. Testing a evaluation different LiDAR-derived canopy height model generation methods for tree height estimation. *International Journal of Applied Earth Observation and Geoinformation*, Vol. 71, September, 2018, pp. 132-143.

Mueller, Amanda R., 2014. Lidar and Image Point Cloud Comparison. Thesis for Master of Science in Remote Sensing Intelligence. Naval Post Graduate School, September 2014. Retrieved from: https://calhoun.nps.edu/handle/10945/43960.

SCDNR, 2011. South Carolina Department of Natural Resources, LiDAR metadata contained within LiDAR product delivery to Pickens County SC.

Seo, Suyoung, 2003. Model Based Automatic Building Extraction from LiDAR and Aerial Imagery. Dissertation, Ohio State University. Retrieved from: https://etd.ohiolink.edu/!etd.send_file?accession=osu1048886400&disposition=inline.

Silva, C.A., Klauberg, C., Hudak, A.T., Vierling, L.A., Liesenberg, V., Bernett, L.G., Scheraiber, C.F. and Schoeninger, E.R., 2018. Estimating Stand Height and Tree Density in Pinus taeda plantations using in-situ data, airborne LiDAR and k Nearest Neighbor Imputation. *Anais da Academia Brasileira de Ciências*, 90(1), March, 2018, pp.295-309.

Shi, Yifang, Tiejun Wang, Andrew K. Skidmore, Marco Heurich, 2018. Important LiDAR metrics for discriminating forest tree species in Central Europe. *ISPRS Journal of Photogrammetry and Remote Sensing*, Vol. 137, March 2018, pp. 163 174.

Song, Jeong-Heon, Soo-Hee Han, Kiyun Yu, Yong-Il Kim, 2002. Assessing the possibility of land-cover classification using lidar intensity data**.** International Archives of Photogrammetry, Remote Sensing and Spatial Information Sciences, 34 (Part3B) (2002),pp. 259-262.

Tang, Lina, Guofan Shao, 2015. Drone remote sensing for forestry research and practices. *Journal of Forestry Research.* Vol. 26, Issue 4, December 2015, pg. 791-797.

Van der Zande, D., Stuckens, J., Verstraeten, W.W., Mereu, S., Muys, B. and Coppin, P., 2011. 3D modeling of light interception in heterogeneous forest canopies using ground-based LiDAR data. *International Journal of Applied Earth Observation and Geoinformation*, 13(5), October 2011, pp.792-800.

Wang, T., Q. Abdullah, D. Chavez, R. Kandukuri, N. Csanyi-May, and D. Simerlink, 2009. The quality of one-foot contour modeling using lidar data versus photogrammetrically derived solutions, Proceedings International Lidar Mapping Forum, January, New Orleans, Louisiana, unpaginated CD-ROM, 9 p.

Wallace, L., Lucieer, A., Malenovský, Z., Turner, D. and Vopěnka, P., 2016. Assessment of forest structure using two UAV techniques: A comparison of airborne laser scanning and structure from motion (SfM) point clouds. *Forests*, 7(3), March 7, 2016, p.62.

Wang, Z., Wu, J., Wang, Y., Kong, X., Bao, H., Ni, Y., Ma, L. and Jin, J., 2018. Crown Level Tree Species Classification Using Integrated Airborne Hyperspectral and LIDAR Remote Sensing Data. *ISPRS-International Archives of the Photogrammetry, Remote Sensing and Spatial Information Sciences*, May, 2018, pp.2629-2634.

Westoby, M. J., J. Brasington, N. F. Glasser, M. J. Hambrey, J. M. Reynolds, 2012. Structure-from-Motion photogrammetry: A low-cost, effective tool for geoscience applications. *Geomorphology*, Vol. 179, December 15, 2012, pp. 300-314.

APPENDIX A

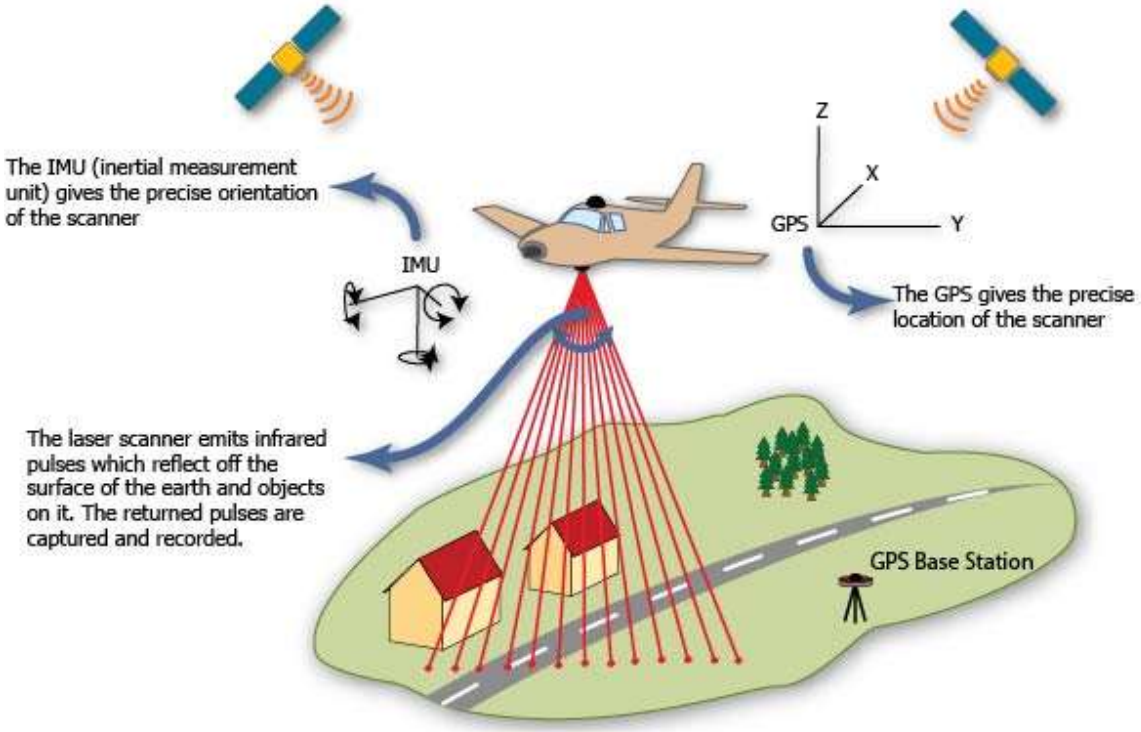

Figure 1 Process of LiDAR data collection. Adapted from: http://www.qpeak.com/scientific-enterprises

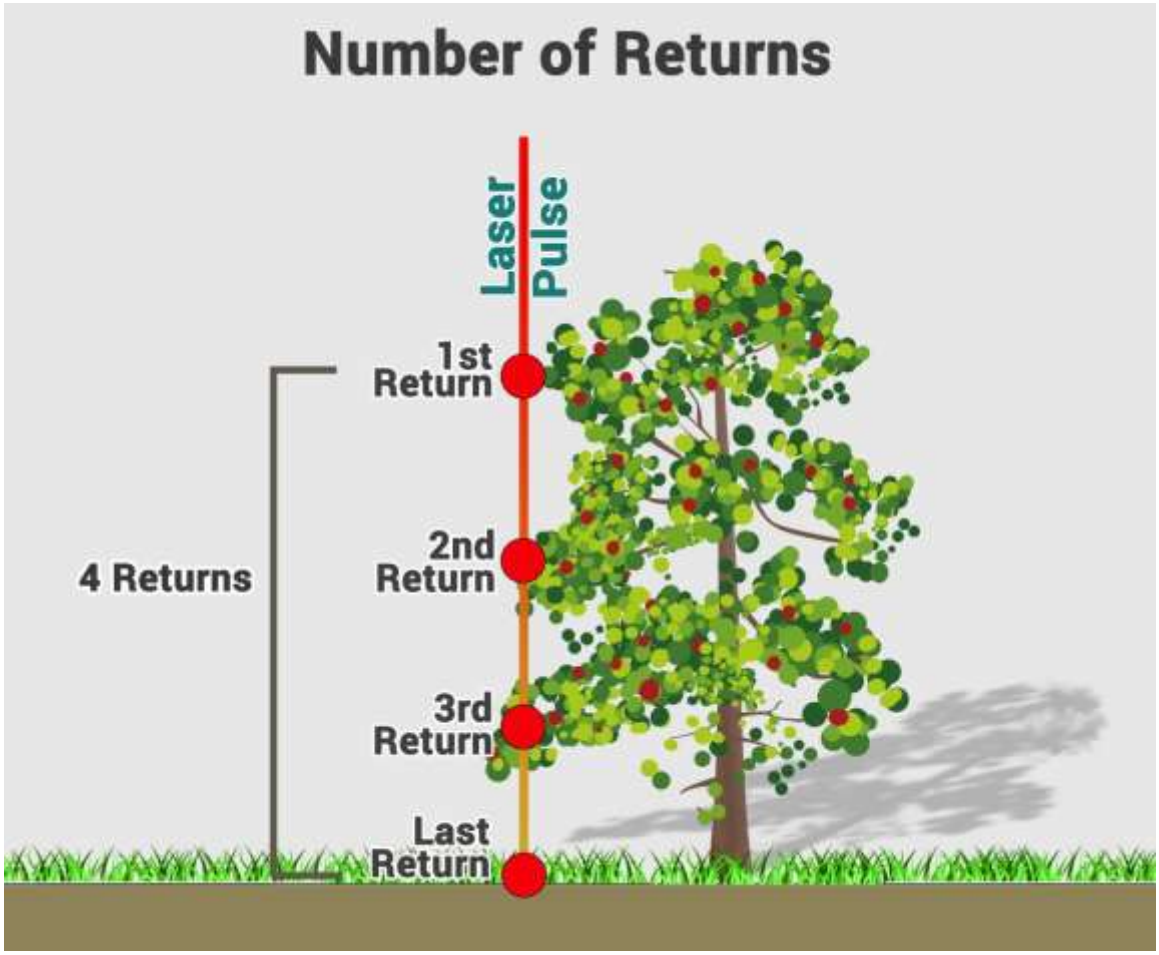

Figure 2 Laser pulse from a LiDAR sensor illustrating the number of returns that could occur when an object is encountered. Adapted from: https://gisgeography.com/lidar-light-detection-and-ranging/

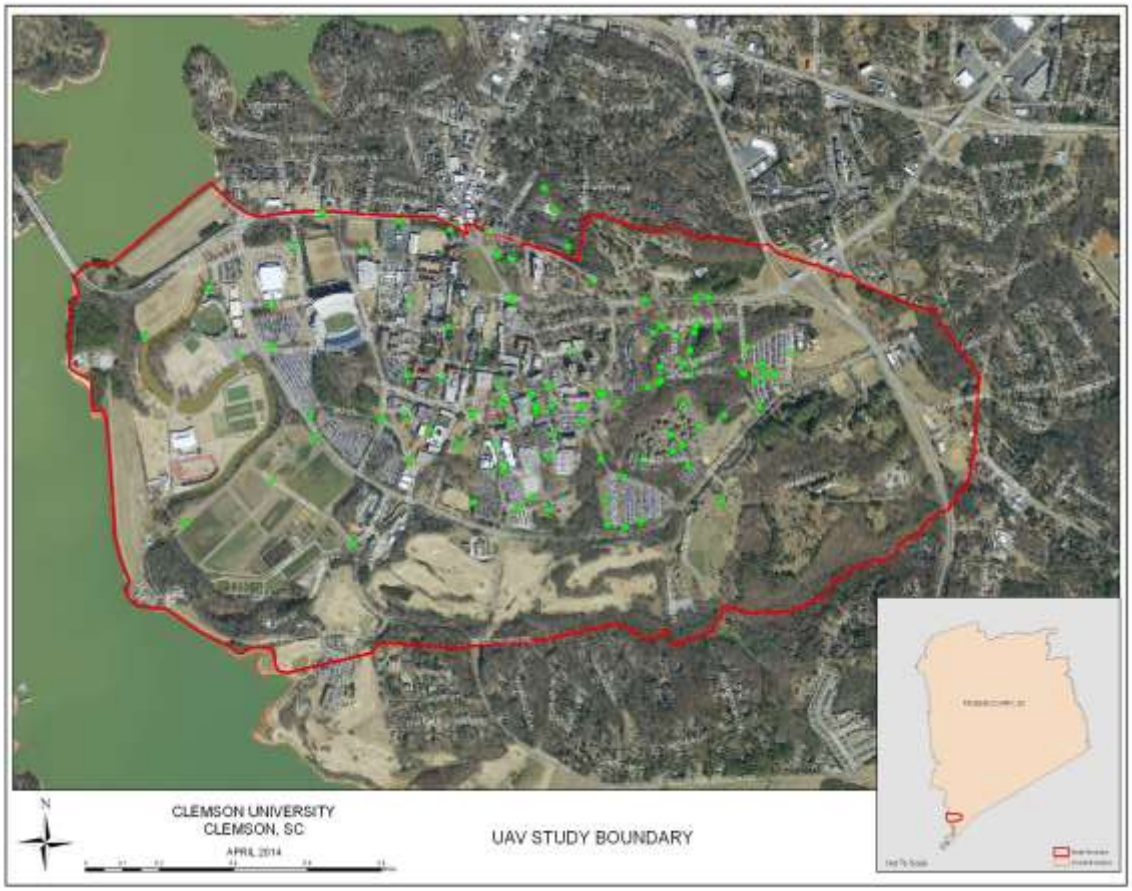

Figure 3 Study boundary used for UAV implementation to collect high resolution imagery. Green dots represent geodetic control points used to correct image spatial inaccuracies if they exist.

Fixed Wing Ebee http://www.sensefly.com/products/swinglet-cam

Multicopter http://diydrones.com/profiles/blogs/a-newbies-guide-to-uavs

Figure 4 General classification categories of UAVs

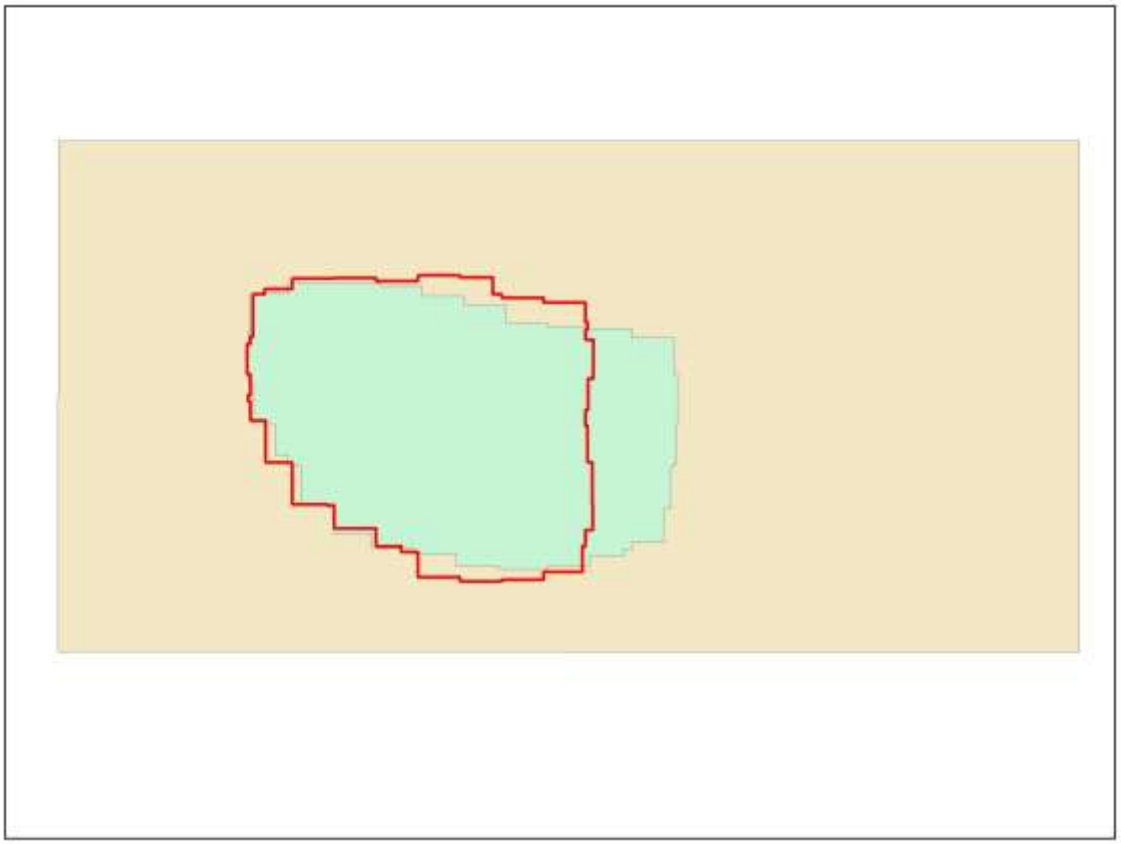

Figure 5 Spatial extents of point cloud LASDatasets converted to polygon: Leaf On = Red, Leaf Off = Green, and LiDAR = Brown

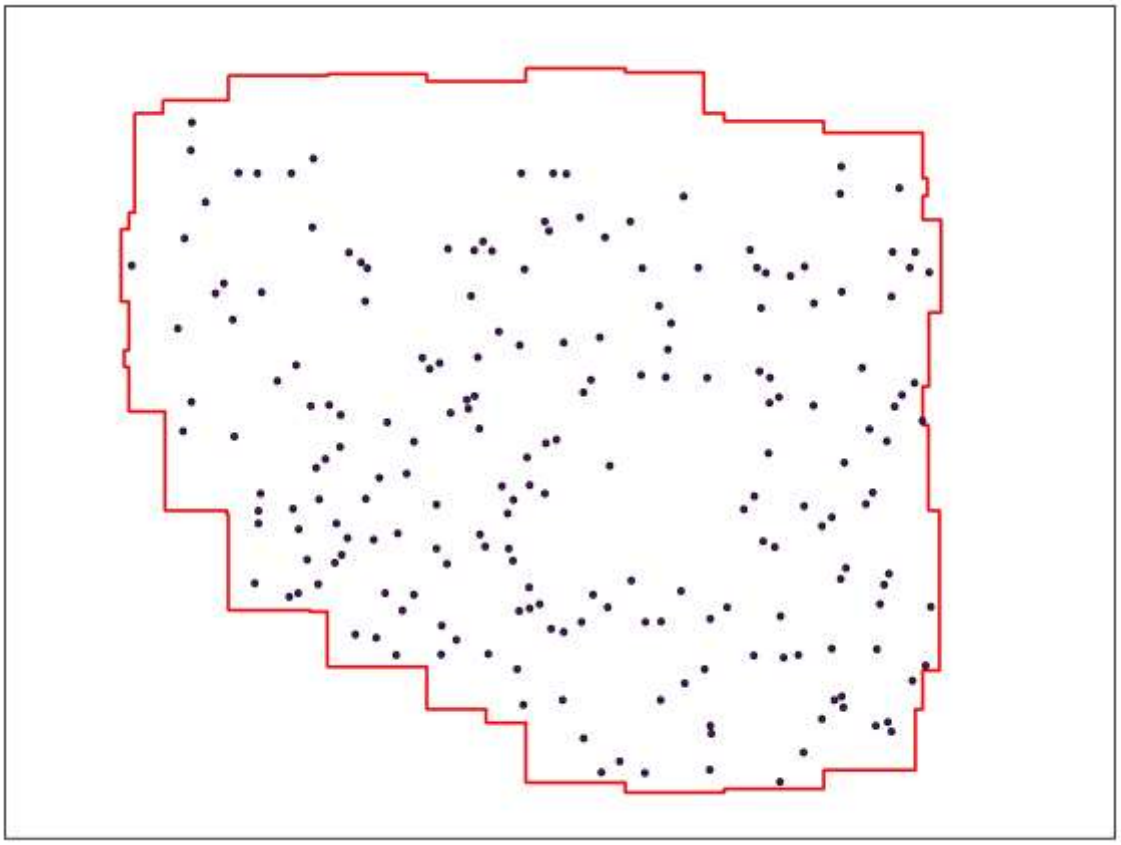

Figure 6 Random points generated for value extraction of DTM an DEM elevation models to test significance (Red Line = Leaf On Boundary)

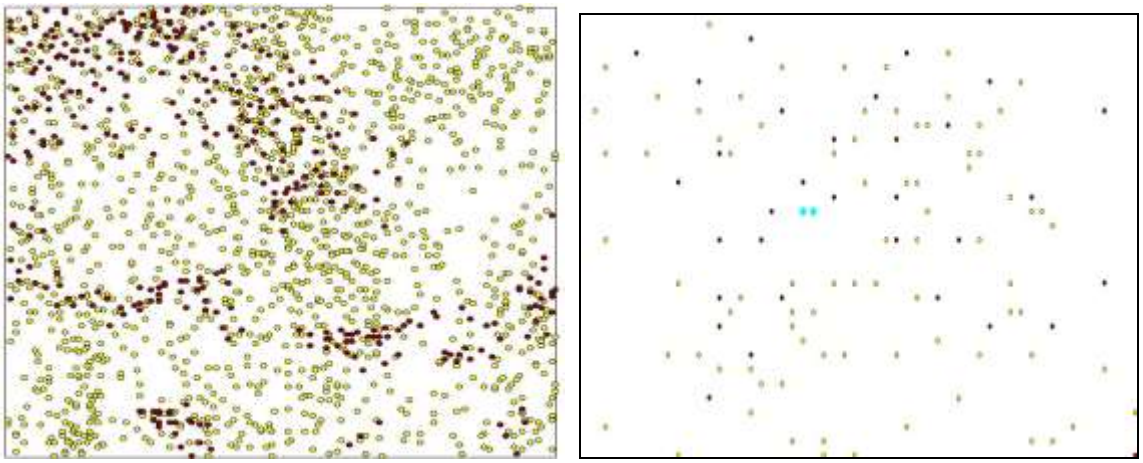

A. B.

Figure 7 Results showing points clipped by 2m x 2m box. Points were used in point to point comparison. A. Leaf Off High Vegetation Points (Brown) and Leaf On High Vegetation Points (Yellow) within 2m x 2m box B. Zoom in area of A showing two closet points selected (Blue) for use in point to point comparison

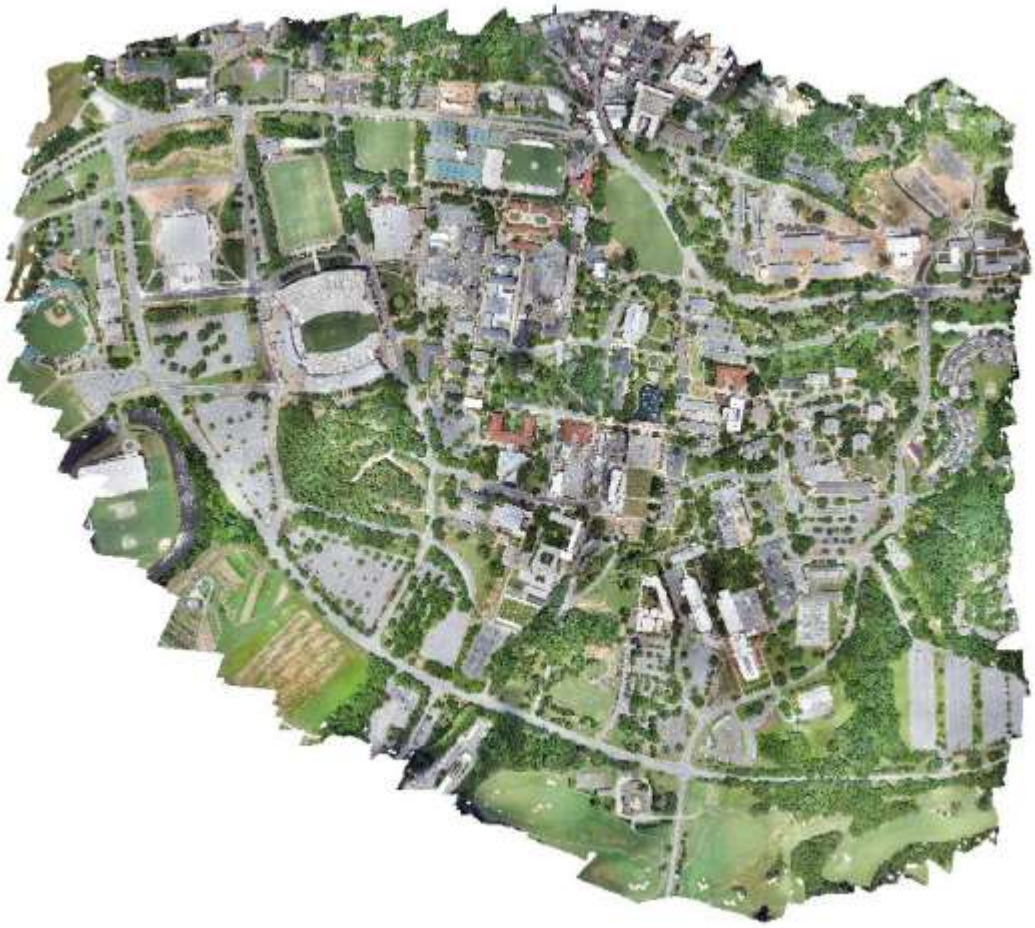

Figure 8 Completed georeference mosaic of Clemson University. This seamless orthomosaic represents leaf on conditions flown on July 8, 2017.

Figure 9 Completed georeference mosaic of Clemson University. This seamless orthomosaic represents leaf off conditions flown on March 4, 2018.

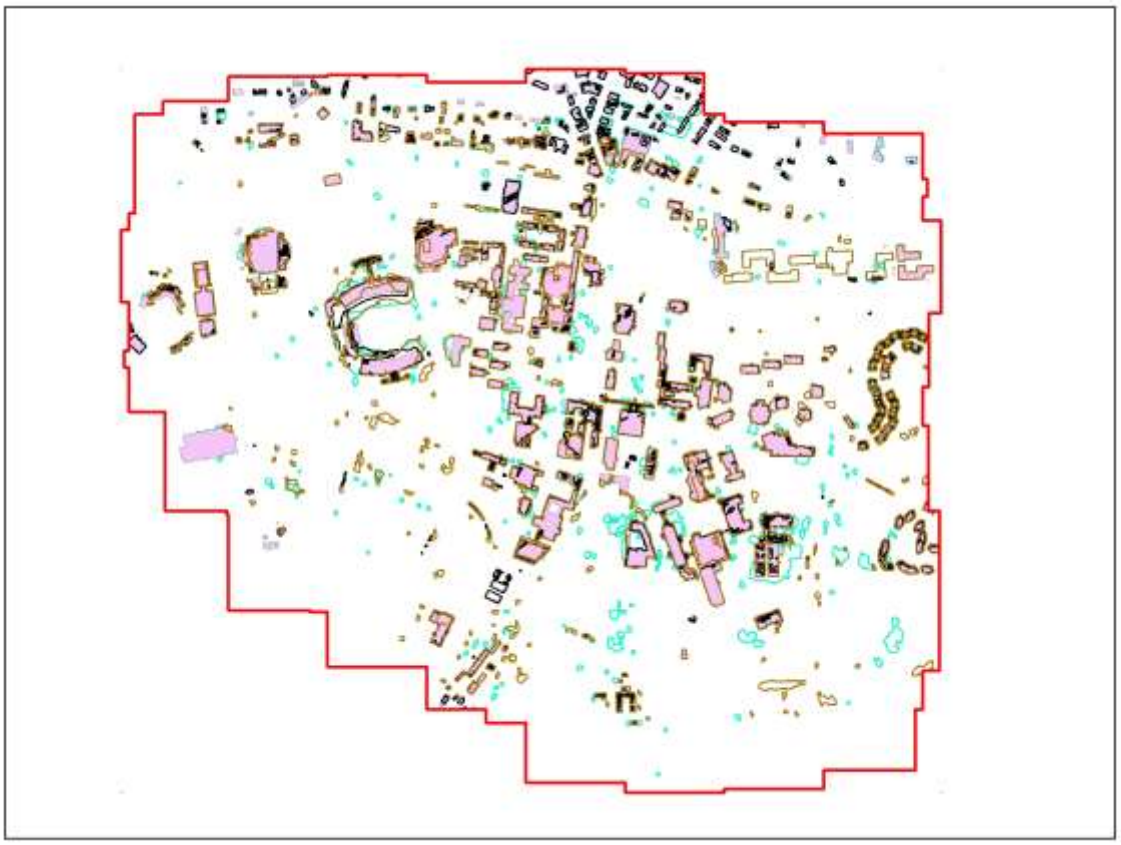

Figure 10 Comparison of building footprints generated using LASBoundary from point clouds using classified building points. Base Buildings from Pickens County GIS = Violet, Leaf Off Buildings = Brown Outline, Leaf On Buildings = Blue Outline and LiDAR Buildings = Black Outline

Table 1 Arial coverage by UAV flights during leaf on (July 8, 2017) and leaf off (March 4, 2018)

Flight	Number of photos	Date
SU01	167	7/8/2017
SU02	597	7/8/2017
SU03	628	7/8/2017
Total	1392	----------
SP01	595	3/4/2018
SP02	512	3/4/2018
SP03	579	3/4/2018
Total	1686	----------

Table 2 Total number of points stratified by point classification

	Classification							
	Unassigned	Ground	Low Vegetation	High Vegetation	Building	Total	Point Spacing (Meter)	Point Density (Sq. Meter)
Leaf Off	617,658,025	390,460,991	11,913,214	70,408,519	124,039,248	1,214,479,997	0.36	54.26
Leaf On	203,780,371	126,440,606	NA	198,440,168	64,665,116	593,326,261	0.19	53.59
LiDAR	3,275,690	20,644,186	NA	7,590,845	1,130,494	32,641,215	2.48	2.27

Table 3 Results of Near Analysis in ArcGIS showing spatial continuity between point clouds

Average Point Distance Spacing (Meter)				
	All Points	Buildings	High Vegetation	Ground
Leaf Off vs. Leaf On	0.0024	86.4900	5.1900	0.1800
Leaf On vs. LiDAR	0.0003	10.9200	3.2500	0.1100
Leaf Off vs. LiDAR	0.0005	12.7400	1.2000	0.1600

Table 4 Quantitative results of building footprints created from LASBoundary and compared with a building footprint obtained from Pickens County GIS

	Building Variation (Percent)		
	Detection Rate	Shape	Size
Leaf Off	56.53	40.42	11.08
Leaf On	55.80	39.96	10.41
LiDAR	72.09	19.48	3.01

Table 5 Results of Mean Absolute Percentage Error (MAPE) when comparing the mean values of total points in a multipoint file. Multipoint files where generated for all, ground, building and high vegetation points.

Mean Comparison Using Mean Absolute Percentage Error (100-MAPE)					
	X (%)	Y (%)	Z (%)	Min Z (%)	Max Z (%)
			All Points		
Lidar vs Leaf Off	99.817430	99.999965	93.763400	99.336580	88.838100
Lidar vs Leaf On	99.773800	99.999207	95.098321	99.969589	90.791058
Leaf Off vs Leaf On	99.956280	99.999172	98.576300	99.359800	97.801670
			Ground Points		
Lidar vs Leaf Off	99.731370	99.995591	95.675842	97.303710	94.109930
Lidar vs Leaf On	99.655680	99.996642	93.493205	95.010910	92.033263
Leaf Off vs Leaf On	99.924110	99.998949	97.718716	97.643667	97.793360
			Building Points		
Lidar vs Leaf Off	99.770720	99.998852	98.084744	99.941015	96.313417
Lidar vs Leaf On	99.743770	99.999433	97.549420	99.271690	95.905962
Leaf Off vs Leaf On	99.972990	99.998285	99.454223	99.330280	99.576949
			High Vegetation Points		
Lidar vs Leaf Off	99.854370	99.998876	93.891506	99.146844	97.740300
Lidar vs Leaf On	99.822100	99.999764	95.924919	98.960570	95.271020
Leaf Off vs Leaf On	99.968090	99.998641	97.834300	98.091130	97.585280

Table 6 Results comparing individual point values and showing that point clouds are correlated at the point to point level.

Point to Point Comparison Using Mean Absolute Percentage Error (100-MAPE)						
	N	X (%)	Y (%)	Z (%)	Min Z (%)	Max Z (%)
			All Points			
Lidar vs Leaf Off	54	99.98485	99.99960	95.34927	94.92352	94.92352
Lidar vs Leaf On	58	99.98661	99.99925	96.05436	93.54977	93.54977
Leaf Off vs Leaf On	61	99.99775	99.99985	95.02662	94.61459	94.61459
			Ground Points			
Lidar vs Leaf Off	36	99.98646	99.99887	98.54030	97.62891	97.65726
Lidar vs Leaf On	49	99.98654	99.99916	98.20544	97.44326	97.36843
Leaf Off vs Leaf On	28	99.99851	99.99989	99.75642	99.64799	99.82437
			Building Points			
Lidar vs Leaf Off	8	99.98389	99.99889	94.52220	98.63900	90.61915
Lidar vs Leaf On	5	99.98099	99.99950	95.29452	97.93526	91.44510
Leaf Off vs Leaf On	19	99.99843	99.99986	96.76570	96.80791	96.68169
			High Vegetation Points			
Lidar vs Leaf Off	10	99.99365	99.99220	95.93801	96.09030	99.11172
Lidar vs Leaf On	4	99.99854	99.99939	91.24626	99.54665	83.70602
Leaf Off vs Leaf On	14	99.99855	99.99990	96.91862	95.18560	96.48352

Table 7 Survey grade points with corresponding DEM values for each point cloud.

Point ID	Northing	Easting	Elevation (Meter)	Horizontal Precision (Meter)	Vertical Precision (Meter)	LiDAR DEM (Meter)	Leaf Off DEM (Meter)	Leaf On DEM (Meter)
51	1040850.804	1443726.654	189.360	0.011	0.018	189.224	189.494	189.281
52	1041106.747	1444315.808	200.755	0.009	0.006	201.280	201.919	201.962
80	1041204.939	1446355.138	214.034	0.010	0.017	214.019	213.785	212.813
72	1040160.581	1449121.254	236.056	0.014	0.016	237.100	236.950	236.210
73	1040328.439	1448208.417	226.499	0.010	0.017	226.219	225.601	225.743
53	1039862.235	1444955.506	196.747	0.010	0.016	197.043	196.617	196.755
54	1039523.494	1445413.246	201.774	0.012	0.021	201.648	201.275	201.461
55	1038703.690	1446121.140	191.981	0.009	0.158	192.118	191.893	191.768
56	1038323.276	1446899.012	210.391	0.011	0.019	209.961	209.975	209.730
57	1039528.338	1446814.947	223.122	0.011	0.025	223.810	223.405	223.122
58	1039064.907	1447602.716	213.572	0.012	0.023	213.046	213.347	213.486
59	1038456.756	1447435.005	201.731	0.017	0.062	201.621	201.434	201.319
63	1038666.698	1448119.667	219.498	0.013	0.026	219.928	219.659	219.042
66	1038614.698	1449483.332	216.348	0.023	0.130	215.702	215.401	212.692
68	1039397.135	1448809.822	226.156	0.198	0.290	225.883	225.479	225.429
69	1039208.663	1449635.771	229.525	0.046	0.105	229.861	229.701	229.484
70	1039846.598	1449173.449	236.785	0.017	0.033	236.801	236.467	236.061
71	1039843.966	1449792.602	238.277	0.011	0.023	237.419	237.279	236.846
81	1039843.845	1444194.417	190.576	0.009	0.016	190.400	190.243	190.252
60	1037748.614	1448084.737	218.394	0.016	0.029	218.466	218.083	217.322
61	1037748.561	1448084.756	218.396	0.014	0.026	218.466	218.082	217.322
62	1037829.756	1447721.064	210.538	0.014	0.026	211.201	210.914	210.046
64	1038071.314	1448290.667	225.005	0.008	0.015	224.984	224.689	224.401
65	1037673.239	1449031.064	217.347	0.014	0.025	216.222	215.076	215.955
67	1037856.106	1450407.347	226.503	0.009	0.015	226.367	226.082	225.969
79	1037026.064	1447743.741	212.065	0.009	0.016	212.030	210.678	209.873
Average			215.055	0.021	0.045	215.032	214.751	214.398

Table 8 Mean Absolute Percentage Error (MAPE) results comparing Actual (Survey Grade Elevation) to Observed (DEM Elevation)

Point Name	LiDAR vs. Actual (Meter)			Leaf Off vs. Actual (Meter)			Leaf On vs. Actual (Meter)		
51	0.1360171	0.0007183	0.0000005	-0.1343238	-0.0007094	0.0000005	0.0784562	0.0030175	0.0000091
52	-0.5252172	-0.0026162	0.0000068	-1.1638698	-0.0057975	0.0000336	-1.2069159	-0.0464198	0.0021548
80	0.0145676	0.0000681	0.0000000	0.2487821	0.0011623	0.0000014	1.2212296	0.0469704	0.0022062
72	-1.0436371	-0.0044211	0.0000195	-0.8942525	-0.0037883	0.0000144	-0.1538363	-0.0059168	0.0000350
73	0.2808122	0.0012398	0.0000015	0.8981497	0.0039654	0.0000157	0.7562408	0.0290862	0.0008460
53	-0.2964415	-0.0015067	0.0000023	0.1298911	0.0006602	0.0000004	-0.0085790	-0.0003300	0.0000001
54	0.1255594	0.0006223	0.0000004	0.4990339	0.0024732	0.0000061	0.3126964	0.0120268	0.0001446
55	-0.1373211	-0.0007153	0.0000005	0.0875815	0.0004562	0.0000002	0.2123458	0.0081671	0.0000667
56	0.4301578	0.0020446	0.0000042	0.4161513	0.0019780	0.0000039	0.6608333	0.0254167	0.0006460
57	-0.6884055	-0.0030853	0.0000095	-0.2824653	-0.0012660	0.0000016	-0.0003348	-0.0000129	0.0000000
58	0.5262792	0.0024642	0.0000061	0.2254668	0.0010557	0.0000011	0.0857152	0.0032967	0.0000109
59	0.1095761	0.0005432	0.0000003	0.2965225	0.0014699	0.0000022	0.4115739	0.0158298	0.0002506
63	-0.4300468	-0.0019592	0.0000038	-0.1612734	-0.0007347	0.0000005	0.4564212	0.0175547	0.0003082
66	0.6459281	0.0029856	0.0000089	0.9475587	0.0043798	0.0000192	3.6566510	0.1406404	0.0197797
68	0.2726368	0.0012055	0.0000015	0.6770263	0.0029936	0.0000090	0.7273888	0.0279765	0.0007827
69	-0.3360624	-0.0014642	0.0000021	-0.1763461	-0.0007683	0.0000006	0.0411701	0.0015835	0.0000025
70	-0.0162770	-0.0000687	0.0000000	0.3183648	0.0013445	0.0000018	0.7245596	0.0278677	0.0007766
71	0.8570734	0.0035970	0.0000129	0.9980261	0.0041885	0.0000175	1.4300981	0.0550038	0.0030254
81	0.1759982	0.0009235	0.0000009	0.3330715	0.0017477	0.0000031	0.3243902	0.0124765	0.0001557
60	-0.0722562	-0.0003309	0.0000001	0.3111353	0.0014247	0.0000020	1.0713676	0.0412064	0.0016980
61	-0.0696521	-0.0003189	0.0000001	0.3138712	0.0014372	0.0000021	1.0743068	0.0413195	0.0017073
62	-0.6627920	-0.0031481	0.0000099	-0.3760000	-0.0017859	0.0000032	0.4921921	0.0189305	0.0003584
64	0.0203659	0.0000905	0.0000000	0.3158833	0.0014039	0.0000020	0.6038809	0.0232262	0.0005395
65	1.1252492	0.0051772	0.0000268	2.2708492	0.0104480	0.0001092	1.3919782	0.0535376	0.0028663
67	0.1359073	0.0006000	0.0000004	0.4205962	0.0018569	0.0000034	0.5338499	0.0205327	0.0004216
79	0.0346517	0.0001634	0.0000000	1.3873467	0.0065421	0.0000428	2.1916415	0.0842939	0.0071055
	Total		0.0000046			0.0000114			0.0017653
	MAPE (%)		0.2140000			0.3380000			4.2020000
	100-MAPE (%)		99.786000			99.662000			95.798000

CHAPTER THREE

Forest metric extraction from photogrammetric point clouds generated from unmanned aerial vehicle (UAV) imagery

Abstract: Field data collection techniques used for forest management are time-consuming but are required for effective decision making. In recent years, remotely sensed data have been effectively used for data extraction. Currency of information and acquisition costs associated with remotely sensed data can limit their use with forest managers who rely on proven field data collection techniques. The unmanned aerial vehicle (UAV) has the potential to reduce costs and currency issues of remotely sensed data. This study examined the use of a UAV with a true color camera to collect high-resolution imagery (< 4 cm). The resulting orthorectified image was used to extract a three-dimensional point cloud. Forest metrics were extracted from the point cloud, including tree height, diameter at breast height (DBH), and canopy metrics, in a similar fashion to Light Detection and Ranging (LiDAR) data. A variety of software applications (Agisoft, ArcGIS 10.3.1, TiFFS, and LASTools) were used in the extraction process. DBH was not extracted directly from the point clouds as ordinary least squares (OLS) regression was used to develop a formula for estimating DBH (Adj. $R^2 = 0.992$). Point cloud classified ground points were used to generate a digital elevation model (DEM). This DEM was comparable to a LiDAR DEM (mean difference < 1 m). The results of this study revealed that the UAV with onboard camera is an affordable alternative to traditional field data collection methods as it provides a high-resolution

remotely sensed product that can be used to extract forest characteristics at the individual tree scale.

Keywords: aerial photography, Clemson University, DEM, diameter at breast height, GIS, LiDAR, remote sensing, tree height, UAV

1. **Introduction**

Forested lands across spatially diverse landscapes are influenced by biological and environmental conditions and are managed according to the objectives of ownership (Beach et al., 2005). Management of these landscapes reflects the quality and character of ownership's directives (Smallidge, 2004). Forest management is defined as "the practical application of biological, physical, quantitative, managerial, economic, social, and policy principles to the regeneration, management, utilization, and conservation of forests to meet specified goals and objectives while maintaining the productivity of the forests" (SAF, 2008). In 1976, the National Commission of Agriculture proposed that forest classification should be based on function (Table 1) (AgriInfo, 2011). Management strategies are based on forest function and services provided by forested landscapes, which are implemented after careful planning that ultimately leads to the implementation of effective management decisions. Planning is an essential part of forest management and contributes significantly to the decision-making process. Based on planning strategies, a forest management plan is devised to encompass seasonal needs that shape the forest to meet short- and long-term objectives (Kangas, 2005, Ryan, 2018).

Once ownership objectives and management directives are established, forest planning begins with the collection of information that will inform management decisions. Each forest stand is mapped using a combination of tools including a geographic information system (GIS), aerial photography, and global positioning system (GPS), which group areas together with similar stand characteristics such as prescription method, species, and/or age. Within these stands, field techniques are used to collect and

inventory resources such as descriptions of water, vegetation, soils, and topography (slope/aspect) along with forest metrics such as diameter, height, species type, percent forest cover, basal area, timber quantity/quality, overall health, and site index (Perez, 2012; Heilligmann, 2002; Wenger, 1984; Lund, 1989). Data gathering predominantly relies upon in situ field visits, which are costly (estimated to be 76% of total forest management cost) (Lund, 1989).

At the landscape level, meticulous in situ observations are not needed to generate an inventory of resources. Prediction models that utilize remotely sensed data can facilitate extraction of forest metrics (Hudak et al., 2013). In recent years, advancements in remote sensing techniques allow for remote capturing of field information, which has reduced costs relative to in situ field visits.

The use of aerial photography is not a new concept as it has been used to develop stand delineation maps and for digitizing visible resources. Multi-spectral (Pasquarella et al. 2018, Dalponte et al., 2018), hyperspectral (Shen, et al., 2018), and Light Detection and Ranging (LiDAR) (Lee et al., 2018) sensors can be used for forest structure and metric extraction (Skowronski, 2012; Means et al., 2000; Evans et al., 2009). The use of LiDAR has become an operative tool within forest applications, limited only by economic considerations and currency of data (Hudak et al., 2013, San Juan and Domingo-Santo, 2018). LiDAR is based on the emission of many narrow pulses of laser light each second by an optical sensor. An infinite number of light reflections from a given object return to the sensor, which records the distance between the sensor and object that ultimately results in a three-dimensional representation of the forest structure.

Definition of physical structures in this way allows for various forest metrics to be extracted, such as volume and height (Evans et al., 2009; Means et al., 2000, San Juan and Domingo-Santo, 2018). Forest structure research has shown that LiDAR is effective in estimating structural variables such as forest age (Farid et al., 2006, Rizeei et al., 2018), which strongly correlates with dominant tree height (Racine et al., 2014). LiDAR has become an operational standard within natural resource disciplines, providing a highly accurate landscape footprint that can also be utilized for spatial analysis (Evans et al., 2009).

UAVs (Figure 1) have been in use since the 1920s (Arjomandi, 2007). Previously utilized mainly within military applications, the UAV has developed into a tool used by natural resource disciplines (Merino et al., 2006, Madden et al., 2017). Recent technological advances allow UAVs to carry an array of different sensor types. Development of sensors such as true color orthophotography, hyperspectral/multi-spectral (Johnston et al., 2003), near infrared (NIR) (Hunt et al., 2010), thermal (Rudol and Doherty, 2008), and LiDAR (Wallace, 2012) allow small UAVs (< 3 kg) (Figure 1) to serve as effective tools for capturing landscape structure. UAVs have developed into an affordable solution that can offer temporal replication across various landscapes to capture high resolution (< 5 cm) remotely sensed data. Data collected by UAVs (Table 2) can be used for forest planning and decision making.

Unmanned Aerial Vehicle (UAV) systems are increasingly being used in forestry operations and are important for replacing gaps within temporal periods while remaining flexible and low cost (Tang and Shao, 2015). Forest managers can use UAVs to collect

data that can be used for time and cost savings when compared to ground GPS and standard measurement techniques. Due to rapid data acquisition and high spatial resolution data, the UAV is a useful tool for forestry applications. Forest mapping includes delineation of compartment boundaries, fire damage, weather events, forest density, stocking, harvesting among others, and can be evaluated using UAVs (Hartley, 2017). Forest structure is an important metric for foresters which is used to describe forest canopies, gather tree (individual and stand) architecture, and calculate tree volume estimates. It can effectively be collected using UAVs to a high degree of accuracy for tree heights, canopy characteristics and individual trees (Wallace et al., 2016). With increased technology available, a host of onboard sensors can be deployed on the UAV for forest monitoring (Sankey, 2017, Dash et al., 2017), biomass estimations (Pena et al., 2018), forest inventory (Goodbody et al., 2017), forest regeneration (Goodbody et al., 2018, Roder et al., 2018), topography mapping (Shidiq et al., 2017). Applications for UAVs are being discovered and developed to increase efficiency and become an effective if not a required tool for the forest manager. In addition, the UAV provides the opportunity for using sensors that previously (in traditional applications) were too costly or unattainable (Hartley, 2017).

This study examined the use of UAVs equipped with a red, green, blue (RGB) 'true color' digital camera to capture high-resolution imagery that was processed into a seamless orthorectified image. Additional processes were used to generate a three-dimensional point cloud from which forest metrics were extracted (extraction was conducted in a similar fashion to that of LiDAR data). The objectives of this study were

to: 1) develop an alternative to high-cost field forest inventories, and 2) develop models based on UAV-derived products for A) extraction of forest metrics such as tree height, DBH, and canopy metrics; and B) production of a digital elevation model (DEM) that can be used for percent canopy, slope, and aspect analysis.

2. Materials and Methods

2.1. Study area

Located in northwest South Carolina, Clemson University is situated in the southwestern corner of Pickens County. Clemson was founded in 1889 from a private gift of Thomas Clemson and was formally opened in 1893. The university's main campus covers 566 ha with an additional 12,949 ha of agriculture and forest land (Clemson, 2014). The campus is a mix of research and teaching facilities with a large core area defined as an urban forest intermixed with open areas. This study was conducted across the main campus located in Clemson, South Carolina (Figure 2).

2.2. UAV aerial imagery

Aerial photos were collected with a UAV that flew multiple missions between April and October 2014 (Table 3). Missions were planned to make efficient use of topography and photographic parameters. Designated flight lines were established utilizing both lateral and longitudinal overlap (70% and 60%, respectively). Flight parameters were managed and transferred to the UAV autopilot using Sensefly, LTD. Emotion2 software. A portable ground control station managed pre-flight and in-flight parameters via radio link to the UAV autopilot. Navigation was controlled utilizing a differential global positioning system (GPS). Autopilot settings controlled the onboard digital camera (senseFly S.O.D.A., 20 megapixel, red (660 nm), green (520 nm), blue (450 nm)) and sensor activation (12.75 x 8.5 mm (1-inch); F 2.8-11; ground resolution of 2.9 cm at 122 m). Images captured during missions were stored on a secure digital (SD)

card onboard the UAV. UAV flight altitude of 90 m was maintained to acquire image resolution of 2.6-3.6 cm. During a previous forest canopy and landscape diversity study (Anderson and Gaston, 2013) these settings were identified to achieve desired outcomes. During pre-flight planning, strategic locations were selected based on suitable topographic characteristics for landing/take off zones (minimum 10 m x 15 m). Ground control communication with the UAV was managed using a 2.4 GHz radio universal serial bus (USB) link. Using a mapping grade GPS (Trimble 7x, Accuracy: horizontal = 25 cm, vertical = 50 cm) (Trimble Inc., Sunnyvale, California), 115 ground control points (GCPs) were established to aid in spatial alignment of images. Results generated across the study area were analyzed and processed into a seamless orthorectified image.

2.3. Image processing

Individual images were removed from storage media located on the UAV. Each image was geotagged with flight log data in preparation for data processing. Flight and camera information were geotagged to each image. Proprietary software (Post Flight Suite) supplied with the UAV was used for geotagging. Camera parameters and spatial x- and y-coordinate information was added to the EXIF header on each image. Images from multiple missions flown on different days across the study area were processed using Agisoft PhotoScan Professional Edition Ver. 1.0.4 (64-bit) (Agisoft, St. Petersburg, Russia), which resulted in a seamless orthorectified image. Agisoft was then used to extract a point cloud in LASer (LAS) file format (www.asprs.org/Committeee General/LASer-Las-File-Format-Echange-Activities.html) for further analysis.

Agisoft modeling allowed for the inclusion of GCP information that aided spatial accuracy. A file containing the name, x-coordinate, y-coordinate, z-value, and horizontal/vertical precision values for each GCP was loaded into Agisoft. Using a manual process in Agisoft, the location of a given GCP identified in the UAV image was tagged with a point using the computer mouse. This point corresponded to the x, y-pixel value on the image. After all images were examined for GCP inclusion, Agisoft rectified the GCP images to their ground location. Images that did not contain a GCP were rectified to adjoining images which created geodetic correlation to ground control. Processing of UAV images in Agisoft consisted of six steps: alignment, the building of geometries, georeferencing, meshed, textured, mosaic, export of the seamless image and point cloud.

In addition to processing photogrammetry data for orthorectification, Agisoft contains functionality for determining DEM and DTM and extraction of three-dimensional point clouds. Within this study, only the point cloud extraction was utilized. The point cloud was extracted into a LAS file format. Native map projection (WGS 1984 Zone 17N) was maintained to limit transformation inaccuracies.

2.4. Tree inventory

An empty point feature class was created with a defined map projection (State Plane NAD 1983 Zone 3900 US Feet) using ArcGIS 10.2.2 software developed by Environmental Systems Research Institute, Inc. (Environmental Systems Research Institute (ESRI), Redlands, California) A heads-up digitizing technique was used to place

a point on each tree identified on the newly created image. These points represent trees identified during visual inspection using pre-identified tree maintenance zones as a guide. The completed process generated a representative tree inventory across the study area.

2.5. Field analysis

Field data collection involved visiting all identified trees within the tree inventory. Collected tree data included species, diameter at breast height (DBH), total height, and general condition. A Biltmore stick was used to measure stem diameter (Black, 2014). Tree heights were calculated using a three-point method of the Nikon Forestry Pro Model 8381 range finder. A technician obtained range measurements taken at three tree positions: eye level, base, and top of tree. These measurements were used by the range finder to calculate a tree height value. Field data were recorded by pen and paper. Key code processing in ArcGIS 10.2.2 was used to add the field data into the tree inventory feature class attribute table.

2.6. Point cloud processing

The extracted point cloud from Agisoft was processed using LASTools (rapidlasso GmbH, Gilching, Germany), and Toolbox for LiDAR Data Filtering and Forest Studies (TiFFS) (www.globalidar.com). Both software applications were developed and designed to process LiDAR data. The UAV point cloud data is similar to LiDAR data and in this study, forest metrics were extracted from the UAV point cloud

data in the same fashion used to process LiDAR data. Point cloud processing in LASTools included; map projection, tiling, ground point classification, height conversion, and high vegetation classification (Table 4). The point classification process converted the non-classified points into LAS version 1.2 specifications. TiFFS is a software that uses grid-based analysis to facilitate identification of individual trees. (Simonson et al, 2018) TiFFS was used for processing the classified point cloud, which generated tree locations (points), crowns (polygons), and statistical attributes as an ESRI shapefile.

The first step for point cloud processing with LASTools was to convert the original map projection (WGS 1984) to UTM WGS 1984 Zone 17 N. This changed the unit measurement of each point from decimal degrees to meters. LASTools are optimally utilized when LAS files contain < 15-million points. The number of points in the UAV point cloud was tiled to meet LASTools requirements for processing. LASTools contains methods that allow for batch tiling. Each tile was classified according to LAS Classifications (Table 5) following processing by a series of tools (LASGroundPro, LASHeightPro, and LASClassifyPro). Tiles were processed in an iterative manner by these tools (in the order listed above) until all tiles were completed. Using LASGroundPro, the tiles were processed to identify ground points (LAS class 2), which created a new set of tiles. These new tiles served as the input to LASHeightPro, which assigned a height value to each point, and also served as input to LASClassifyPro, in which each point was identified as high vegetation (LAS class 5), buildings (LAS class 6), or unclassified (LAS class 1). Upon completion, the resulting tiles contained points

that were classified as unclassified, ground, high vegetation, or building. Tiles generated from LASTools data processing were used as inputs to TiFFS. The TiFFS software processed the LAS tiles following the setting of model parameters by the user. TiFFS utilize an algorithm for auto-detection of points, which generates a point (trees) and polygon (crowns) feature class.

2.7. ArcGIS processing

TiFFS outputs were added to ArcGIS 10.2.2 along with the orthorectified UAV images and tree inventory feature class. The tree inventory feature class was spatially joined to the crown polygon feature class adding crown attributes to each tree. Attributes of the tree inventory feature class were modified to convert standard units to metric equivalents. These attributes included diameter (inches to centimeter) and tree height (feet to meters). DEMs were developed based on the processing of LiDAR and UAV point clouds.

Tools designed for processing LiDAR point clouds are included in ArcMap 10.3.0. These tools were utilized to develop DEM models for both LiDAR and UAV point cloud data. LAS files for LiDAR data were imported into a LASDataset. To generate a DEM, ground points (LAS class 2 - all returns) were used in the LASDataset to Raster tool. The UAV point cloud was processed in a similar fashion. Comparisons between DEMs derived from LiDAR and UAV (LiDAR – UAV) point cloud were made utilizing the Raster Calculator.

2.8. Statistical analysis

Tree heights, measured and predicted, were compared using a paired t-test. If the null hypothesis is not rejected, then it is concluded that the means are equal (i.e., tree heights are equal). Point cloud data processing did not generate diameter values directly as the functionality of this process was not a software component. To estimate diameters, an Ordinary Least Squares (OLS) regression model was created in ArcGIS 10.3.0. OLS is shown to work well with LiDAR data as a predictor in forestry applications (Hill and Mandallaz, 2018, Meng et al., 2018). OLS was chosen due to its popularity and applicability for parameter estimations (Li et al., 2014). To determine potential variables needed for regression modeling, an exploratory regression was performed in ArcGIS 10.3.0. This exploratory regression identified variables that contribute to diameter estimations that were then used in ArcGIS 10.3.0 OLS regression modeling. Based on the OLS results, a formula to estimate tree diameters was developed. DEMs developed in ArcGIS from LiDAR and UAV point clouds were compared using a paired t-test to determine equivalency.

3. Results and discussion

3.1. UAV aerial imagery

A total of 19 UAV missions were flown between July and October 2014 across the study area (Table 3). Upon completion of UAV missions, 2,164 color images were captured. The UAV was an effective solution for obtaining high-resolution aerial photographs at low altitudes and functioned reliably during missions.

3.2. Image processing

Orthorectification and mosaic rendering into a seamless image were completed in Agisoft (Figure 3). Variations in-flight parameters across flight dates resulted in tonal imbalances, excessive shading (sun-angle differences), and color inconsistencies that introduced a certain degree of visual inaccuracies. Agisoft processing was repeated with altered model parameters to limit these visual inaccuracies. GCP inclusion during processing with Agisoft, increased horizontal spatial accuracy (< ~15 cm) and is recommended for image processing.

Utilizing structure from motion (SfM), Agisoft is able to construct a three-dimensional (3D) architecture from the two-dimensional (2D) images in the form of a point cloud. The resulting point cloud yielded 1,190,594,445 points. It is important to note that Agisoft processing strained computer resources (8 core processor, 32-gb RAM); when a large number of images (>500) are processed. In future studies, resources will need to be evaluated for efficiency prior to implementation. Time to complete processing using Agisoft was four days of continuous operation.

3.3. Tree inventory

The high-resolution orthomosaic UAV image made identification of individual trees simple because each tree crown was clearly visible. The seamless image was added to ArcGIS 10.2.2 along with an empty point feature class that represented individual trees. Individual trees were identified based upon their concave form relative to one another under the mosaics oblique view (Figure 4). Relative to neighboring shadows and sun angles, crown tonal balances were lighter at higher crown positions. Crown differentiation was aided by flight parameters set to minimize sun angle effects. The concave form and tonal differences allowed for individual tree identification. Using heads-up digitizing within ArcGIS 10.2.2, a point was added for each identified tree that was assigned a unique x, y-coordinate by clicking on the tree inventory feature class with the computer mouse (Figure 5). To guide data collection, a polygon feature class representing tree management zones was added to the map. A total of 6,920 trees were identified using this method.

3.4. Field analysis

Field operations were used to visit each tree for data collection which was a time-consuming process. The time needed to collect the data both in terms of in field and from point cloud processes was evaluated. A total of 29.3 days was needed to complete field work which represents potential savings if it is possible to derive the same metrics using point cloud processing for tree inventories. At the conclusion of field inventory, all data was key coded into the inventory feature class using ArcGIS (Figure 6). Within the

6,920 trees evaluated during tree inventory, a total of 96 unique tree species were identified through field observations. Tree diversity was represented by 51 genera and 96 species.

3.5. Point cloud processing

Utilizing LASTile produced a total of 115 tiles and when generated stratified the points into manageable (in terms of point totals) tiles of data. Batch processing within LASTools was efficient and resulted in an effective way to process and classifies 3D point clouds. The result of classification shows the points stratified as follows: unassigned: 36.5%, ground: 33.2%, high vegetation: 5.8%, building: 4.4%, and never classified: 20.0%. The results (Table 7) for processing LiDAR and 3D point clouds indicate that additional research is needed to validate different classification parameters that will reduce the percentage of never classified points. The unassigned category contains classified points that do not fall within ground, building and or high vegetation classes (i.e. water, noise, rail, model key, etc.).

TiFFS filters a ground and non-ground classified point within a morphological process and with a watershed segmentation routine locates tree tops and crown boundaries (Simonson et al., 2018). The results of TiFFS processing were added to ArcMap 10.3.0. The polygon feature class represented tree crowns (Figure 7) of each tree with an attribute table containing statistical information, crown radius, crown volume, and tree heights. In contrast to the manual tree inventory method, the point feature class from TIFFS can be used for a tree inventory. In this study, the manually-derived tree

inventory was used. Further investigation is needed to optimize the points generated by TIFFS before using them as a valid tree inventory. The results were visually inspected and compared to the original tree inventory and high-resolution mosaic. In some instances, multiple tree points from the manual tree inventory were contained within a single TiFFS crown (Figure 7). Further investigation of these results is needed, but it is surmised that this result is due to dissimilarities between LiDAR and UAV point clouds, coalescing of tree species with similar heights, and detection algorithm processing. The miss-detection of the crown(s) at these locations indicates that modifications to the detection algorithm and/or model parameters are needed to accurately process UAV point clouds. The occurrence of coalesced crowns was not widespread and did not follow any spatial or topographical pattern. Multiple trees contained within a single crown polygon were removed from further analysis.

Use of TiFFS to generate forest metrics was user-friendly due to its automated processing of LAS files. Specifically, TiFFS was designed to utilize LiDAR information for forest structure analysis and is a well-known remote sensing software for forestry (Dong et al., 2018). TiFFS performed well and showed the ability to be valid software for processing 3D point clouds. In addition to point (tree) and polygon (crown) shapefiles (Dong et al., 2018), other outputs include digital elevation models (DEM), digital terrain models (DTM) (McRoberts et al., 2018, Lee et al., 2017), object height models (OHM) and ground and object LAS point clouds (Lee et al., 2017). Tree height values in the attribute table were statistically compared with tree inventory measured heights and using a paired t-test shows that both are equal ($p = 0.76$; at the level of

significance of $\alpha = 0.05$). Comparison of manual tree inventory points and TiFFS generated tree points revealed spatial differences (mean distance 6.13 m) (Figure 8). This difference is hypothesized to be a result of crown placement by detection algorithms designed for LiDAR data.

3.6. ArcGIS processing

DEM differences were not significant across the majority of the study area (Figure 9). Areas of large differences in DEM were predominantly located in areas of moderate to heavy forest canopy. When comparing classified ground points (LAS class 2), gaps in the UAV coverage where point densities are low or zero were detected. The point distributions for LiDAR (LAS class 2) ground points were evenly distributed across the study area, with clustering of UAV ground points (LAS class 2). These areas of difference were expected in areas of moderate to heavy canopy cover where LiDAR can pass through to record ground returns (Figure 10).

3.7. Statistical analysis

Statistical comparisons between measured and estimated tree heights were made. Descriptive statistics for mean, standard deviation, and N were calculated in ArcGIS 10.3.1 and were subjected to a paired t-test (GraphPad, La Jolla, CA) to determine equivalency. Trees with measured and estimated heights (11% of total inventory) were used for comparison of means. This test concluded that measured and estimated tree heights were equal ($p = 0.76$; at the level of significance of $\alpha = 0.05$).

The Zonal Statistics tool in ArcGIS 10.3.1 was used to derive descriptive statistics for both LiDAR and UAV DEMs. These statistics were used to evaluate the means within and between LiDAR and UAV DEMs. Comparison of individual DEM results revealed minimal differences in means (UAV = ±0.123 m, LiDAR = ±0.114 m). Comparison of two DEM means revealed only a slight variation (±0.175 m). A t-test (GraphPad) was conducted to compare UAV and LiDAR DEM means, which revealed the means are equal ($p = 0.058$; at the level of significance of $\alpha = 0.05$) (CI = (0.1695, 0.1750)).

Point cloud processing did not generate DBH values for inventoried trees. Instead, DBH was estimated using ArcGIS 10.3.1 regression tools. Exploratory regression was conducted to determine if independent variables contributed to DBH estimates. OLS does not require normality among dependent and independent variables (ESRI, 2015). Several independent variable candidates were chosen based upon their potential correlation to DBH: crown diameter (Gering and May, 1995; Hemery et al., 2005, Dalponte, et al., 2018), tree height (O'Brien et al., 1995; Zhang et al., 2004, Dalponte et al., 2018, Sullivan et al., 2017), tree age (O'Brien et al., 1995; Leak, 1985, Berra et al., 2017), and environmental influences (Kaufmann and Merrill, 1986; Racine et al., 2014; De Luis et al., 2009). OLS was used to estimate DBH (cm), based on tree height (m), tree age, and canopy radius (m). The results revealed that additional independent variables were needed to estimate DBH. Site Index (m) and crown diameter (m) (which replaced canopy radius (m)) were added to the model. Site index was computed, and values were added to the tree inventory attribute table. Site index curves

(Carmean et al., 1989) were referenced using the mean age and height values of specific species. If a curve did not exist for a specific species, mean age and height of a closely related species (same family) were used in a site index curve. An additional attribute was added to the tree inventory table to represent crown diameter. The values for each tree were calculated (radius x 2) using the crown radius (computed from TiFFS results). Upon determining contributory candidates, they were processed using the OLS tool.

Within forest stands as well as within other similar ecological locations, autocorrelation (i.e., spatial dependence) is present, which documents relationships between adjacent individuals across vegetative populations that have similar/dissimilar patterns (Lu, 2011; Zhang et al., 2006, Ver Planck, et al., 2018). Spatial autocorrelation was present and residual mapping did not explain the spatial anomalies (inherent or induced) (Lu, 2011). A semi-variogram was created using the Geostatistical Analyst toolset in ArcGIS 10.3.1. These conclusions did not produce conclusive anisotropy results. It was surmised that the presence of autocorrelation indicated a missing independent variable. After the inclusion of potential variables that were significant in exploratory regression, it was concluded that characteristics influencing DBH growth (either ±) were tested. A third-order undetermined complexity may be present in the model, but further research is needed to explain the autocorrelation that occurred.

Although dependent and independent variable normality was not required, the OLS results revealed complexity among candidates in which variable transformation was needed. Transformations were performed in ArcGIS 10.3.1 and included square, triple, log, log square, log triple, square log, and triple log for each independent and dependent

variable. OLS iterations were performed to evaluate various combinations between transformations. Each result was compared to previous iterations for statistical validation.

At the conclusion of model iteration, a model was selected to use for DBH estimations. The selected model had high overall performance (Adj. $R^2 = 0.992$, Akaike's Information Criterion (AICc) = -1,769.76). For independent variables, age and tree height (m) had a positive relationship to DBH while crown radius (cm) and site index (m) had a slight negative influence. All independent variables were statistically significant providing a valid relationship with DBH. All independent variables did not possess redundancy, as indicated by their variance inflation factor (VIF < 2.0). Additional statistical tests, including Joint F, Joint Wald, Koenker (BP), and Jarque Bera, were performed on the model; each test generated statistically significant results ($p < 0.01$ at the level of significance of $\alpha = 0.05$). These results indicate that the model was valid; however, a statistically significant Jarque Bera result can indicate that residuals did not follow a normal distribution, a result that was expected due to the presence of autocorrelation. Although heteroscedasticity could explain this result, it was not present in the data. The statistically significant Jarque Bera test result could also have been due to data outliers. A scatterplot graph was created using ArcGIS 10.3.1 that plotted standard residuals (Y) and predicated DBH (X) (Figure 11). This graph directly correlated with the attribute table in that the points on the graph correspond to data in the attribute table, which allowed selection of residuals and further analysis to qualify the position of the data points within the scatterplot. A group of points was selected (residual < -2) that

correspond to flowering dogwood (*Cornus florida*) (99.06%) and pecan (*Carya illinoinensis*) (0.04%). Examination of these trees revealed that the site index for flowering dogwood and the age for pecan trees were not accurate and misrepresented the trees within the model. Thus, these trees need to be re-evaluated and their values updated. The scatterplot also showed vertical and horizontal patterns within the data, which happens when values among independent and dependent variables are compared using a mix of integer and float data types. A two-tailed unpaired t-test (GraphPad https://www.graphpad.com/) was used to compare measured DBH with estimated DBH (OLS results) which show OLS derived DBH was equal to measured DBH (p-value = 0.94, at the level of significance $\alpha = 0.05$). Overall, the OLS model is statistically significant and these results can be used to construct a formula for estimating DBH, as follows:

DBH =Diameter at Breast Height (cm)
A = Log [Age]
B = Log [Site Index ^{2} (m)]
C = Log [Tree Height ^{2}(m)]
D = Log [Crown Radius ^{2} (cm)]

$$DBH = \sqrt{-\text{Log}\left[-0.05 + (1.89)(A) - (0.11)(B) + (0.003)(C) - (0.02)(D) + 1\right]} \quad (1)$$

This formula can be used to estimate DBH from these independent variables. It is important to note that independent variables (tree height and crown radius) were measured using UAV point cloud extraction methods and were not validated for applications using measurements from other methods (i.e., LiDAR or ground).

4. Conclusions

The objective of this study was to evaluate the contribution of three-dimensional point clouds generated from UAV high-resolution imagery to models used for generating DEMs, forest metrics (crown volume, crown radius, and tree height), and DBH extractions (Table 6). Although this study was conducted across an urban interface, implementation can be applied to rural forests. For a stand-level approach, identification of individual trees can enhance results by incorporation of micro-site characteristics captured at the tree level (Kaufmann and Ryan, 1986). A mix of applications (Agisoft, LASTools, ArcGIS, and TiFFS) was effective in the extraction of forest metrics. A DEM generated from a LASDataset using ArcGIS was comparable to a LiDAR DEM (mean difference < 1 m), which represents a viable alternative to the high cost and currency of LiDAR data. It is expected that further research will refine detection parameters for point cloud classification and will enhance the UAV DEM to increase its similarity to the LiDAR DEM. Forest structure (tree height, canopy metrics and DBH) can be extracted from three-dimensional point clouds and are equivalent to using LiDAR in a similar fashion. This study revealed that UAV remotely sensed data can be used for forest metric extraction and generates an accurate DEM, which can be used to provide the data required for landscape-level forest management utilizing a tree level approach.

REFERENCES

AgriInfo, 2011. My Agriculture Information Bank Website. Available online at: www.agriinfo.in/page=topic&superid=2&ropicid=1605.

Arjomandi, M. 2007. *Classification of Unmanned Aerial Vehicles*. The University of Adelaide, Australia.

Beach, Robert H., Subhrendu K. Pattanayak, Jui-Cen Yang, Brian C. Murray, Robert C. Abt. Econometric studies of non-industrial private forest management: a review and synthesis. *Forest Policy and Economics* 7(3), 261-281.

Berra, E.F., Fontana, D.C. and Kuplich, T.M., 2017. TREE AGE AS ADJUSTMENT FACTOR TO NDVI. *Revista Árvore*, 41(3), May 3,2017.

Black, Justin, 2014. Measuring Tree Volume with a Biltmore Stick. Utah State University. Available online at http://forestry.usu.edu/htm/rural-forests/forest-management/forest-timber-management/measuring-tree-volume-with-a-biltmore-stick/.

Carmean, Willard H., Jerold T. Hahn, Rodney D. Jacobs, 1989. Site Index Curves for Forest Tree Species in the Eastern United States. USDA Forest Service, North Central Forest Experiment Station. General Technical Report NC-128, published February 1, 1989. Available online at: www.2.ca.uky.edu/Forestry/FOR250/SiteIndexCurves.pdf.

Clemson, 2014. Clemson University Website History Page; http://www.clemson.edu/about/history/ About the Clemson University Land Use Property Page; http://www.clemson.edu/administration/public-affairs/landuse/about.html Graduate School Information page; http://www.grad.clemson.edu/GeneralInformation.php.

Dalponte, M., Ene, L.T., Gobakken, T., Næsset, E. and Gianelle, D., 2018. Predicting Selected Forest Stand Characteristics with Multispectral ALS Data. *Remote Sensing*, 10(4), April 10, 2018, pp.586.

Dalponte, M., Frizzera, L., Ørka, H.O., Gobakken, T., Næsset, E. and Gianelle, D., 2018. Predicting stem diameters and aboveground biomass of individual trees using remote sensing data. *Ecological indicators*, 85, February, 2018, pp.367-376.

Dash, J.P., Watt, M.S., Pearse, G.D., Heaphy, M. and Dungey, H.S., 2017. Assessing very high resolution UAV imagery for monitoring forest health during a simulated disease outbreak. *ISPRS Journal of Photogrammetry and Remote Sensing*, 131, September 2017, pp.1-14.

De Luis, Martin, Klemen Novak, Katarina Cufar and Jose Raventos, 2009. Size mediated climate-growth relationships in *Pinus halepensis* and *Pinus pinea*. Trees, 23(5): 1065-1073.

Dong, T., Zhou, Q., Gao, S. and Shen, Y., 2018. Automatic Detection of Single Trees in Airborne Laser Scanning Data through Gradient Orientation Clustering. *Forests*, 9(6), May, 2018, p.291.

Environmental Systems Resource Institute (ESRI), 2018. ESRI website. Available online at: http://www.esri.com.

Environmental Systems Resource Institute (ESRI), 2018. Online ArcGIS Resource Center. Help Desk ArcGIS version 10.6. Available online at http://desktop.arcgis.com/en/arcmap/latest/manage-data/las-dataset/what-is-lidar data-.htm.

Evans Jeffrey S., Andrew T. Hudak, Russ Faux, Alistair M.S. Smith, 2009. Discrete Lidar in Natural Resources: Recommendations for Project Planning, Data Processing, and Deliverables. *Journal of Remote Sensing*, 1, 776-794.

Farid, A., Goodrich, D.C. and Sorooshian, S., 2006. Using airborne lidar to discern age classes of cottonwood trees in a riparian area. *Western Journal of Applied Forestry*, 21(3), July 1, 2006, pp.149-158.

Gering, Lawrence R., Denise M. May, 1995. The Relationship of Diameter at Breast Height and Crown Diameter for Four Species Groups in Hardin County, Tennessee. *Southern Journal of Applied Forestry*, 19(4): 177-181.

Globalidar, 2014. TIFFS, The Lidar Information Engine. Available online at http://www.globalidar.com/Pages/default.aspx.

Goodbody, T.R., Coops, N.C., Marshall, P.L., Tompalski, P. and Crawford, P., 2017. Unmanned aerial systems for precision forest inventory purposes: A review and case study. *The Forestry Chronicle*, 93(1), March, 2017, pp.71-81.

Goodbody, T.R., Coops, N.C., Hermosilla, T., Tompalski, P. and Crawford, P., 2018. Assessing the status of forest regeneration using digital aerial photogrammetry and unmanned aerial systems. *International journal of remote sensing*, *39*(15-16), November, 2018, pp.5246-5264.

Hartley, R., 2017. Unmanned aerial vehicles in forestry-reaching for a new perspective. *New Zealand Journal of Forestry*, 62(1), May, 2017, pp.31-39.

Heilligmann, Randall B., 2002. Forest Management, Developing a Plan to Care for Your Forest. Ohio State University Extension Fact Sheet, F-34-02.

Hemery, G. E., P. S. Savill, and S. N. Pryor, 2005. Applications of the crown diameter stem diameter relationship for different species of broadleaved trees. *Forest Ecology and Management* 215(1): 285-294.

Hill, A., Buddenbaum, H. and Mandallaz, D., 2018. Combining canopy height and tree species map information for large-scale timber volume estimations under strong heterogeneity of auxiliary data and variable sample plot sizes. *European Journal of Forest Research*, August 2018, pp.1-17.

Hudak, Andrew T., A. Tod Haren, Nicholas L. Crookston, Robert J. Liebermann, and Janet L. Ohmann, 2013. Imputing Forest Structure Attributes from Stand Inventory and Remotely Sensed Data in Western Oregon, USA. *Forest Science*, 60(2): 253-269.

Hunt, E. R., Hively, W. D., Fujikawa, S. J., Linden, D. S., Daughtry, C. S., & McCarty, G. W. (2010). Acquisition of NIR-green-blue digital photographs from unmanned aircraft for crop monitoring. *Remote Sensing*, *2*(1), 290-305.

Johnston, L. F., Herwitz, S., Dunagan, S., Lobitz, B., Sullivan, D., Slye, R., 2003. Collection of Ultra High Spatial and Spectral Resolution Image Data over California Vineyards with a Small UAV. Proceedings, International Symposium on Remote Sensing of Environment, 2003. Available online at http://www.uav-applications.org/gallery/img/5.pdf .

Kangas, Jyrki, Annka Kangas, 2005. Multiple criteria decision support in forest management-he approach, methods applied, and experiences gained. *Forest Ecology and Management 207* (2005) 133-143.

Kaufmann, Merrill R. and Michael G. Ryan, 1986. Physiographic, stand and environmental effects on individual tree growth efficiency in subalpine forests. *Tree Physiology*, 2(1-2-3): 47-59.

Lee, J., Coomes, D., Schonlieb, C.B., Cai, X., Lellmann, J., Dalponte, M., Malhi, Y., Butt, N. and Morecroft, M., 2017. A graph cut approach to 3D tree delineation, using integrated airborne LiDAR and hyperspectral imagery. *arXiv preprint arXiv:1701.06715*.

Lee, J., Im, J., Kim, K. and Quackenbush, L.J., 2018. Machine Learning Approaches for Estimating Forest Stand Height Using Plot-Based Observations and Airborne LiDAR Data. *Forests*, 9(5), May 2018, p.268.

Leak, William B., 1985. *Relationships of tree age to diameter in old-growth northern hardwoods and spruce-fir*. Vol. 329. U.S. Department of Agriculture, Forest Service, Northeastern Experiment Station.

Li, M., Im, J., Quackenbush, L.J. and Liu, T., 2014. Forest biomass and carbon stock quantification using airborne LiDAR data: A case study over Huntington Wildlife Forest in the Adirondack Park. *IEEE Journal of Selected Topics in Applied Earth Observations and Remote Sensing*, 7(7), pp.3143-3156.

Lu, Junfeng, Lianjun Zhang, 2011. Modeling and Prediction of Tree Height-Diameter Relationships Using Spatial Autoregressive Models. *Forest Science*, 57(3): 252-264.

Lund, Gyde H., Charles E. Thomas, 1989. A Primer on Stand and Forest Inventory Designs. United States Department of Agriculture Forest Service, General Technical Report WO-54, September 1989.

Madden, M., Jordan, T., Cotten, D., O'Hare, N., Pasqua, A. and Bernardes, S., 2017, January. The future of unmanned aerial systems (UAS) for monitoring natural and cultural resources. In *Photogrammetric Week* (Vol. 15, pp. 369-384).

McRoberts, R.E., Chen, Q., Gormanson, D.D. and Walters, B.F., 2018. The shelf-life of airborne laser scanning data for enhancing forest inventory inferences. *Remote Sensing of Environment*, 206, March 2018,pp.254-259.

Means, Joseph E., Steven A. Acker, Brandon J. Fitt, Michael Renslow, Lisa Emerson, Chad J. Hendrix, 2000. Predicting Forest Stand Characteristics with Airborne Scanning Lidar. *Photogrammetric Engineering & Remote Sensing* Vol. 66, 11, pp. 13678-1371.

Meng, R., Dennison, P.E., Zhao, F., Shendryk, I., Rickert, A., Hanavan, R.P., Cook, B.D. and Serbin, S.P., 2018. Mapping canopy defoliation by herbivorous insects at the individual tree level using bi-temporal airborne imaging spectroscopy and LiDAR measurements. *Remote Sensing of Environment*, 215, September 2018, pp.170 183.

Merino, L., Caballero, F., Martinez-de Dios, J. R., Ferruz, J., Ollero, A. 2006. *A cooperative perception system for multiple UAVs: Application to automatic detection of forest fires.* Journal of Field Robotics, Vol. 23, Iss. 3-4, March-April 2006 pp. 165-184, Available online at http://www3.interscience.wiley.com/cgi-bin/jhome/111090262 Wiley Periodicals Inc.

O'Brien Sean T., Stephen P. Hubbell, Peter Spiro, Richard Condit and Robin B. Foster, 1995. Diameter, Height, Crown and Age Relationship in Eight Neotropical Tree Species. *Ecology*, 76(6): 1926-1939.

Pasquarella, V.J., Holden, C.E. and Woodcock, C.E., 2018. Improved mapping of forest type using spectral-temporal Landsat features. *Remote Sensing of Environment*, 210, June 2018, pp.193-207.

Peña, J.M., de Castro, A.I., Torres-Sánchez, J., Andújar, D., San Martín, C., Dorado, J., Fernández-Quintanilla, C. and López-Granados, F., 2018. Estimating tree height and biomass of a poplar plantation with image-based UAV technology. *Agriculture and Food*, Vol. 3(3), September 2018, pp. 313-326.

Perez, Dennis Lisa, 2012. Forest Management Planning. Utah State University Cooperative Extension. Fact sheet NR/FF/003 Revised.

Racine, Etienne B., Nicholas C. Coops, Benoit St-Onge, and Jean Begin, 2014. Estimating Forest Stand Age from LiDAR-Derived Predictors and Nearest Neighbor Imputation. *Forest Science*, 60(1):128-136.

Rapidlasso, 2014. Creator of LASTools for LiDAR. http://rapidlasso.com/.

Rizeei, H.M., Shafri, H.Z., Mohamoud, M.A., Pradhan, B. and Kalantar, B., 2018. Oil palm counting and age estimation from WorldView-3 imagery and LiDAR data using an integrated OBIA height model and regression analysis. *Journal of Sensors*, January, 2018, pp. 13.

Röder, M., Latifi, H., Hill, S., Wild, J., Svoboda, M., Brůna, J., Macek, M., Nováková, M.H., Gülch, E. and Heurich, M., 2018. Application of optical unmanned aerial vehicle-based imagery for the inventory of natural regeneration and standing deadwood in post-disturbed spruce forests. *International Journal of Remote Sensing*, pp.1-22.

Rudol, P., & Doherty, P., 2008. Human body detection and geolocalization for UAV search and rescue missions using color and thermal imagery. In *Aerospace Conference, 2008 IEEE* (pp. 1-8). IEEE.

Ryan, C.M., Cerveny, L.K., Robinson, T.L. and Blahna, D.J., 2018. Implementing the 2012 Forest Planning Rule: Best Available Scientific Information in Forest Planning Assessments. *Forest Science*, 64(2), March 1, 2018, pp.159-169.

San Juan, R.F.D.V. and Domingo-Santos, J.M., 2018. The Role of GIS and LIDAR as Tools for Sustainable Forest Management. *GIS-An Overview of Applications*, *1*, pp.124-148.

Sankey, T., Donager, J., McVay, J. and Sankey, J.B., 2017. UAV lidar and hyperspectral fusion for forest monitoring in the southwestern USA. *Remote Sensing of Environment*, *195*, June 2017, pp.30-43.

Shen, X., Cao, L., Chen, D., Sun, Y., Wang, G. and Ruan, H., 2018. Prediction of Forest Structural Parameters Using Airborne Full-Waveform LiDAR and Hyperspectral Data in Subtropical Forests. *Remote Sensing*, 10(11), November 2018, p.1729.

Shidiq, I.P.A., Wibowo, A., Kusratmoko, E., Indratmoko, S., Ardhianto, R. and Nugroho, B.P., 2017, December. Urban forest topographical mapping using UAV LIDAR. In *IOP Conference Series: Earth and Environmental Science* (Vol. 98, No. 1, p. 012034). IOP Publishing.

Simonson, W., Allen, H. and Coomes, D., 2018. Effect of Tree Phenology on LiDAR Measurement of Mediterranean Forest Structure. *Remote Sensing*, 10(5), April 24, 2018, p.659.

Skowronski, Nicholas S., Andrew J. Lister, 2012. The Utility of LiDAR for Large Area Forest Inventory Applications. Forest Inventory and Analysis Symposium. United States Department of Agriculture, Forest Service. General Technical Report NRS-P-105.

Smallidge, Peter, 2004. Enhancing the Stewardship of Your Forest. Chapter 8, Ownership Objectives-What you Want and Need. Cornell University, Department of Natural Resources, Cornell Cooperative Extension Publications. Available online at: www2.dnr.cornell.edu/ext/info/pubs/Stewardsjipmanual/8ManagementObjectives.pdf.

Society of American Foresters (SAF), 2008. Society of American Foresters Website. The Dictionary of Forestry. Available online at http://dictionaryofforestry.org/dict/term/forest_management.

Sullivan, F.B., Ducey, M.J., Orwig, D.A., Cook, B. and Palace, M.W., 2017. Comparison of lidar-and allometry-derived canopy height models in an eastern deciduous forest. *Forest Ecology and Management*, 406, December 2017, pp.83-94.

Tang, L. and Shao, G., 2015. Drone remote sensing for forestry research and practices. *Journal of Forestry Research*, 26(4), December 2015, pp.791-797.

Ver Planck, N.R., Finley, A.O., Kershaw Jr, J.A., Weiskittel, A.R. and Kress, M.C., 2018. Hierarchical Bayesian models for small area estimation of forest variables using LiDAR. *Remote Sensing of Environment*, 204, January 2018, pp.287-295.

Wallace, L., Lucieer, A., Malenovský, Z., Turner, D. and Vopěnka, P., 2016. Assessment of forest structure using two UAV techniques: A comparison of airborne laser scanning and structure from motion (SfM) point clouds. *Forests*, 7(3), March 2016, p.62.

Wallace, L., Lucieer, A., Watson, C., & Turner, D., 2012. Development of a UAV-LiDAR system with application to forest inventory. *Remote Sensing*, *4*(6), 1519-1543.

Wenger, Karl F., 1984. *The Forestry Handbook*. John Wiley and Sons, New York. Section 17 & 8.

Zhang, Lianjun, Huiquan Bi, Pengfei Cheng, Craig J. Davis, 2004. Modeling spatial variation in tree diameter-height relationships. *Forest Ecology and Management*, 189(1): 317-329.

APPENDIX A

Fixed Wing Swinglet Cam http://www.sensefly.com/products/swinglet-cam

Multicopter http://diydrones.com/profiles/blogs/a-newbies-guide-to-uavs

Figure 1 General classification categories of UAV's

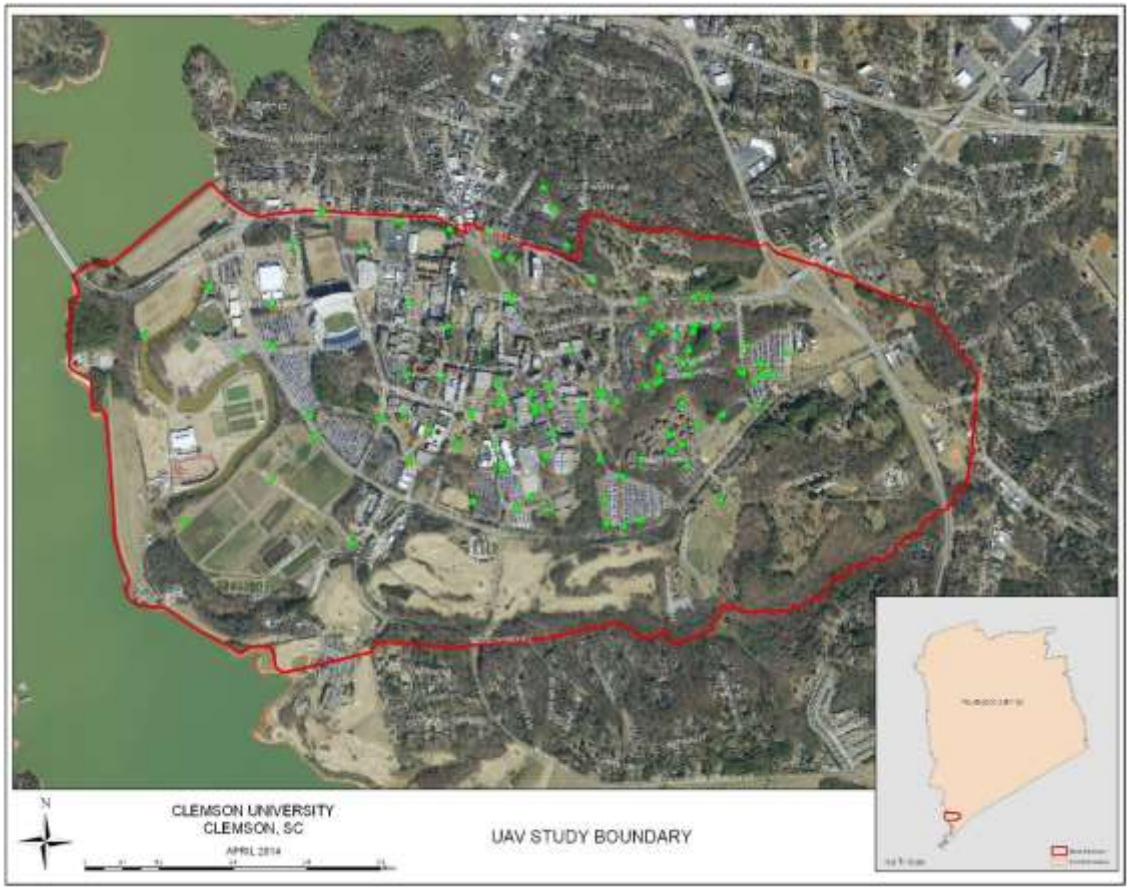

Figure 2 Study boundary used for UAV implementation to collect high resolution imagery. Green dots represent geodetic control locations used to correct image spatial inaccuracies if they exist.

Figure 3 Completed georeference mosaic of Clemson University. This seamless orthomosaic was used for point cloud extraction

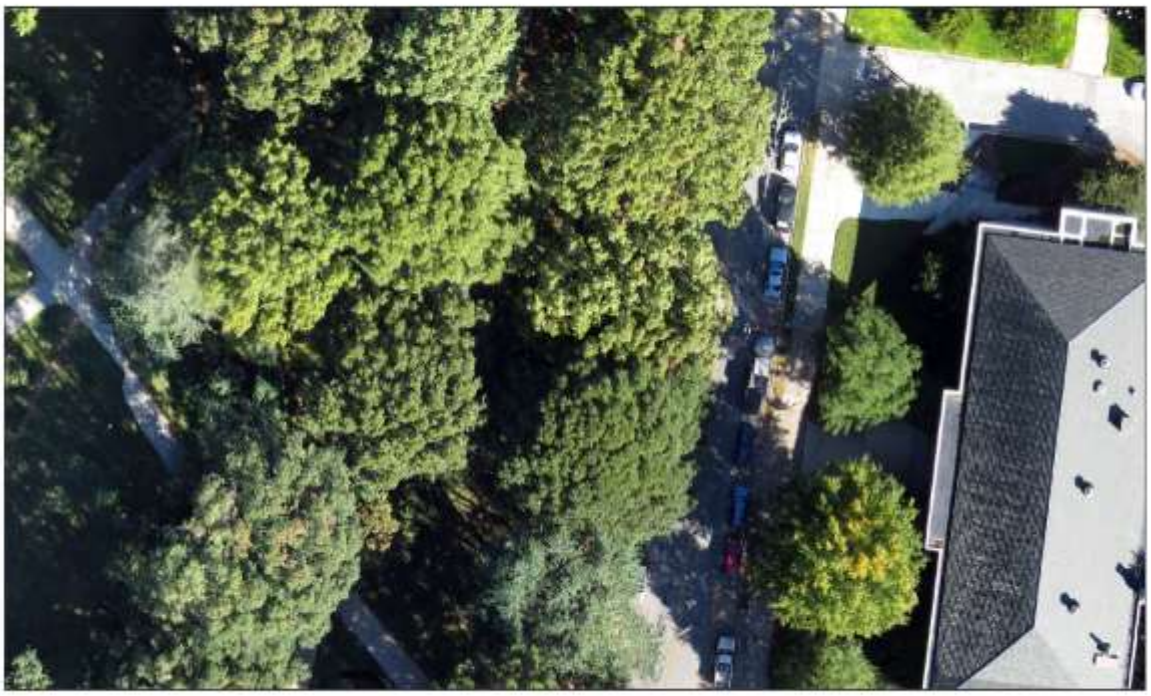

Figure 4 Isolated portion of orthorectified image showing individual trees. Note concave structure with tonal changes (light to dark) moving from crown peak to crown width.

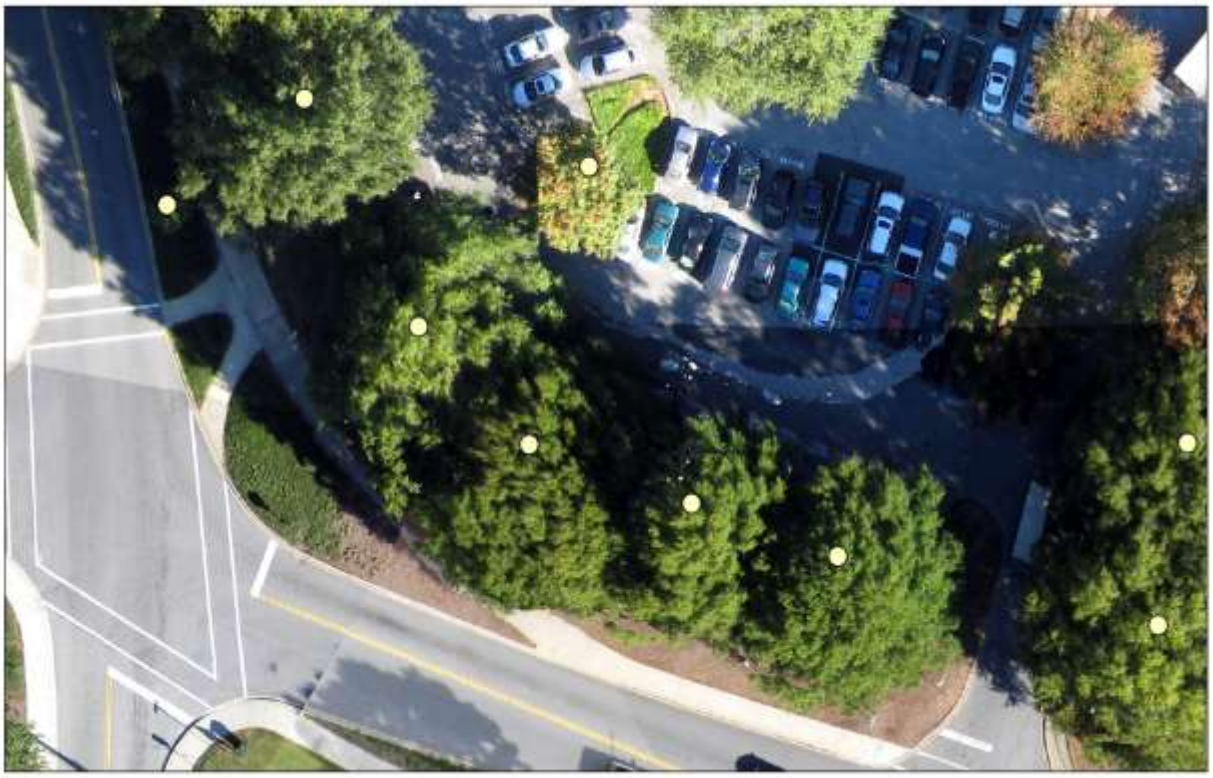

Figure 5 Tree inventory results using high resolution mosaic of Clemson campus

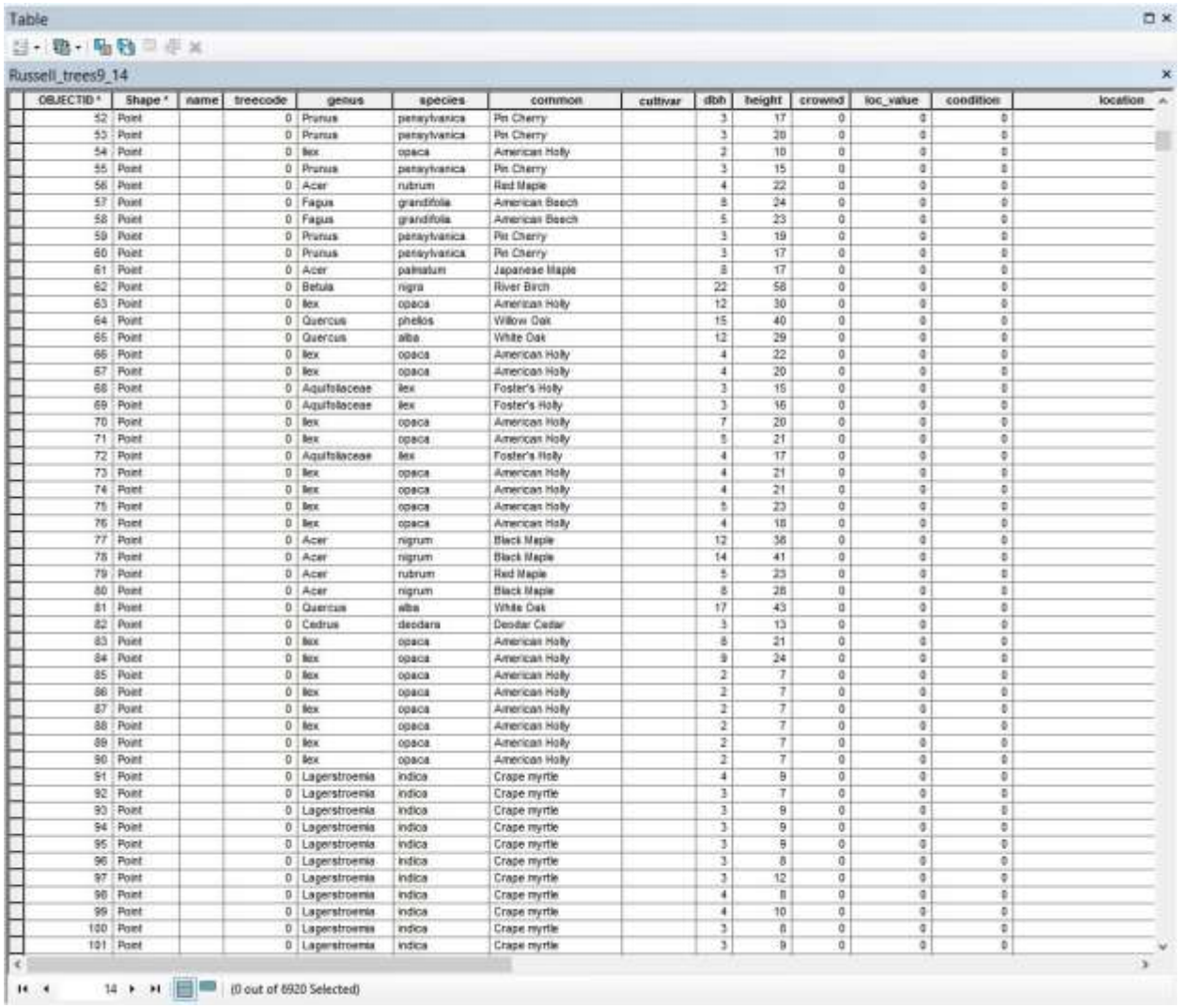

Figure 6 Screen capture of tree inventory attribute table in ArcGIS after field data was collected and key coded into the table

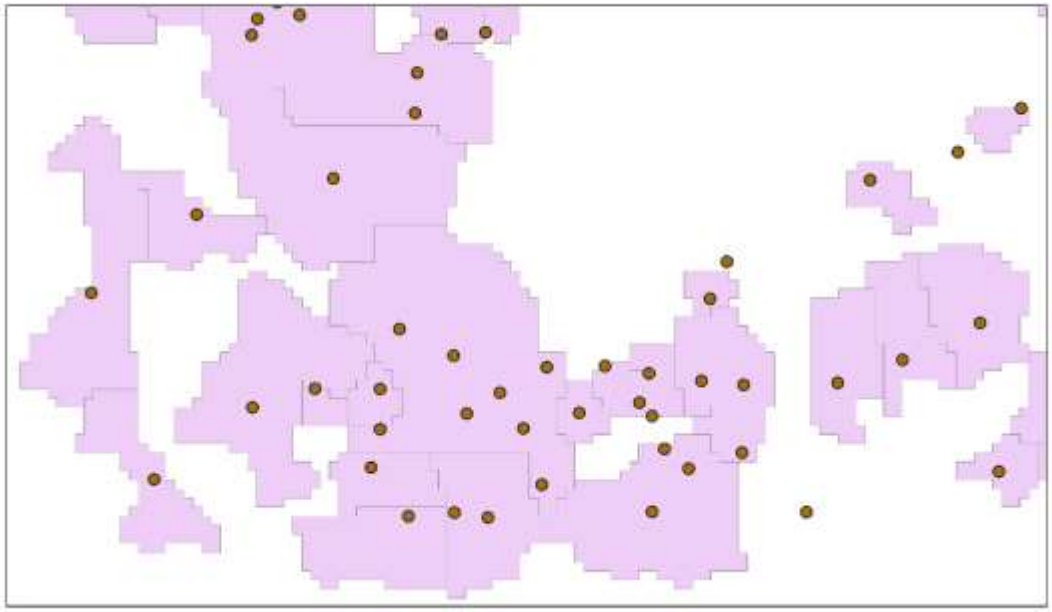

Figure 7 TiFFS crown results showing tree inventory points. Multiple trees were detected as single tree crown by the detection algorithm. Crowns = Purple, Original Tree Inventory = Brown

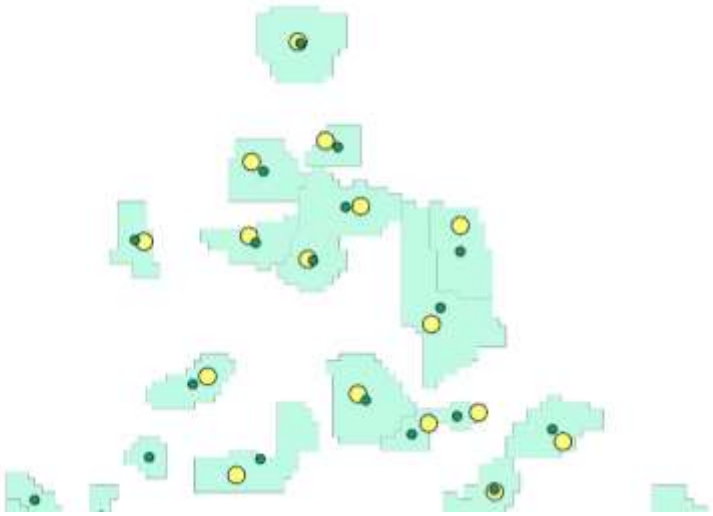

Figure 8 Crowns and tree locations generated from TiFFS. Manual tree inventory was added to show comparison of results. TiFFS Generated Crowns = Green Polygon, Manual Tree Inventory = Yellow Points, TiFFS Generated Tree Location = Dark Green Points

Figure 9 LiDAR and UAV point cloud DEM comparison results. Colored areas represent dissimilarities between derived rasters. Areas of similarity (< 1 m difference) are removed for clarity.

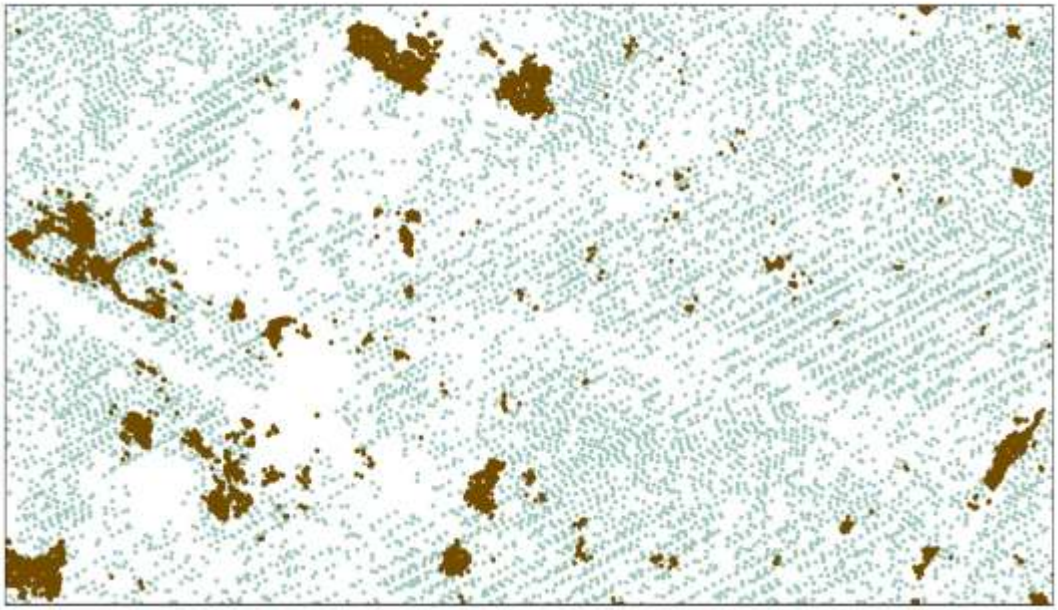

Figure 10 LiDAR and UAV ground point (LAS class 2) comparison. Areas of dissimilar point density reflect the greatest differences between respective DEM's. Green = LiDAR Ground Points, Brown = UAV Ground Points

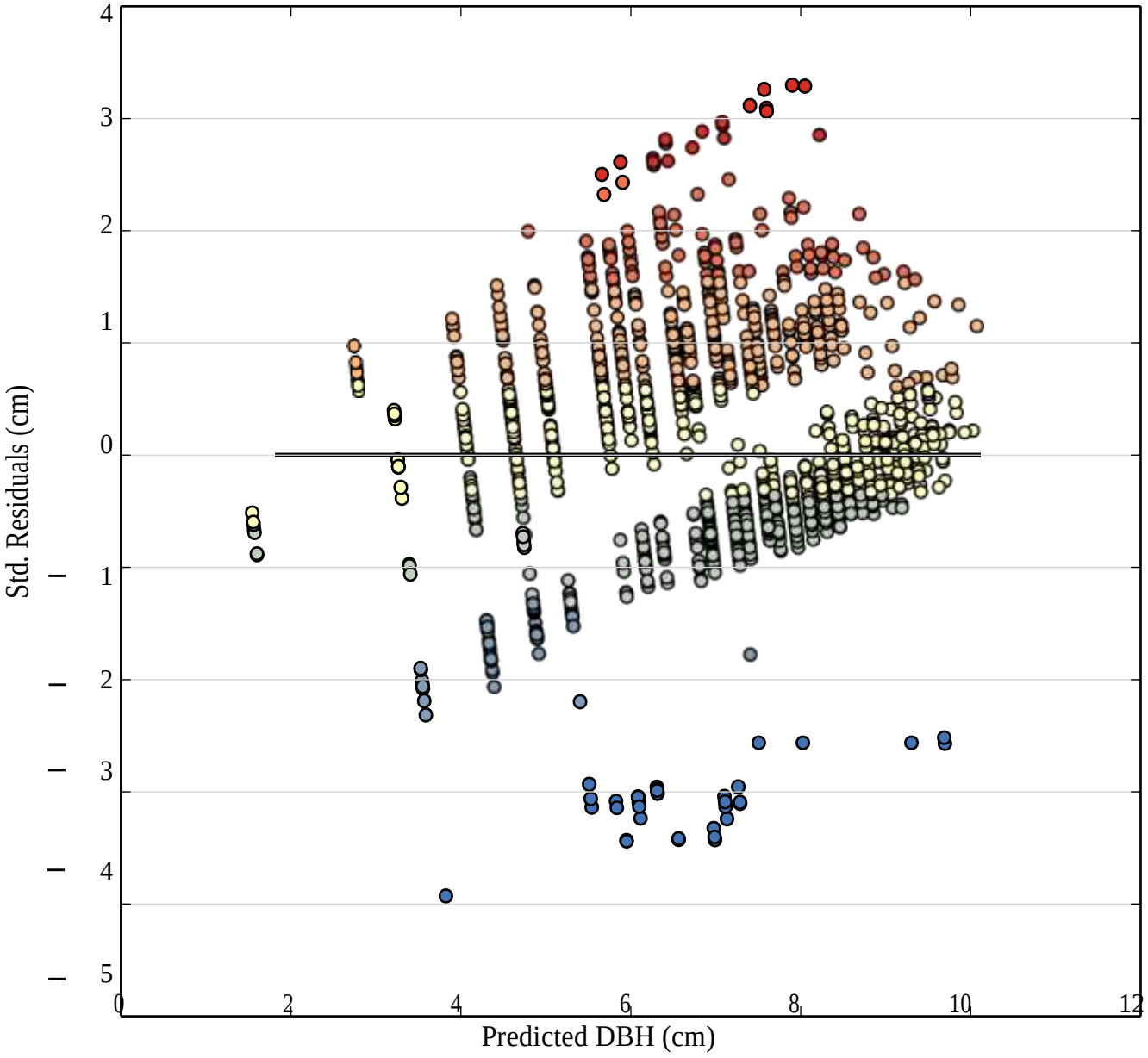

Figure 11 Using OLS results, a scatterplot created in ArcGIS 10.3.1 graphed standard residuals against predicted DBH.

Table 1 Forest classified by their function as proposed by the National Commission on Agriculture (1976).

Function	Definition
Protection Forest	Protection of the forest due to terrain instability, nature of soil, geological formations etc. Where the forest is protected to conserve other resources contained within.
Production Forest	Objective is to produce maximum quantity of forest products
A. Commercial Forestry	Maximum quantity of forest products as a business
B. Industrial Forestry	Timber production as required for industry with focus on production and economic factors
Social Forests	Forestry that meets the demands of rural and urban populations
A. Community Forestry	Forestry on lands outside conventional locations for the benefit of local communities in which the community is involved in management
B. Farm Forestry	Forestry that is integrated with other farm operations
C. Extension Forestry	Raising trees on farm lands, along sides of roads, wasteland, etc. and to maximize timber production under agroforestry
D. Agro-Forestry	A sustainable land system that combines crop, forest, and or animal production simultaneously within the same unit of land
E. Recreational Forestry	Practice of forestry with the objective for maintaining and developing forest for their scenic beauty and leisure activities

Table 2 Unmanned aerial vehicle (UAV) products related to Forestry uses

UAV products	Urban forestry uses
Color aerial photography	- Land cover/use mapping - Tree inventory - Historical documentation - Vegetation analysis (crown density) - Temporal comparison - Planning - Maintenance - Planting - Wildlife corridors - Landscape fragmentation
Near Infrared (NIR) photography	- Vegetation analysis - Tree monitoring - Vegetation health monitoring (e.g. insect/disease detection)
LiDAR	- Tree heights - Topographic analysis - Watershed analysis - Infrastructure analysis - Soil moisture, - Forest structure - Riparian analysis
DEM	- 3D modeling - Contours - Road/trail design - Slope/aspect - Elevation
Thermal imaging	- Vegetative analysis, - Insect/disease monitoring - Drought sensitivity

Note: Digital elevation model (DEM) is a product of color images and is used to support other analysis. Technology for LiDAR sensors are creating smaller packages which in time can be incorporated into a UAV platform.

Table 3 Arial coverage by UAV flights in summer of 2014

Flight	Number of photos	Date
F01	163	4/24/2014
F02	114	4/24/2014
F03	99	4/24/2014
F01	183	4/28/2014
F02	128	4/28/2014
F03	85	4/28/2014
F04	106	4/28/2014
F01	162	5/09/2014
F02	58	5/09/2014
F01	133	5/19/2014
F02	88	5/19/2014
F01	88	7/16/2014
F02	74	7/16/2014
F03	64	7/16/2014
F01	174	10/1/2014
F01	47	10/3/2014
F01	333	10/7/2014
F01	65	10/28/2014
Total	2164	----------

Table 4 Flow design of processing UAV point cloud using LASTools

Step	Input File	Tool	Output File
1	pointcloud.las	LAS2LAS	pointcloud_prj.laz
3	pointcloud_prj.laz	LASTILE	*Multiple* _temp.laz files
4	*Multiple* laz Files	LASGROUNDPRO	*Multiple* _tile_g.laz files
5	*Multiple* _tile_g.laz files	LASHEIGHTPRO	*Multiple* _temp_g_h.laz Files
6	*Multiple* _temp_g_h.laz Files	LASCLASSIFYPRO	*Multiple* _temp_g_h_c.las Files

Table 5 LAS Classification codes for LAS 1.1-1.4 specifications as defined by the American Society for Photogrammetry and Remote Sensing (ASPRS) (ESRI, 2015)

Classification Value	Meaning
0	Never Classified
1	Unassigned
2	Ground
3	Low Vegetation
4	Medium Vegetation
5	High Vegetation
6	Building
7	Low Point
8	Reserved
9	Water
10	Rail
11	Road Surface
12	Reserved
13	Wire- Guard (Shield)
14	Wire- Conductor (Phase)
15	Transmission Tower
16	Wire-Structure Connector (Insulator)
17	Bridge Deck
18	High Noise
19-63	Reserved
63-255	User Definable

					TiFFS Results									OLS Results
OBJECTID	Genus	Species	Common	Elevation	Crown Radius (cm)	Tree Height (m)	Canopy Volume (m^2)	Mean Height (m)	Standard Deviation Height (m)	Skewness Height (m)	Kurtosis Height (m)	QuadMean Height (m)	Percent Height (%)	DBH (cm)
503	Quercus	alba	White Oak	206.63	3.29	25.84	593.29	20.22	2.37	-6.38	53.10	20.88	22.48	109.22
477	Quercus	alba	White Oak	211.67	5.94	23.40	1673.14	18.51	3.24	-4.38	24.25	19.25	21.62	114.30
478	Quercus	alba	White Oak	212.35	6.96	24.09	2331.28	17.59	1.82	-7.55	68.92	18.16	18.92	91.44
476	Quercus	alba	White Oak	209.02	11.38	27.96	7957.79	18.04	7.69	-1.09	3.03	20.06	27.96	121.92
475	Quercus	alba	White Oak	209.08	4.72	27.48	900.54	24.94	0.74	-0.17	1.84	25.49	26.49	127.00
468	Lagerstroemia	indica	Crape myrtle	212.06	4.03	8.45	215.24	3.03	1.30	1.05	4.80	3.78	7.54	10.16
419	Quercus	alba	White Oak	213.80	3.34	17.12	557.63	16.24	0.48	-1.74	6.55	16.76	16.98	134.62
474	Prunus	pensylvanica	Pin Cherry	208.87	1.95	3.12	26.38	1.65	0.67	0.47	2.89	2.24	3.46	17.78
469	Lagerstroemia	indica	Crape myrtle	211.61	2.71	6.45	103.26	4.57	1.68	-1.31	3.72	5.33	7.08	10.16
467	Cupressus	x leylandii	Leyland Cypress	212.58	2.88	12.47	182.53	5.99	3.43	0.33	1.94	7.30	12.82	5.08
466	Cupressus	x leylandii	Leyland Cypress	215.25	2.46	9.57	116.65	5.66	2.65	-0.19	1.93	6.69	10.98	7.62
470	Lagerstroemia	indica	Crape myrtle	219.70	2.65	5.77	86.16	3.16	1.53	0.09	1.81	3.96	7.00	10.16
471	Lagerstroemia	indica	Crape myrtle	217.76	2.46	6.31	84.63	3.33	1.81	0.08	1.61	4.25	6.92	10.16
465	Cupressus	x leylandii	Leyland Cypress	208.27	2.88	5.35	93.42	2.92	1.13	-0.09	2.15	3.61	5.57	12.70
524	Quercus	palustris	Pin Oak	204.17	2.76	9.95	102.64	4.97	3.67	-0.04	1.28	6.59	10.40	30.48
658	Quercus	alba	White Oak	202.96	3.24	8.31	169.71	5.20	1.65	-1.01	4.06	5.89	8.08	20.32
659	Quercus	palustris	Pin Oak	203.08	4.48	15.02	511.72	10.43	3.21	-0.67	3.17	11.39	15.54	35.56
351	Ulmus	parvifolia	Chinese Elm	203.17	3.48	7.57	173.36	5.79	1.05	-3.05	14.08	6.46	6.95	17.78
352	Ulmus	parvifolia	Chinese Elm	203.07	3.39	7.33	192.16	5.95	1.35	-3.19	12.67	6.61	7.11	17.78

Table 6 A portion of the tree inventory attribute table after joining: digital elevation model (DEM), tree heights, canopy metrics and diameter at breast height (DBH) results from point cloud data extraction using Toolbox for LiDAR Data Filtering and Forest Studies (TiFFS) and ArcGIS Ordinary Least Squares (OLS) regression processes

	Classification					
	Unassigned	Ground	High Vegetation	Building	Never Classified	Total
3D Point Cloud	434,964,534	395,227,776	69,570,766	52,712,480	238,118,889	1,190,594,445
LiDAR	10,350,419	61,368,599	29,192,217	1,861,121	0	102,772,356

Table 7 Point count after classification processing was completed using LASTools

Glossary

Agisoft:

a commercial based 3D reconstruction software that uses digital photos. The professional edition allows authoring of geographic information system (GIS) data to produce seamless imagery and 3D point clouds

ArcGIS:

a commercial based geographic information system (GIS) developed by Environmental Systems Research Institute

Autonomous:

operation of a UAV by onboard computer or ground based pilot by remote control

Canopy:

uppermost layer of the forest formed by tree crowns

Canopy Height Model (CHM):

raster based model representing the canopy elevation of the forest and or trees

Diameter at Breast Height (DBH):

measurement location to obtain tree diameter usually at 4.5’ off the ground

Digital Elevation Model (DEM):

raster based model representing ground or surface elevations

Digital Terrain Model (DTM):

raster based model representing vegetation height elevations

Geodetic Control Point (GCP):

global positioning system (GPS) derived point that can be used to accurately position non-spatially referenced geographic data by serving as reference object that can be tied to its complimentary location in geographic data

Geographic Information System (GIS):

a computer based software that captures, manages, analyzes, edits and displays geographic data

Geotagging:

process of adding geographic metadata to photographs or imagery

Global Positioning System (GPS):

satellite based navigation system that provides locational information

Ground Control Station:

facilities and computer hardware that maintains human control over unmanned aerial vehicles during flight

Heads-Up-Digitizing:

GIS process for creating feature objects from data (i.e. imagery) displayed on a computer screen

Hyperspectral:

imaging technique that collects data by scanning objects across the electromagnetic spectrum using three techniques: scanning spatial images, sequential capture of full spectral data, or capture spatial and spectral data at the same time

Imagery:

images representing spatial objects on the earth's surface

LASTools:

toolset developed by Martin Isenburg for LiDAR las formatted data. Can be used through DOS command window and as a toolkit or pipeline in ArcGIS

Light Detection and Ranging (LiDAR):

remote sensing technique that uses a laser to measure distance by analyzing reflected light of a laser illuminated object on the earth

Log ASCII Standard (LAS):

standard file format for exchanging LiDAR data

Mosaic:

process of creating a single image from a collection of images

Multi-Spectral:

process of capturing image data at specific frequencies of the electromagnetic spectrum

Multi-Temporal:

data that contains information which spans across different time ranges i.e. multiply years

Near Infrared (NIR):

image data collected in the near infrared region of the electromagnetic spectrum this is closest to the radiation detected by the human eye

Orthomosaic:

combination of orthorectification and mosaicing to create a rectified image with limited distortion to form a single image from a collection of images

Orthorectification :

process of correcting imagery distortion by using based data such as elevation along with camera metadata to match map projection

Photogrammetry:

the scientific process(s) of developing measurements from photographs

Point Cloud:

consists of data points referenced to a coordinate system so that each point contains a value for the x, y, and z

Random Access Memory (RAM):

a type of computer data storage for accessing and writing data at the same speed regardless of the order it is accessed

Spatialtemporal:

term used to describe spatial data over a period of time

Structured Query Language (SQL):

programming language used to managing data within a relational database

Toolbox for LiDAR Data Filtering and Forest Studies (TiFFS):

commercial based computer software for automatic viewing and analysis of LiDAR point clouds

Urban Forest:

a collection of trees or forest stands within a city, town or suburb

Unmanned Aerial Vehicle (UAV):

term used to describe a remotely operated airborne vehicle that is flown in absence of a human pilot

Unmanned Aerial System (UAS):

ground control equipment, communication system and other support equipment including the unmanned aerial vehicle to maintain flight mission objectives

X,Y:

coordinate pair point representing values of a map projection that spatially locates an object on the earth's surface

Z-Value:

spatial value of a map projection that represents elevation of a located object

Flow Diagram for LASTool Batch Processing

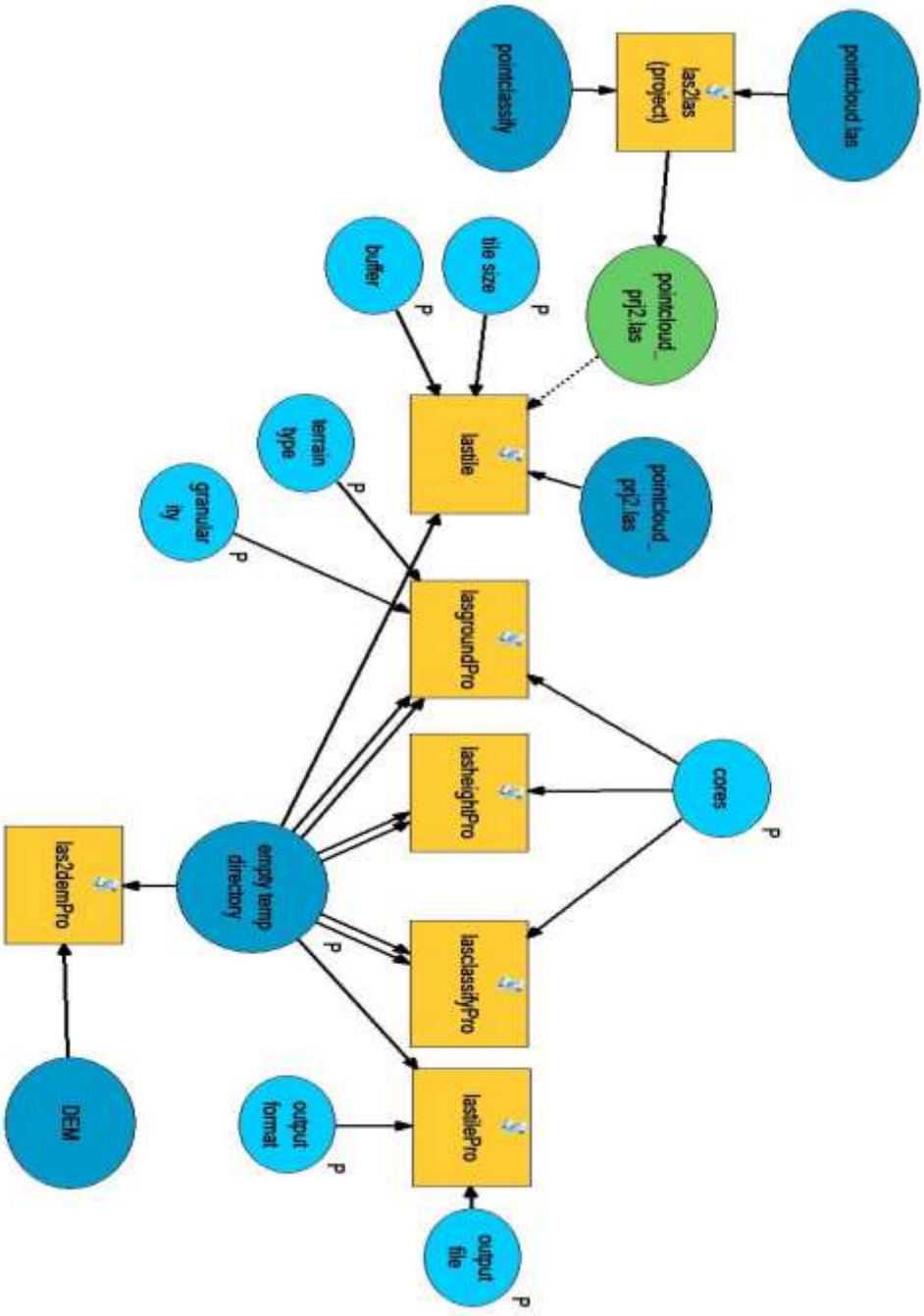

CHAPTER FOUR

Identifying Forest Tree Species using Object-Based Image Analysis (OBIA) of Unmanned Aerial Vehicle Imagery (UAV)

Abstract: Remotely sensed data performs an important role in modeling large ecological areas with a high degree of detail to aid natural resource decisions. However, collection of remotely sensed products can have temporal and economical limitations. This can be overcome by the use of unmanned aerial vehicles (UAV) that allow multi-temporal flights which are reliable and economical. Photogrammetry analysis has often relied upon classification processes to extract information such as forest metrics, land cover, and buildings. UAV ultra-high-resolution imagery can improve photogrammetry analysis. Processing of ultra-high-resolution data uses a different approach than traditional methods. Object Based Image Analysis (OBIA) goes beyond traditional pixel levels and groups similar pixels into objects. These objects can then be classified by supervised processes such as Random Forest (RF) to label these objects based upon ground-verified data. This work used R-Studio to develop a hybrid approach (OBIA and RF) for classifying individual trees at the genus/species level. This process was successful in classifying tree species within an urban forest landscape (93.4%). These results demonstrate that the UAV is an economically effective tool for data collection and that

the hybrid model can be applied within a forested landscape to delineate individual trees by species.

Keywords: aerial photography, Clemson University, OBIA, GIS, random forest, tree classification, UAV

1. Introduction

Remotely sensed products have been used extensively by natural resource disciplines in a variety of applications. (Madden et al., 2017) Spatial, environmental, and ecosystem derived analyses, among others, depend upon remote sensing products. Image resolution refers to the raster cell size (width and height) and/or the total number of image pixels. The larger the cell size, the courser the resolution and the smaller the cell size, the higher the resolution, which yields more detailed information (Microbus, 2015). Analyses that use remotely sensed data are typically conducted at the pixel level. These pixels are similar in size to that of objects detected within the data (Blaschike et al., 2012). Spatial and temporal analysis was performed at the pixel or spectral level and was limited to course resolutions. Pixel-based analysis ignores shape, location, and neighbor association (Addink, 2010). Technology improvements in sensor and data acquisition techniques resulted in smaller pixels with higher resolution (< 1 m). Analysis approaches using these highly detailed products began to branch utilize algorithms for feature extraction. Features were designated as objects (i.e., grouping of similar pixels) that are characterized by their spectral, spatial, and neighborhood relationships. The process of image segmentation (i.e., feature extraction of objects) began in the 1970s and slowly changed the paradigm of feature extraction. Object Based Image Analysis (OBIA) (i.e., image segmentation) is now commonly used for high resolution analysis (Blaschike, 2010, Chen et al., 2018, Ye et al., 2018).

Human perception of image-based features is mimicked by OBIA which allows the computer to recognize these features and group pixels into objects through image

segmentation. (Gustafson et al., 2018) The object-based approach has overtaken traditional pixel by pixel analysis. (Chen and Weng, 2018) There are both strengths and weakness to the OBIA approach (Table 1), which is the logical choice for multispectral high-resolution imagery analysis (Hay and Castilla, 2006). Image segmentation can be implemented through algorithmic methods, each having unique importance. (Chen and Weng, 2018) The separation of objects from each other and from background environment is the result of image processing through segmentation. (Craciun et al., 2018) Two general approaches for method classification are local and global segmentation using region-based, edge-based, and watershed approaches (Kaur and Kaur, 2014). The mean shift segmentation algorithm is a local region-based segmentation method utilized for multi-resolution color images in vegetation classification (Zheng et al., 2009; Ferraz et al., 2012). Having a good performance reputation for unsupervised clustering, the mean shift algorithm can be used with a comprehensive group of images. (Craciun et al., 2018) The mean shift approach analyzes the mean pixel value along a moving window to determine pixel clusters. The window recalculates the mean at each iteration and decides which clusters should be bound together to form an object that exhibits certain shape, spectral, and spatial characteristics (Esri, 2018). The mean shift is a non-parametric density function (introduced by Fukunaga and Hostetler in 1975 (Fukunaga and Hostetler, 1975)) that uses the nearest neighbor and kernel approach of pattern recognition to cluster pixels. (Ming, et al., 2012, Wu et al., 2018)

Classification of remotely sensed data results in the labeling of objects that mirrors their on-ground counterparts. Different types of classification methods are

available, and each has its own degree of accuracy. Classification methods rely upon an algorithmic process to assess spectral similarities and to cluster pixels into classes of objects. (Hasmadi et al., 2017) The algorithm is based on user-defined characteristics, performance, and measurements of accuracy (Pal and Mather, 2003). Classification can be divided into two distinct groups: supervised and unsupervised. (Hasmadi et al., 2017) Supervised classification uses sets of training data that represent specific classes of objects that define how pixels are labeled. These training data are integrated into the algorithm that in turn classifies pixels based upon their similarity to the training data. Conversely, unsupervised classification does not use training data and the outcomes are based upon algorithm analysis to determine group labels and to classify pixels to represent ground objects (Extension, 2017). The maximum likelihood classifier (MLC) is a supervised classification algorithm that is widely used in remote sensing. The MLC is based on the Gaussian probability density function and uses class statistics from training samples (Foody et al., 1992). Random Forest (RF) is a classification process that is an improvement over MLC when classifying high resolution imagery (Fredl, 1997, Feng et al., 2015). RF uses a collection of decision trees to produce accurate classification results of multi-dimensional remotely sensed data. (Belgiu and Dragut, 2016) Bagging or boosting is used within RF to improve accuracy. Boosting is a weighting function while bagging or bootstrapping performs classification using a regression (i.e., decision) tree. A random set of data are selected with or without replacement and a decision tree is formed. Multiple iterations of bootstrap decision trees are performed in which nodes are split from a random set of predictors. A random selection of variables occurs at each

split in the tree to minimize correlations. RF is not influenced by noise nor does it result in overtraining, whereas boosting can overtrain the data due to weighting effects (Gislason et al., 2006; Liaw and Wiener, 2002, Zabihi et al., 2016).

The use of unmanned aerial vehicles (UAVs) (Figure 1) is widely used by natural resources disciplines. (Madden et al., 2017, Hogan et al., 2017) UAVs provide low cost and flexible technology that generates ultra-high-resolution imagery (< 5 cm) (Merino et al., 2006; Tang, 2015). The UAV can carry different sensor types: true color (Milas et al., 2017), hyperspectral/multispectral (Johnston et al., 2003, Shen, et al., 2018, Pasquarella et al. 2018, Dalponte et al., 2018), thermal (Rudol and Doherty, 2008), LiDAR (Wallace, 2012, Lee et al., 2018), and near infrared (Hunt et al., 2010, Zhu et al., 2018). Within forestry, these sensors can be used for: biomass estimations (Pena et al., 2018), forest regeneration (Goodbody et al., 2018, Roder et al., 2018), forest inventory (Goodbody et al., 2017), topography mapping (Shidiq et al., 2017) and forest monitoring (Sankey, 2017, Dash et al., 2017) The UAV becomes an opportunity for the forest manager to utilize sensor technology previously inaccessible or too costly within traditional deployments. (Hartley, 2017)

The use of UAVs for mapping forest structure and complicated landscapes (e.g., urban forests) is cost-efficient and the collected data provides necessary detail for object extraction (Feng et al., 2015). Forest structure is an integral aspect to the forest manager. Structure describes the architecture and forest canopy in addition to providing data regarding tree heights, canopy characteristics and placement of individual trees (tree inventory) just to name a few. The UAV is very capable tool for obtaining the data

needed to extract this information for the forest manager. (Wallace et al., 2016) Traditional remote sensing methods have long been utilized by natural resource communities. Since its introduction, the use of UAVs for remote sensing–along with sensor advancements–offers an economical and efficient alternative to traditional methods (Colomina and Molina, 2014).

Remotely sensed data within natural resources can become inadequate due to temporal inconsistencies while UAV systems are becoming increasingly popular within forestry applications supplanting temporal shortages. The UAV provides flexibility within data collections while remaining low cost. (Tang and Shao, 2015, Liebermann et al., 2018) Forestry applications benefit from low turnaround time to collect data over large areas. Not only is time and costs savings realized, high spatial resolutions accompany UAV remotely sensed products. UAV applications are becoming a basic tool for the forest manager and as new purposes are developed will be a fundamental necessity. (Hartley, 2017)

Forest exist across spatially diverse landscapes that results in complex properties residing within remotely sensed data. Extraction of objects from remote data requires object-based analysis in conjunction with point cloud data for object extraction. Forest landscapes are stratified for modeling predictions using object-oriented classifications. (Gonzalez et al., 2018, Ruiz et al., 2018) Utilizing UAV derived high resolution imagery (and corresponding SfM point cloud), utilizes and necessitates the combination of OBIA and RF analysis for high accuracy results (when compared to pixel-pixel analysis). (Liu and Abd-Elraman, 2018, Franklin and Ahmed, 2017) Not just in forestry but within

natural systems across many spatial environments, changes occur both from natural and anthropogenic causes. The UAV is a capable tool to capture high resolution data to enrich datasets with accuracy to meet specific needs to help understand these complex dynamic changes. Utilization of high-resolution imagery within advanced image analysis processes is becoming the trend for obtaining beneficial knowledge leading to more efficient and sound management decisions. (Fraser and Congalton, 2018)

Within natural resource disciplines, decisions are based on in situ data collection methods that provide information critical to the decision-making process. Forest managers use in situ visits as the primary method of data collection which are costly and time consuming. (Lund, 1989, Gonzalez et al., 2018). Recent advances in remote sensing provide a way to capture forest stand level data. Light Imaging Detection and Ranging (LiDAR) can be used to estimate vertical forest structures (Marino et al., 2018), define forest characteristics such as; stand volume (Yoga et al., 2018), canopy metrics (Simonson et al., 2018), basal area (Stovall and Shugart, 2018), and biomass. (Jeronimo et al., 2018) In addition, this information can be used for habitat mapping (Guo et al., 2018, Campbell et al., 2018, Garabedian et al., 2018), wildlife management (Dubayah, 2000; Lim, 2003), and land cover classification (Ekhtari et al., 2018, Huo et al., 2018). High resolution imagery (< 1 m) provides added accuracy when delineating landscape level results (i.e., forests, pasture, crops, buildings). In forest management, in situ operations define not only forest stands but also collect the composition of tree species. High resolution images generated by new sensor technology combined with UAVs raises the possibility that this technology can be used to detect and classify species of trees. The

objectives of this study were to: 1) utilize UAV systems to capture ultra-high resolution imagery, 2) determine image segmentation that can be effectively used in a classification model, and 3) develop a hybrid classification model based on OBIA and RF to delineate tree species for urban and traditional forest management.

2. Materials and Methods

2.1. Study Area

Clemson University campus has an array of research and teaching facilities across 566 ha. The core area of campus contains an urban forest embedded with the facilities that support students, faculty, and staff. Clemson opened in 1893 based on a private gift from Thomas Clemson. Clemson University is located at the southern end of Pickens County that is in the northwest corner of South Carolina. In addition to the core campus, Clemson utilizes an additional 12,949 ha of forested and agriculture land for research. The study area for this work covered the core campus of Clemson University in Clemson, South Carolina (Figure 2) (Clemson, 2014). Within the study area, a sub-sample area was used to improve efficiency and to limit stress on computer resources during processing.

2.2. UAV Aerial Imagery

Ultra-high resolution imagery was collected using an eBee UAV (senseFly, Cheseaux-sur-Lausanne, Switzerland) with onboard digital camera (senseFly S.O.D.A., 20 MP, red (660 nm), green (520 nm), blue (450 nm)) and sensor activation (12.75 x 8.5 mm (1-inch), F 2.8-11, ground resolution of 2.9 cm at 122 m), and differential GPS for navigation. In flight controls and camera activation were managed by onboard autopilot. Multiple missions were flown on July 8, 2017 between the hours of 10 AM and 2 PM. Flight parameters were designated during pre-flight planning and then transferred into the Emotion3 flight software. Flight lines were designated with a lateral and longitudinal overlaps of 70% and 60%, respectively. Flight control was managed with a portable

ground control station. Flight parameters were transferred by radio link to the autopilot onboard the UAV. Landing/take off zones that adhered to topographic and photographic requirements were designated prior to take off. Ground control points (GCP) were established across the Clemson campus. A mapping grade global positioning system (GPS) (Trimble 7x, Accuracy: horizontal = 25 cm, vertical = 50 cm), was used to collect 102 locations that were used during orthorectification to aid in horizontal control.

2.3. Image Processing

After each UAV flight, images were removed from the secure digital card and transferred to a computer for processing. Camera and spatial information were tagged to each image's exchangeable image file (EXIF) header. Parameters for orthorectification were designated using Agisoft PhotoScan Professional Edition Ver. 1.3 (64-bit) (Agisoft, St. Petersburg, Russia). After loading the images, a six-step process was used to process the images, which included alignment, building geometries, georeferencing (i.e., GCP inclusion), mesh, texture, mosaic, export of the seamless image, and point cloud extraction. GCPs were incorporated into the process to improve the horizontal accuracy of the resulting image. A text file was generated in ArcGIS 10.5.0 from the GCP feature class and was formatted to the Agisoft schema. A manual process was implemented in Agisoft to progress through each GCP. As a GCP is selected, the corresponding image (i.e., the image containing the GCP) appears in the console. The user selects each image, locates the GCP, and, if needed, moves the GCP to match its location on the image. This

process is repeated along each image before moving to the next GCP and repeating this same manual process.

2.4. Data Collection

The characteristics displayed when adding the new UAV mosaic image to ArcGIS allowed for visual identification of individual trees. Heads up digitizing was used in ArcGIS 10.3.0 software ((Environmental Systems Research Institute (ESRI), Redlands, California) (ESRI, 2016). An empty point feature class was established using Universal Transverse Mercator (UTM) NAD 1983 Zone 17N meters projection to record digitized points that represent trees found on the UAV image. Using heads up digitizing techniques, a new point was placed on each tree object found on the image. This identification process relied upon tree crown structures and spectral changes that occurred while viewing from the nadir perspective. Crown tonal balances at the higher positions (exposed to greater sunlight) were lighter than shadows cast by interior branches, leaves, and adjacent crowns. UAV pre-flight discussions focused on flight patterns (image overlap, time of day, weather) that would aid in crown isolation. Along with these tonal effects, the concave structure of tree crowns simplified visual identification. To aid in tree inventory, campus management zones were added as a polygon feature class to the map. Upon completion of the tree inventory, attributes were added and populated with the spatial position (x, y) of each tree.

In situ data collection followed tree inventory. Field observations were made at each tree to collect DBH, total height, species, and general condition. A Biltmore stick was used to capture DBH by measuring the tree stem at 1.4 m above the ground (Black,

2014). Tree heights were measured using a three-point method with a Nikon Forestry Pro Model 8381(Nikon Inc., USA Headquarters: Melville, NY) range finder. This three-point method involved taking range finder measurements of the stem at eye level, the base of the tree, and the top of the tree. Based on these three measurements, the range finder internally computed the total height of the tree. All field collected data were recorded by pen and paper and were added to the tree inventory feature class using key coding methods in ArcMap 10.3.0.

2.5. ArcGIS processing

The mean shift segmentation tool of ESRI's ArcGIS (version 10.5.0) was utilized to pre-process UAV imagery. This tool uses a window that moves across an image to iteratively look at three key properties: spectral detail, spatial detail, and minimum segment size. User input varies the characterization of each property to define objects. Once window processing initiates, average pixel values are computed to determine the object for pixel grouping. This process is calculated for each band within the input image. The completed multi-spectral object segmented image was used within the species classification model. This image was divided using three methods: random, vertical, and horizontal. Each division was then subdivided into three zones; each zone (total of 9) was utilized within the classification model. Training samples were generated using ArcMap 10.5.0 from the tree inventory point feature class. A buffer (1 m) was generated around each tree point that produced a polygon feature class that was used in R-Studio (Boston, MA) classification model. After the buffer was created, a spatial join was utilized to add the attribute(s) of each tree to the buffer. In addition, an attribute field

(TreeID) was created and populated that associated the common tree species name to a number for raster processing in R-Studio.

2.6. R processing

R-Studio was used to build the species classification model. This integrated development environment (IDE) allows for direct code execution along with a console that can utilize additional tools within its syntax editor. R is a programming language utilized in statistical computing. Two versions of R are available: commercial and free open source, both of which can be run on Windows, macOS and Linux. Packages, written by R community users, increase the dimensionality and applicability of R to many innovative research initiatives. Combinations of these packages, along with included sets of tools, allows R to be productive and robust (R, 2017). The free open source version was used in this study. The species classification model took advantage of classification and statistical packages to produce a hybrid model (OBIA and supervised classification) for identifying and validating the composition of tree species across the study area. The model used training samples and segmented imagery representing a subsample of the study area. For each segmented image and associated training sample, individual classification models were constructed and implemented using R-studio.

2.7. Statistical Analysis

During the execution of the tree species classification model in R-Studio, several statistical libraries were employed for validation and model tuning. The RF classification

algorithm was implemented using defined parameters. Tuning parameters were determined to identify the number of bootstraps needed, based on error rates. Graphs were generated to evaluate each classification error to determine how many bootstrap trees were needed at a specific error return. To determine classification and miss-classification results, a confusion matrix was constructed for each class. Overall model validation was performed by calculating a kappa value and confidence intervals. A final validation was performed in which the model was repeated against the un-used bootstrap data. An Out of Bag (OOB) error was generated to examine the effectiveness of the model against this sample for model validation. The OOB represents the misclassification rate that was applied to the leftover data sample. A smaller OOB rate indicates a better model. To further stress and validate the model, ArcGIS 10.5.0 was used to sub-divided the study sample into three equal parts (total of nine): random, vertical, and horizontal sub-divisions. The model was iterated across each and results were exported to a working directory.

3. Results and Discussion

3.1. UAV Aerial Imagery

A total of three eBee UAV flights were conducted within the study area on July 8, 2017 between the hours of 10 AM and 2 PM that captured ultra-high-resolution true color images across the study boundary (Figure 2). Following pre-flight preparations, the UAV was launched and a total of 1,392 images were collected during the three flights (Table 2). Images with resolutions of 2.4-3.5 cm were captured at an altitude of 118.8 m. These parameters and image resolutions were based on a previous forest canopy and landscape diversity study (Anderson and Gaston, 2013). Autonomous take-offs and landings were completed in open landing zones (minimum 10 m x 15 m) with communication between the UAV and ground control mediated by a 2.4 GHz radio universal serial bus (USB) link. The UAV did not encounter any issues during flight and provided an economical and effective alternative for capturing true color images as compared to traditional methods.

3.2. Image Processing

Using Agisoft, orthorectification was completed to result in a seamless image for the mission flown on July 8, 2017. Inclusion of GCPs within the orthomosaic process resulted in increased horizontal accuracies (< 15 cm) and is necessary for UAV image processing. The resulting seamless orthomosaic image (Figure 3) is a four-band image with a resolution of 4.1 cm.

3.3. Data Collection

Utilizing the high-resolution seamless image trees were identified by tonal signatures and structure of their crowns. This tree inventory was beneficial to assisting in situ field data collection. Field data collection was implemented, and data was transferred to computer via key coding. This manual operation was evaluated in terms of time between collection methods; in field and point cloud processing. A realized savings (~29 days) was found by using point cloud processing for field inventories. Tree inventory resulted with a total of 6,920 trees in the study area. These results contained 96 unique tree species spread across 51 genera. There was a total of 39 unique tree species representing a total of 332 trees (Table 3) distributed across the sub-sample boundary used for hybrid model analysis.

3.4. ArcGIS Processing

ArcGIS 10.5.0 was used in several applications to prepare data for the classification model. The large file size of the original mosaic image could not be processed due to limited computer resources (Two Xeon Processors (8 Core Each) Duel Thread (Total 32 Threads), 96 Gb Random Access Memory (RAM), Nvidia GeForce GTX 10 Series Video Card). Data was extracted for subsequent processing from a subset of the study area. In ArcMap, a polygon feature class was created to represent the study area (Figure 4). This polygon feature class was used to clip both the orthomosaic and training sample data. To stress and validate the classification model, the original

subsample was divided into random, vertical, and horizontal sub-divisions (Figure 5) and data were extracted using the same clip technique for each of the sub-divisions.

OBIA modeling required a segmented image. Several segmentation routines are available to prepare the image for processing, including watershed (Yang et al., 2017), mean shift (Ellis and Mathews, 2018), K-means (Niedzielski et al., 2017), normalized graph, interactive, and maximized clustering (Liu et al., 2012). The mean shift segmentation was selected based on its characteristics for remote sensing applications relative to the other techniques (Mohan and Leela, 2013, Maschler et al., 2018, Ellis and Mathews, 2018, Silalahi et al., 2018). Several commercial and open source applications are available for mean shift segmentation: QGIS (www.qgis.org/en/site), SAGA (www.saga-gis.org/en/index.html), GRASS (https://grass.osgeo.org), Orfeo (www.orfeo-toolbox.org), ArcGIS (www.ESRI.com), and Ecognition (http://www.ecognition.com). Several of these applications were used to determine the best segmented image for species classification. Some of the applications (QGIS, SAGA and GRASS) produced a single band output while ArcGIS and Ecognition produced a three-band image. Ecognition is robust and relevant, however the user needs aptitude with the software before use. ArcGIS contained useful parameters for mean shift implementation and was executed directly from a tool menu. The mean shift results from ArcGIS (Figure 5) were selected for use within the classification model.

3.5. R processing

The hybrid classification model (Appendix A) was developed in blocks to differentiate the model implementation steps. These blocks of code include library designation, loading data, data preparation, tuning, RF classification, model validation, predictions, and exporting results. Code was also added to aid with model efficiency and to take advantage of parallel computer processing. Upon completion of code, development debugging was completed, and trials were executed. These trials offered insight into tool and model efficiency.

Single band segmented images (SAGA, ORFEO, QGIS) did not produce quality results (OOB mean error of 17.89%). It was decided to use a multi-band segmented image as input for the model. The multi-band segmented image improved the results significantly (61.5% improvement) as compared to the model classification results generated with the single band segmented image. These results support the use of ultra-high-resolution images captured by UAV along with RF to classify trees based on genus and species.

To further extend and validate the multiband results, additional model iterations were performed. To stress the model, the sub-sample boundary was divided (Figure 5) to determine how the model would perform. The results were similar across each sub-division with the exception of Random Sec 2 and Horizontal Sec 0 (Table 4), which had a 40.9% and 37.9% higher OOB error, respectively. The classification model was used to test possible explanations for these results. In ArcMap 10.5.0, training samples that intersected between both sub-divisions were selected and used to create a new feature

class. Intersected training samples were selected based upon the assumption that the high OOBs occurred at the same location within both sub-divisions. Each sub-division segmented image along with this training sample was input into the classification model and executed. Both results show that Foster's Holly (*Aquifoliaceae ilex*, TreeID 11) was misclassified as Crepe Myrtle (*Lagerstroemia indica*, TreeID 6). The model also indicated that the reverse (Crepe Myrtle classified as Foster's Holly) was not true, indicating an accurate species classification of Crepe Myrtle. Additional research is needed to determine the cause of this misclassification, but it is surmised that canopy structure and training sample size (buffer radius too large or small) are possible causes.

3.6. Statistical Analysis

Random Forest uses a decision tree process and averaging to determine object or pixel classification. Using RF has been proven highly effective for classification of high-resolution imagery from UAV acquisitions. (de Castro, et al., 2018) The RF method allows the model to assemble the combination of all trees rather than individual parts of the decision tree. The RF can grow a significant number of models with averaged outcomes or voted on to find the best model for classification of each species. (Melville et al., 2018, Berhane et al., 2018) RF can grow each tree as far as possible; however, a source of randomness is needed to make each tree unique. There are two ways to achieve randomness. Bagging or bootstrapping takes a randomized sample with replacement. Approximately one-third of the sampled data is omitted when bootstrapping. (Teluguntla et al., 2018) Evolution of decision tree growth (Figure 6) differs slightly when a different

sample set for each tree is used. Strong variables will still dominate the first decision in most tree results (Stephens, 2016). Using tuning methods, a graph was generated to determine the total number of trees (ntree variable) (Figure 7). From this graph, error rates for each class flatten out past 50 trees except for one class that begins to diminish at 200 trees, resulting in an ntree of 200. OOB error rates are at their lowest rate of return at approximately 60 trees, and then begin to stabilize at 200 trees.

A second randomness application is using only a subset of available variables. By default, the number of variables is the square root of the total. (Berhane et al., 2018) The selection of variables changes for each node in the decision tree to allow for additional randomness. This number can be manually set by the user using the mtry parameter. The current model is based on a three-band segmented image, resulting in three variables. Reduction of mtry reduces correlation and strength; conversely increases of mtry result in increased correlation and strength. The square root default limited the overall effectiveness of the model and a decision was made to use all variables, resulting in mtry being set to three. Randomness in the RF decision tree generates a collection of unique trees, with each collection classified differently. From the culmination of unique trees, votes are tallied and used to determine classification assignments. This modeling system avoids over-fitting by growing a multitude of trees where mistakes are averaged across the results (Stephens, 2016).

R-Studio code was used to generate a graph (Figure 8) that was used to determine variable importance. This graph shows the mean decrease in accuracy and the mean decrease Gini. (Berhane et al., 2018) The order of each variable in terms of importance

is from the top down (most important to least important). The mean decrease in accuracy was due to the exclusion of a variable during OOB error calculations. The graph shows that band 3 is more important than band 2 and band 1. The mean decrease in Gini refers to a coefficient that measures how each variable affects the homogeneity of nodes and leaves in the decision tree. This coefficient measures variable importance as compared to the impurity index at each tree node. These results reveal band 2 is more heterogeneous than band 1 and band 3 (Cutler et al., 2007; ListenData, 2017; Rodriguez-Galiano et al., 2012).

At the completion of RF classification, a confusion matrix was code generated in R-Studio. A matrix table was constructed and used to describe classification model performance. (Teluguntla et al., 2018) Objects at specific locations were classified and accuracy was assessed based on how well the objects were correctly classified. Comparisons of the classified objects vs. known classifications were made within a confusion matrix, with informative and analytical descriptions used to encapsulate accuracy (Lewis and Brown, 2001). The confusion matrix further dissected accuracy across individual classes to indicate model success (Story and Congalton, 1986). A confusion matrix (Table 5) was constructed during each model iteration to validate both model and class accuracy.

Analytical measurements were calculated from the confusion matrix to describe the results of each tree species classification (Table 6). Accuracy (AC), recall (true positive rate TP), false positive rate (FP), true negative rate (TN), false negative rate

(FN), precision (P), specificity, sensitivity, and F-Score are measurements derived from the confusion matrix. Explanations of these measurements can be illustrated, where:

A is the number of correct predictions that are negative

B is the number of incorrect predictions that are positive

C is the number of incorrect predictions that are negative

D is the number of correct predictions that are positive

$$AC = A + D / A + B + C + D \quad (1)$$

$$TP = D / C+D \quad (2)$$

$$FP = B / A + B \quad (3)$$

$$TN = A / A + B \quad (4)$$

$$FN = C / C + D \quad (5)$$

$$P = D / B + D \quad (6)$$

Specificity identifies the probability that the results are true negatives. Higher specificity values identify classifications that are not misclassified. Sensitivity is the probability that results are true positives. Higher sensitivity values identify classifications that are classified correctly (Cutler et al., 2007, Ohsaki et al, 2017). Precision or confidence is the positive predictive value representing the proportion of predicted positive results that are positive. To compare precision and sensitivity, the harmonic average is calculated to formulate the F-Score. The F-Score yields a summary of both metrics (precision and sensitivity) as a single value for evaluation (Ericson and Rohm, 2017). In addition to individual class measurements, model measurements were calculated (Table 4), including Kappa, model accuracy, confidence interval (CI), OOB, and p-value. Kappa measures

how well RF classified results as compared to training samples. Kappa indicates how well the classification model performed, which represents the expected model and classification accuracy.

Model summaries (Table 4) had an OOB average (5.7% - 7.98%) that was consistent with whole model results (6.88%) across the sub-sample divisions. Model accuracies (92.0% - 94.3%) also exhibited a close relationship to the results generated from the whole segmented image (93.1%), with small confidence interval ranges. P-values and sub-division Kappa values (90.6% - 93.5%) were also consistent with whole classification (92.5%) results. The whole segmented image model results indicate a close relationship among sub-division iterations. Sub-division results generated from stressing the classification model show consistency to the model when applied to the whole segmented image, for qualitative and quantitative validation of the tree classification process.

Using a sample boundary to execute the R classification model showed good performance in the identification of tree species. Applying stress to the model with implementation across sub-sample boundaries produced similar results. Although computer resource limitations required sample parameters, these results indicate that the model should perform well across the larger study area. UAV ultra-high-resolution images showed greater detail across multiple bands, resulting in increased classification accuracy (as compared to single band segmentation).

4. Conclusions

The objectives of this research were to evaluate the use of a UAV system to capture ultra-high-resolution images for use in a hybrid tree species classification model for individual tree identification. The images were useful when converted to multi-band segmented images then analyzed by both the OBIA and RF classifier. Multi-band segmented images provided a 61.5% improvement in tree species classification compared to single band segmented images. Tree species classification was executed using a combination of open source and commercial software applications. ArcGIS was effective in using the mean shift algorithm to produce a segmented three band image for data preparation. R-studio provided an effective and flexible environment to develop a hybrid (OBIA and supervised classification) model with statistical validation. These results showed model efficiency within the urban forest and the model is expected to perform equally well in traditional forest applications. Further research is needed to identify why two trees (Crepe Myrtle and Fosters Holly) were misclassified and to apply the model against a spatially discrete set of tree species. Overall results from this study showed that ultra-high-resolution images along with a hybrid approach (OBIA and RF classifier) was effective (mean accuracy 94.3%) in identifying individual tree species down to the genus/species taxonomic level.

REFERENCES

Addink, Elisabeth, 2010. Object-based Image Analysis. GIM International published online, 1/28/2010. https://www.gim-international.com/content/article/object-based-image-analysis.

Anderson, Karen, Kevin J. Gaston, 2013. Lightweight unmanned aerial vehicles will revolutionize spatial ecology. *Frontiers in Ecology and the Environment.* Vol. 11, Issue 3, April 2013, pg. 138-146.

Belgiu, M. and Drăguţ, L., 2016. Random forest in remote sensing: A review of applications and future directions. *ISPRS Journal of Photogrammetry and Remote Sensing*, 114, April, 2016,pp.24-31.

Berhane, T.M., Lane, C.R., Wu, Q., Autrey, B.C., Anenkhonov, O.A., Chepinoga, V.V. and Liu, H., 2018. Decision-Tree, Rule-Based, and Random Forest Classification of High-Resolution Multispectral Imagery for Wetland Mapping and Inventory. *Remote Sensing*, 10(4), April, 2018, p.580.

Black, Justin, 2014. Measuring Tree Volume with a Biltmore Stick. Utah State University. Available online at http://forestry.usu.edu/htm/rural-forests/forest-management/forest-timber-management/measuring-tree-volume-with-a-biltmore-stick/ .

Campbell, M.J., Dennison, P.E., Hudak, A.T., Parham, L.M. and Butler, B.W., 2018. Quantifying understory vegetation density using small-footprint airborne lidar. *Remote Sensing of Environment*, *215*, pp.330-342.

de Castro, A.I., Torres-Sánchez, J., Peña, J.M., Jiménez-Brenes, F.M., Csillik, O. and López-Granados, F., 2018. An automatic random forest-obia algorithm for early weed mapping between and within crop rows using UAV imagery. *Remote Sensing*, 10(2), April, 208, p.285.

Chen, G. and Weng, Q., 2018. Special issue: Remote sensing of our changing landscapes with Geographic Object-based Image Analysis (GEOBIA). *GISScience and Remote Sensing*,Vol. 55 No. 7, Febuary 9, 2018, pp. 155-158.

Chen, G., Weng, Q., Hay, G.J. and He, Y., 2018. Geographic object-based image analysis (GEOBIA): emerging trends and future opportunities. *GIScience & Remote Sensing*, 55(2), January 2018, pp.159-182.

Clemson, 2014. Clemson University Website History Page; http://www.clemson.edu/about/history/ About the Clemson University Land Use Property Page; http://www.clemson.edu/administration/public-affairs/landuse/about.html Graduate School Information page; http://www.grad.clemson.edu/GeneralInformation.php.

Colomina, I, P. Molina, 2014. Unmanned aerial systems for photogrammetry and remote sensing: A review. *ISPRS Journal of Photogrammetry and Remote Sensing.* Vol. 92, June 2014, pg. 79-97.

Craciun, S., Kirchgessner, R., George, A.D., Lam, H. and Principe, J.C., 2018. A real-time, power-efficient architecture for mean-shift image segmentation. *Journal of Real-Time Image Processing*, 14(2), February, 2018, pp.379-394.

Cutler, Richard D., Thomas C. Edwards Jr., Karen H. Beard, Adele Cutler, Kyle T. Hess, Jacob Gibson, Joshua J. Lawler, 2007. Random Forests for Classification in Ecology. *Ecology* Vol. 88(11), 2007, pg. 2783-2792.

Dalponte, M., Frizzera, L., Ørka, H.O., Gobakken, T., Næsset, E. and Gianelle, D., 2018. Predicting stem diameters and aboveground biomass of individual trees using remote sensing data. *Ecological indicators*, 85, February, 2018, pp.367-376.

Dubayah, Ralph, Jason B. Drake, 2000. Lidar Remote Sensing for Forestry. *Journal of Forestry.* Vol. 98, No. 6, June 2000, pg. 44-46.

Ekhtari, N., Glennie, C. and Fernandez-Diaz, J.C., 2018. Classification of Airborne Multispectral Lidar Point Clouds for Land Cover Mapping. *IEEE Journal of Selected Topics in Applied Earth Observations and Remote Sensing*, Vol. 11 (6), June 2018, pp. 2068-2078.

Ellis, E.A. and Mathews, A.J., 2018. Object-based delineation of urban tree canopy: assessing change in Oklahoma City, 2006–2013. *Computers, Environment and Urban Systems*, Vol. 73, January 2019, pp. 85-94.

Environmental Systems Resource Institute (ESRI), 2016. Online ArcGIS Resource Center. Help Desk ArcGIS version 10.5. Available online at http://desktop.arcgis.com/en/arcmap/latest/manage-data/raster-and images/segment-mean-shift-function.htm.

Ericson, Gary, William Anton Rohm, 2017. How to evaluate model performance in Azure Machine Learning. Microsoft Azure website, https://docs.microsoft.com/en-us/azure/machine-learning/studio/evaluate-model-performance.

Extension, 2017. What's the difference between a supervised and unsupervised image classification? USDA Extension Newsletter. October 17, 2013. Can be found online at: https://articles.extension.org/pages/40214/whats-the-difference-between-a-supervised-and-unsupervised-image-classification.

Feng, Quanlong, Jiantao Liu, Jianhua Gong, 2015. UAV Remote Sensing for Urban Vegetation Mapping Using Random Forest and Texture Analysis. *Remote Sensing.* 7(10), pg. 1074-1094.

Ferraz, Antonio, Frederic Bretar, Stephane Jacquemoud, Gil Goncalves, Luisa Pereira, Margarida Tome, Paula Soares, 2012. 3-D mapping of multi-layered Mediterranean forest using ALS data. *Remote Sensing of Environment.* Vol. 121, June 2012, pg. 210-233.

Fraser, B. and Congalton, R., 2018. Issues in Unmanned Aerial Systems (UAS) Data Collection of Complex Forest Environments. *Remote Sensing*, 10(6), June 2018, p.908.

Friedl, M. A., C. E. Brodley, 1997. Decision tree classification of land cover from remotely sensed data. *Remote Sensing of Environment.* Vol. 61, Issue 3, September 1997, pg 399-409.

Foody, G. M., N. A. Campbell, N. M. Trodd, T. F. Wood, 1992. Derivation and Applications of Probabilistic Measures of Class Membership from the Maximum-Likelihood Classification. *Photogrammetric Engineering & Remote Sensing.* American Society for Photogrammetry and Remote Sensing, Vol. 58, No. 9, September 1992, pg 1335-1341.

Franklin, S.E. and Ahmed, O.S., 2017. Deciduous tree species classification using object based analysis and machine learning with unmanned aerial vehicle multispectral data. *International Journal of Remote Sensing*, 39(15-16), August 10, 2017, pp.5236-5245.

Fukunaga, K., L. Hostetler, 1975. The estimation of the gradient of a density function, with applications in pattern recognition. *IEEE Transactions on Information Theory.* Vol. 21, Issue 1, January 1975.

Garabedian, J.E., Moorman, C.E., Peterson, M.N. and Kilgo, J.C., 2018. Relative importance of social factors, conspecific density, and forest structure on space use by the endangered Red-cockaded Woodpecker: A new consideration for habitat restoration. *The Condor*, *120*(2), pp.305-318.

Gislason, Pall Oskar, Jon Atli Benediktsson, Johannes R. Sveinsson, 2006. Random Forests for land cover classification. *Pattern Recognition Letters.* Vol. 27, Issue 4, March 2006, pg. 294-300.

Guo, X., Coops, N.C., Gergel, S.E., Bater, C.W., Nielsen, S.E., Stadt, J.J. and Drever, M., 2018. Integrating airborne lidar and satellite imagery to model habitat connectivity dynamics for spatial conservation prioritization. *Landscape Ecology*, 33(3), January 20, 2018. pp.491-511.

Gustafson, K.B., Coates, P.S., Roth, C.L., Chenaille, M.P., Ricca, M.A., Sanchez Chopitea, E. and Casazza, M.L., 2018. Using object-based image analysis to conduct high-resolution conifer extraction at regional spatial scales. *International Journal of Applied Earth Observation and Geoinformation*, 73, December, 2018, pp.148-155.

Hasmadi, M., Pakhriazad, H.Z. and Shahrin, M.F., 2017. Evaluating supervised and unsupervised techniques for land cover mapping using remote sensing data. *Geografia-Malaysian Journal of Society and Space*, *5*(1).

Hay, G. J., G. Castilla, 2006. Object-Based Image Analysis: Strengths, Weaknesses, Opportunities and Threats (SWOT). In *Proc. 1st Int. Conf. OBIA* (pp. 4-5).

Hogan, S., Kelly, M., Stark, B. and Chen, Y., 2017. Unmanned aerial systems for agriculture and natural resources. *California Agriculture*, 71(1), February 2017, pp.5-14.

Hunt, E. R., Hively, W. D., Fujikawa, S. J., Linden, D. S., Daughtry, C. S., & McCarty, G. W. (2010). Acquisition of NIR-green-blue digital photographs from unmanned aircraft for crop monitoring. *Remote Sensing*, *2*(1), 290-305.

Huo, L.Z., Silva, C.A., Klauberg, C., Mohan, M., Zhao, L.J., Tang, P. and Hudak, A.T., 2018. Supervised spatial classification of multispectral LiDAR data in urban areas. *PloS one*, 13(10), October, 2018, p.e0206185.

Jeronimo, S.M., Kane, V.R., Churchill, D.J., McGaughey, R.J. and Franklin, J.F., 2018. Applying LiDAR individual tree detection to management of structurally diverse forest landscapes. *Journal of Forestry*, *116*(4), pp.336-346.

Johnston, L. F., Herwitz, S., Dunagan, S., Lobitz, B., Sullivan, D., Slye, R., 2003. Collection of Ultra High Spatial and Spectral Resolution Image Data over California Vineyards with a Small UAV. Proceedings, International Symposium on Remote Sensing of Environment, 2003. Available online at http://www.uav-applications.org/gallery/img/5.pdf .

Kaur, Dilprett, Yadwinder Kaur, 2014. Various Image Segmentation Techniques: A Review. *International Journal of Computer Science and Mobile Computing.* Vol. 3, Issue 5, May 2014, pg. 809-814.

Lee, J., Coomes, D., Schonlieb, C.B., Cai, X., Lellmann, J., Dalponte, M., Malhi, Y., Butt, N. and Morecroft, M., 2017. A graph cut approach to 3D tree delineation, using integrated airborne LiDAR and hyperspectral imagery. *arXiv preprint arXiv:1701.06715*.

Lewis, H. G., M. Brown, 2001. A generalized confusion matrix for assessing area estimates from remotely sensed data. *International Journal of Remote Sensing*. Vol. 22, No. 16, 2001, pg. 3223-3235.

Liaw, Andy, Matthew Wiener, 2002. Classification and Regression by randomForest. *R News.* Vol. 2/3, December 2002, pg. 18-22.

Liebermann, H., Schuler, J., Strager, M.P., Hentz, A.K. and Maxwell, A., 2018. Using Unmanned Aerial Systems for Deriving Forest Stand Characteristics in Mixed Hardwoods of West Virginia. *Journal of Geospatial Applications in Natural Resources*, *2*(1), January 12, 2018, p.2.

Lim, Kevin, Paul Treitz, Michael Wulder, Benoit St-Onge, Marin Flood, 2003. Lidar remote sensing of forest structure. *Progress in Physical Geography.* Vol. 27, Issue 1, March 2003, pg. 88-106.

ListenData, 2017. Random Forest in R: Step by Step Tutorial. Online at: http://www.listendata.com/2014/11/random-forest-with-r.html.

Liu, Dingding, Bilge Soran, Gregg Petrie, and Linda Shapiro. "A review of computer vision segmentation algorithms." *Lecture notes* 53, 2012.

Lund, Gyde H., Charles E. Thomas, 1989. A Primer on Stand and Forest Inventory Designs. United States Department of Agriculture Forest Service, General Technical Report WO-54, September 1989.

Madden, M., Jordan, T., Cotten, D., O'Hare, N., Pasqua, A. and Bernardes, S., 2017, January. The future of unmanned aerial systems (UAS) for monitoring natural and cultural resources. In *Photogrammetric Week* (Vol. 15, pp. 369-384).

Marino, E., Montes, F., Tomé, J.L., Navarro, J.A. and Hernando, C., 2018. Vertical forest structure analysis for wildfire prevention: Comparing airborne laser scanning data and stereoscopic hemispherical images. *International Journal of Applied Earth Observation and Geoinformation*, *73*, pp.438-449.

Maschler, J., Atzberger, C. and Immitzer, M., 2018. Individual Tree Crown Segmentation and Classification of 13 Tree Species Using Airborne Hyperspectral Data. *Remote Sensing*, 10(8), Vol. 10 (8), August 2018.

Melville, B., Lucieer, A. and Aryal, J., 2018. Object-based random forest classification of Landsat ETM+ and WorldView-2 satellite imagery for mapping lowland native grassland communities in Tasmania, Australia. *International journal of applied earth observation and geoinformation*, 66, April, 2018, pp.46-55.

Merino, L., Caballero, F., Martinez-de Dios, J. R., Ferruz, J., Ollero, A. 2006. *A cooperative perception system for multiple UAVs: Application to automatic detection of forest fires.* Journal of Field Robotics, Vol. 23, Iss. 3-4, March-April 2006 pp. 165-184, Available online at http://www3.interscience.wiley.com/cgi-bin/jhome/111090262 Wiley Periodicals Inc.

Microbus, 2015. Microbus website, http://www.microscope-microscope.org/imaging/image-resolution.htm . Image Resolution, size, and compression: What does it really mean?

Milas, A.S., Arend, K., Mayer, C., Simonson, M.A. and Mackey, S., 2017. Different colours of shadows: classification of UAV images. *International journal of remote sensing*, *38*(8-10), January 13, 2017, pp.3084-3100.

Ming, D., Ci, T., Cai, H., Li, L., Qiao, C. and Du, J., 2012. Semivariogram-based spatial bandwidth selection for remote sensing image segmentation with mean-shift algorithm. *IEEE Geoscience and Remote Sensing Letters*, 9(5), pp.813-817.

Mohan Sambhu Surya, Sushma Leela, 2012. Importance of Mean Shift in Remote Sensing Segmentation. *IOSR Journal of Computer Engineering*, Col. 14, Issue 6, September-October 2013, pg. 80-83.

Niedzielski, T., Jurecka, M., Stec, M., Wieczorek, M. and Miziński, B., 2017. The nested k-means method: A new approach for detecting lost persons in aerial images acquired by unmanned aerial vehicles. *Journal of Field Robotics*, 34(8), May 2017, pp.1395-1406.

Ohsaki, M., Wang, P., Matsuda, K., Katagiri, S., Watanabe, H. and Ralescu, A., 2017. Confusion-matrix-based kernel logistic regression for imbalanced data classification. *IEEE Transactions on Knowledge and Data Engineering*, 29(9), September 2017, pp.1806-1819.

Pal, Mahesh, Paul M. Mather, 2003. An assessment of the effectiveness of decision tree methods for land cover classification. *Remote Sensing of Environment.* Vol. 86, Issue 4, August 30, 2003, pg. 554-565.

Pasquarella, V.J., Holden, C.E. and Woodcock, C.E., 2018. Improved mapping of forest type using spectral-temporal Landsat features. *Remote Sensing of Environment*, 210, June 2018, pp.193-207.

R, 2017. R website, https://www.rstudion.com.

Rodriguez-Galiano, V. F., B. Ghimire, J. Rogan, M. Chica-Olmo, J. P. Rigol-Sanchez, 2012. An assessment of the effectiveness of a random forest classifier for land-cover classification. ISPRS Journal of Photogrammetry and Remote Sensing. Vol. 67, 2012, pg. 93-104.

Rudol, P., & Doherty, P., 2008. Human body detection and geolocalization for UAV search and rescue missions using color and thermal imagery. In *Aerospace Conference, 2008 IEEE* (pp. 1-8). IEEE.

Shen, X., Cao, L., Chen, D., Sun, Y., Wang, G. and Ruan, H., 2018. Prediction of Forest Structural Parameters Using Airborne Full-Waveform LiDAR and Hyperspectral Data in Subtropical Forests. *Remote Sensing*, 10(11), November 2018, p.1729.

Silveyra Gonzalez, R., Latifi, H., Weinacker, H., Dees, M., Koch, B. and Heurich, M., 2018. Integrating LiDAR and high-resolution imagery for object-based mapping of forest habitats in a heterogeneous temperate forest landscape. *International journal of remote sensing*, pp.1-26.

Silalahi, R.P., Jaya, I.N.S., Tiryana, T. and Mulia, F., 2018. Assessing the Crown Closure of Nypa on UAV Images using Mean-Shift Segmentation Algorithm. *Indonesian Journal of Electrical Engineering and Computer Science*, 9(3), March 2018, pp.722-730.

Simonson, W., Allen, H. and Coomes, D., 2018. Effect of Tree Phenology on LiDAR Measurement of Mediterranean Forest Structure. *Remote Sensing*, 10(5), April, 2018, June, 2018, p.659.

Stephens, Trevor, 2016. Titanic: Getting Started with R- Part 5: Random Forests. Website, http://trevorstephens.com/kaggle-titanic-tutorial/r-part-5-random-forests.

Story, Michael, Russell G. Congalton, 1986. Accuracy Assessment: A User's Perspective. *Photogrammetric Engineering and Remote Sensing*. Vol. 52, No 3, March 1986, pg. 397-399.

Stovall, A.E. and Shugart, H.H., 2018. Improved Biomass Calibration and Validation With Terrestrial LiDAR: Implications for Future LiDAR and SAR Missions. *IEEE Journal of Selected Topics in Applied Earth Observations and Remote Sensing*, Vol. 11 (10), October, 2018, pp. 3527-3537.

Tang, Lina, Guofan Shao, 2015. Drone remote sensing for forestry research and practices. *Journal of Forestry Research.* Vol. 26, Issue 4, December 2015, pg. 791-797.

Teluguntla, P., Thenkabail, P., Oliphant, A., Xiong, J., Gumma, M.K., Congalton, R.G., Yadav, K. and Huete, A., 2018. A 30-m landsat-derived cropland extent product of Australia and China using random forest machine learning algorithm on Google Earth Engine cloud computing platform. *ISPRS Journal of Photogrammetry and Remote Sensing*, 144, October, 2018, pp.325-340.

Wallace, L., Lucieer, A., Watson, C., & Turner, D., 2012. Development of a UAV-LiDAR system with application to forest inventory. *Remote Sensing*, *4*(6), 1519-1543.

Wu, T., Xia, L., Luo, J., Zhou, X., Hu, X., Ma, J. and Song, X., 2018. Computationally Efficient Mean-Shift Parallel Segmentation Algorithm for High-Resolution Remote Sensing Images. *Journal of the Indian Society of Remote Sensing*, September. 2018, pp.1-10.

Yang, J., He, Y., Caspersen, J.P. and Jones, T.A., 2017. Delineating Individual Tree Crowns in an Uneven-Aged, Mixed Broadleaf Forest Using Multispectral Watershed Segmentation and Multiscale Fitting. *IEEE Journal of Selected Topics in Applied Earth Observations and Remote Sensing*, 10(4), April 2017, pp.1390 1401.

Ye, S., Pontius, R.G. and Rakshit, R., 2018. A review of accuracy assessment for object based image analysis: From per-pixel to per-polygon approaches. *ISPRS journal of photogrammetry and remote sensing*, 141, July, 2018, pp.137-147.

Yoga, S., Bégin, J., Daigle, G., Riopel, M. and St-Onge, B., 2018. A Generalized Lidar Based Model for Predicting the Merchantable Volume of Balsam Fir of Sites Located along a Bioclimatic Gradient in Quebec, Canada. *Forests*, *9*(4), p.166.

Zabihi, M., Pourghasemi, H.R., Pourtaghi, Z.S. and Behzadfar, M., 2016. GIS-based multivariate adaptive regression spline and random forest models for groundwater potential mapping in Iran. *Environmental Earth Sciences*, 75(8), April, 2016 p.665.

Zheng, Liying, Jingtaoe Zhang, Qianyu Wang, 2009. Mean-shift-based color segmentation of images containing green vegetation. *Computers and Electronics in Agriculture.* Vol. 65, Issue 1, January 2009 pg. 93-98.

Zhu, W., Huang, Y. and Sun, Z., 2018, August. Mapping Crop Leaf Area Index from Multi-Spectral Imagery Onboard an Unmanned Aerial Vehicle. In *2018 7th International Conference on Agro-geoinformatics (Agro-geoinformatics)* (pp. 1 5). IEEE.

APPENDIX A

Fixed Wing Ebee http://www.sensefly.com/products/swinglet-cam

Multicopter http://diydrones.com/profiles/blogs/a-newbies-guide-to-uavs

Figure 1 General classification categories of Unmanned Aerial Vehicles (UAV)

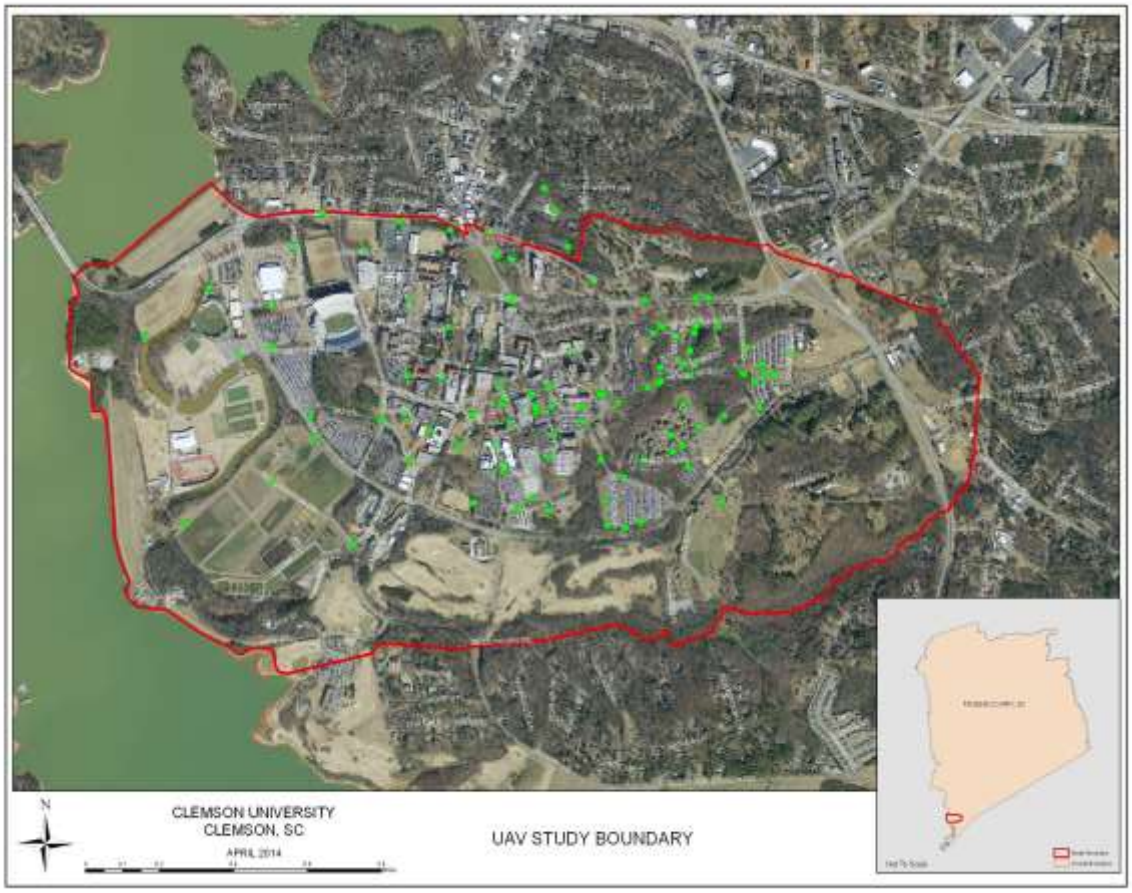

Figure 2 Study boundary used for Unmanned Aerial Vehicle (UAV) implementation to collect high resolution imagery. Green dots represent geodetic control points used to correct image spatial inaccuracies if they exist.

Figure 3 Completed georeference mosaic of Clemson University. This seamless orthomosaic was used for object-based species classification.

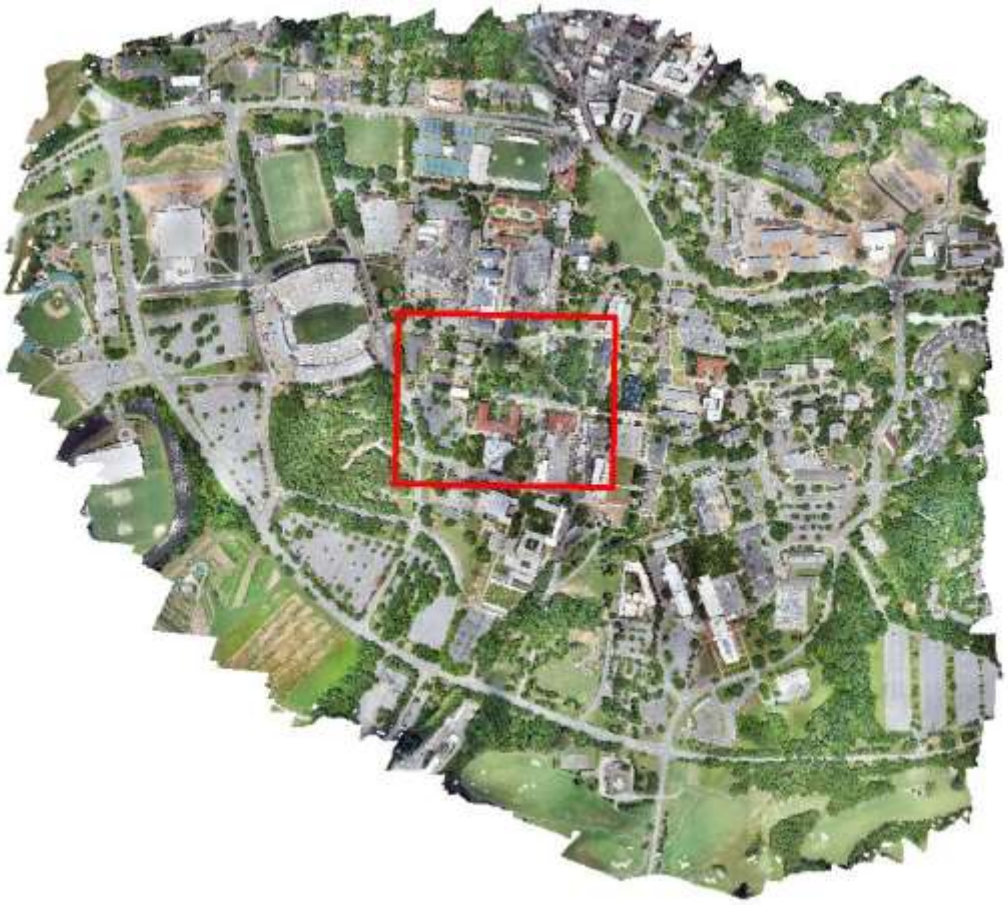

Figure 4 Subset boundary polygon used to extract data for classification model in R-Studio

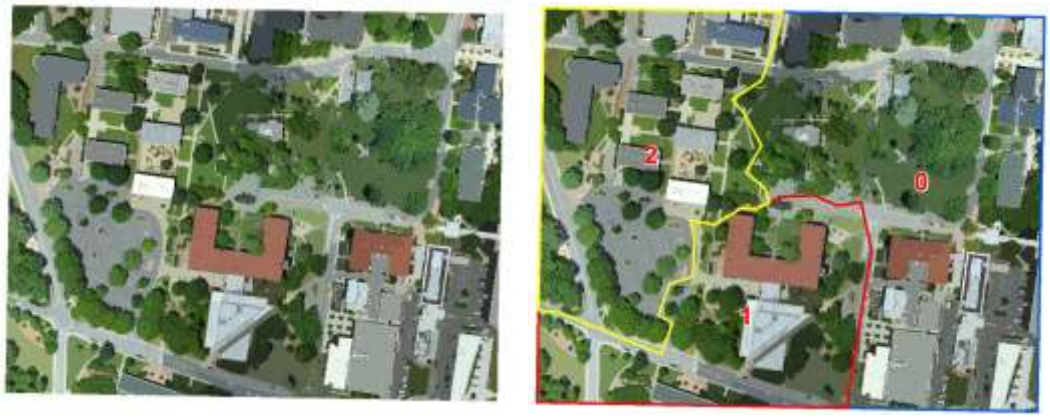

A B

C D

Figure 5 Result of using the Mean Shift Segmentation tool in ArcGIS 10.5.0. Segmented results were sub-divided: A. Whole Section B. Random division C. Horizontal division and D. Vertical division for processing in R-Studio

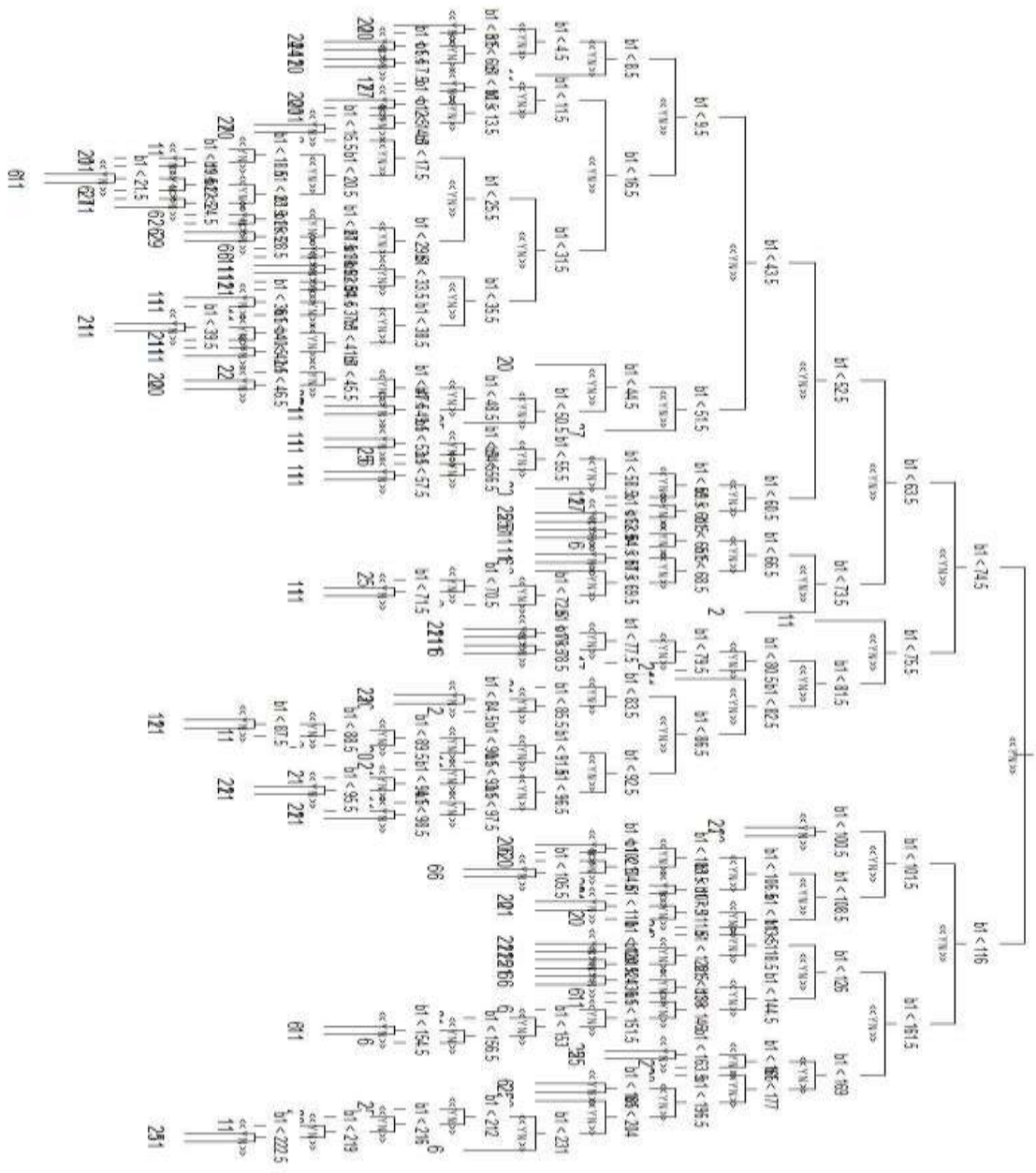

Figure 6 Decision tree results from running the classification model in R-Studio against the whole segmented image Note: For clarity, only the branch for band 1 is shown

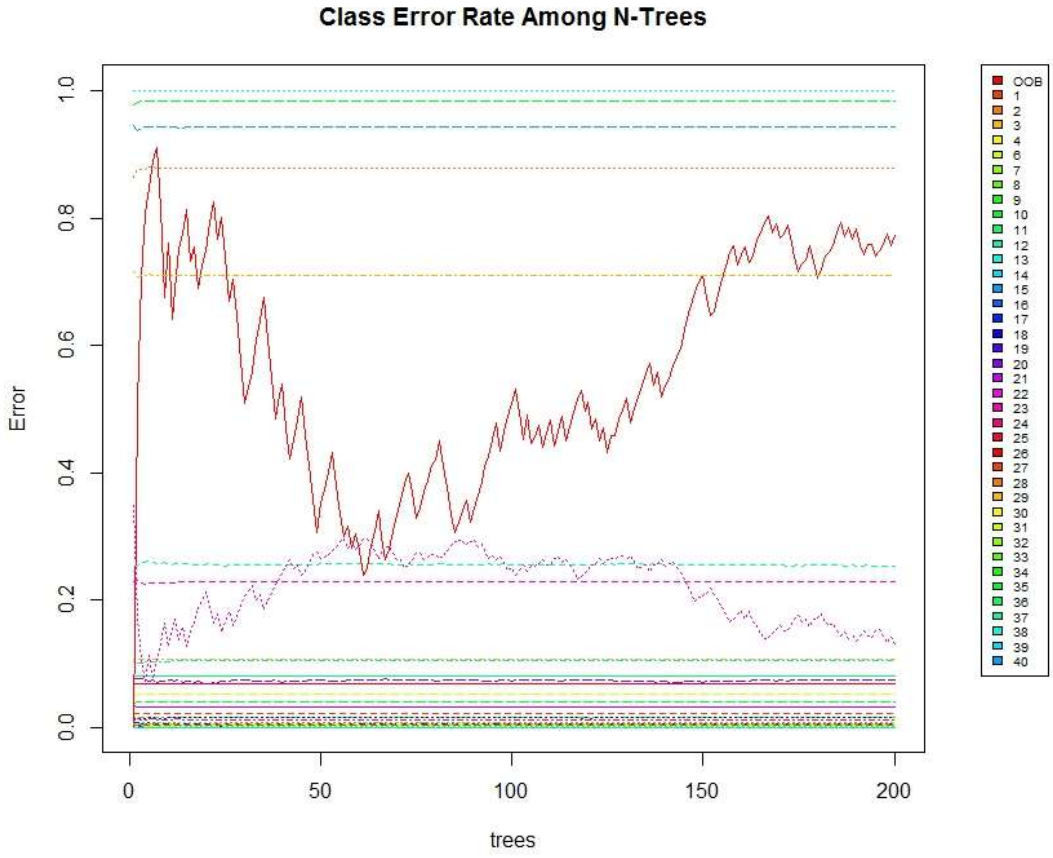

Figure 7 Class Error Rate graph showing change as number of bootstrapping trees increases Note: Graph is from using the Whole Section model

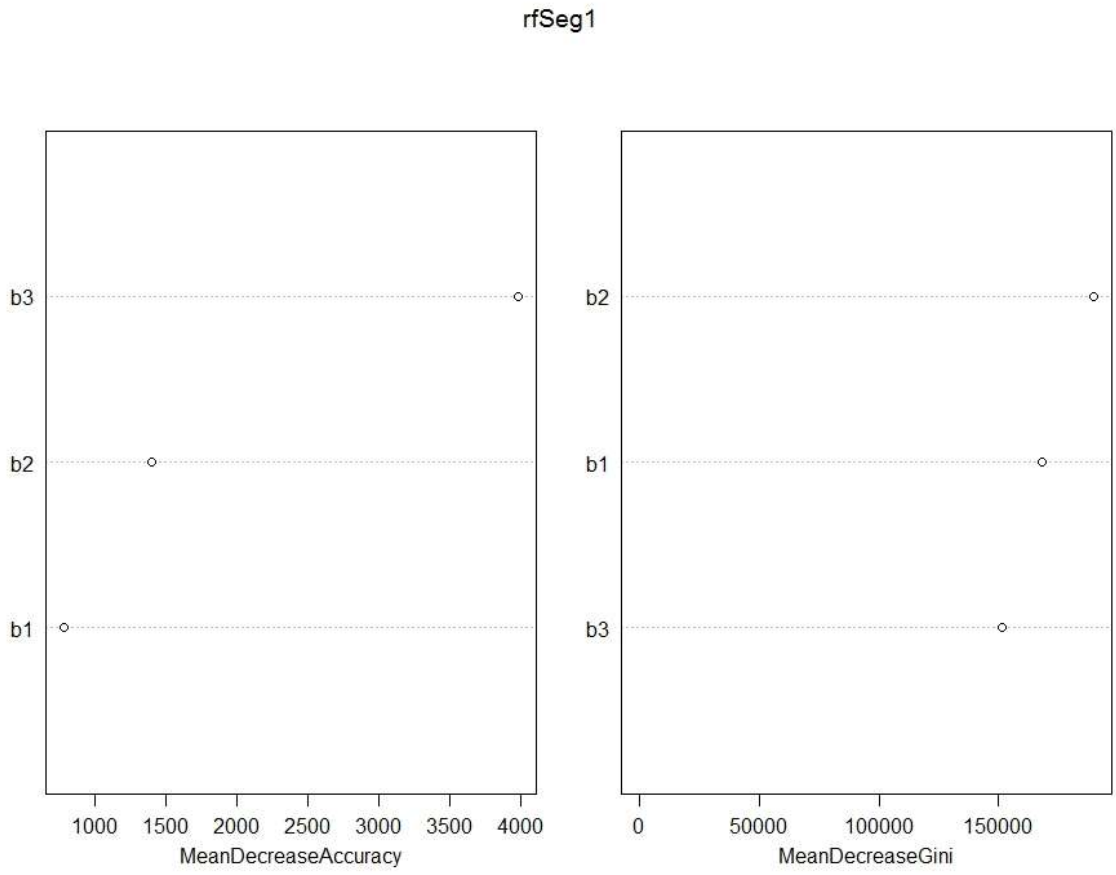

Figure 8 Graphs showing segmented image band importance for use in the classification model Note: Graph is from using the Whole Section model

Table 1 Strengths and Weakness of Object Based Image Analysis (OBIA) proposed by Hay and Castilla (2006).

Strengths	Weakness
Image segmentation mimics human perception of image objects	Current OBIA software has complicated options
User can take advantage of non-parametric techniques while reducing computational load	Large datasets pose a challenge especially with multispectral images
Useful features contain shape, texture, and context that are absent with pixel based methods	Heterogeneity can lead to different segmentations with no unique solution
Objects are readily utilized within vector based application such as GIS	Limited accuracy assessment of segmentation processes
Commercial and Open Source software solutions are built upon OBIA	Poor understanding of scale and hierarchical relationships at different resolutions

Table 2 Arial coverage by Unmanned Aerial Vehicle (UAV) flights in summer of 2017

Flight	Number of photos	Date
F01	167	7/8/2017
F02	597	7/8/2017
F03	628	7/8/2017
Total	1392	----------

Table 3 Tree species distribution within sub-sample boundary

Common	Genus	Species	Tree Count	Avg. DBH (cm)	Avg.Height (m)	Avg.Canopy (m^2)	Tree ID
American Beech	*Fagus*	*grandifolia*	1	35.56	12.80	1085.73	35
American Holly	*Ilex*	*opaca*	22	32.21	15.77	1038.07	1
Black Maple	*Acer*	*nigrum*	6	48.68	18.78	1895.85	2
Bradford Pear	*Pyrus*	*calleryana*	18	42.47	18.58	1465.26	3
Bur Oak	*Quercus*	*macrocarpa*	1	30.48	17.18	370.62	31
Chinese Elm	*Ulmus*	*parvifolia*	4	53.34	19.49	1238.37	4
Common Fig	*Ficus*	*carica*	1	7.62	20.85	1207.31	32
Crape myrtle	*Lagerstroemia*	*indica*	41	13.13	12.90	1715.05	6
Deodar Cedar	*Cedrus*	*deodara*	6	102.45	17.06	1305.30	7
Eastern Red Cedar	*Juniperus*	*virginiana*	6	70.27	11.91	323.22	8
Eastern White Pine	*Pinus*	*strobus*	1	43.18	8.96	302.50	9
Flowering Dogwood	*Cornus*	*florida*	27	10.35	16.49	1300.81	10
Foster's Holly	*Aquifoliaceae*	*ilex*	60	12.23	15.94	1501.31	11
Ginkgo	*Ginkgo*	*biloba*	3	44.87	10.36	218.11	12
Golden raintree	*Laburnum*	*x watereri*	1	22.86	8.83	243.26	36
Green Ash	*Fraxinus*	*pennsylvanica*	1	38.10	10.23	481.18	37
Kousa Dogwood	*Cornus*	*kousa*	1	7.62	18.97	685.02	13
Live Oak	*Quercus*	*virginiana*	8	94.61	16.18	2492.81	33
Norway Spruce	*Picea*	*abies*	1	66.04	22.51	543.97	34
Pecan	*Carya*	*illinoinensis*	1	66.04	20.59	4352.38	38
Persian Ironwood	*Parrotia*	*persica*	1	10.16	4.78	26.06	39
Pin Cherry	*Prunus*	*pensylvanica*	3	16.09	9.77	214.59	23
Pin Oak	*Quercus*	*palustris*	3	53.34	15.14	868.27	24
Port Orford Cedar	*Chamaecyparis*	*lawsoniana*	2	76.20	17.22	1538.99	14
Red Maple	*Acer*	*rubrum*	9	41.20	21.26	994.69	25
River Birch	*Betula*	*nigra*	1	55.88	18.71	519.92	15
Sawtooth Oak	*Quercus*	*acutissima*	1	45.72	15.39	644.21	16
Scarlet Oak	*Quercus*	*coccinea*	4	77.47	18.42	1470.91	17
Silver Maple	*Acer*	*saccharinum*	1	30.48	8.18	160.97	26
Southern Magnolia	*Magnolia*	*grandiflora*	17	58.57	17.93	1512.24	18
Star Magnolia	*Magnolia*	*stellata*	1	38.10	12.32	341.87	40
Sugar Maple	*Acer*	*saccharum*	4	86.36	20.44	996.37	27
Swamp Chestnut Oak	*Quercus*	*michauxii*	1	30.48	13.15	604.26	28
Trident Maple	*Acer*	*buergeranum*	1	12.70	19.53	867.42	19
Water Oak	*Quercus*	*nigra*	5	80.26	23.16	1449.97	29
Wax Myrtle	*Myrica*	*cerifera*	1	10.16	6.58	220.96	30
White Oak	*Quercus*	*alba*	35	83.75	21.43	2240.45	20
Willow Oak	*Quercus*	*phellos*	28	74.48	20.54	1976.97	21
Yoshino Cherry	*Prunus*	*x yedoensis*	4	41.28	13.02	925.22	22

Table 4 Classification model iteration results when applied to the sub-sample area and each sub-division

Model	OOB	Accuracy	95% CI	NIR	P-Value [Acc > NIR]	Kappa
Whole	6.88%	0.9312	(0.9306, 0.9319)	0.1811	< 2.2e-16	0.9246
			Whole Area Sub-Divisions			
Random Sec 1	9.65%	0.9032	(0.9017, 0.9047)	0.2817	< 2.2e-16	0.8839
Random Sec 2	2.66%	0.9734	(0.9728, 0.974)	0.1668	< 2.2e-16	0.9705
Random Sec 3	11.64%	0.8836	(0.8821, 0.885)	0.3177	< 2.2e-16	0.8628
Average	7.98%	0.9201		0.2554		0.9057
Horizontal Sec 0	11.08%	0.8892	(0.8879, 0.8905)	0.2136	< 2.2e-16	0.8751
Horizontal Sec 1	3.46%	0.9654	(0.9646, 0.9662)	0.3056	< 2.2e-16	0.9597
Horizontal Sec 2	4.21%	0.9579	(0.9569, 0.9588)	0.2348	< 2.2e-16	0.9509
Average	6.25%	0.9375		0.2513		0.9286
Vertical Sec 0	4.39%	0.9561	(0.9551, 0.957)	0.3334	< 2.2e-16	0.9476
Vertical Sec 1	9.23%	0.9077	(0.9066, 0.9088)	0.1768	< 2.2e-16	0.8967
Vertical Sec 2	3.47%	0.9653	(0.9644, 0.9662)	0.2327	< 2.2e-16	0.9611
Average	5.70%	0.9430		0.2476		0.9351
Sub-Division Average	6.64%	0.9335		0.2514		0.9231

Table 5 Confusion matrix results from the Vertical Sec 2 sub-division. Values outside diagonal are considered miss-classified pixels

	Reference																	
Predicted	X1	X6	X7	X8	X10	X11	X12	X14	X15	X17	X18	X20	X21	X22	X25	X29	X33	X34
1	11155	0	0	0	1	0	0	0	0	0	0	1	0	0	0	1	0	0
6	1	16720	0	1	0	0	0	0	0	6	0	0	1	0	0	0	0	0
7	0	0	5566	0	0	0	0	0	0	0	0	0	0	0	0	0	0	0
8	0	0	0	1864	0	0	0	0	0	0	0	0	0	0	0	0	0	0
10	0	0	0	0	9276	0	0	0	0	0	0	0	0	0	0	0	0	0
11	0	0	0	0	0	5582	0	0	0	0	0	0	0	0	0	0	0	0
12	0	1	0	0	1396	0	4173	0	0	0	0	1	0	0	0	0	0	0
14	0	0	0	0	0	0	388	3322	0	0	0	0	0	0	0	0	0	0
15	0	0	0	0	0	0	0	0	1854	0	0	0	0	0	0	0	0	0
17	0	0	0	0	0	0	0	0	0	1853	0	1	0	0	0	0	0	0
18	0	0	0	0	0	0	0	0	0	0	14862	0	0	0	0	0	0	0
20	1	0	1604	0	241	0	0	1	0	0	0	35299	27	0	0	0	0	0
21	0	1	0	0	0	0	0	0	0	0	0	0	16698	0	0	0	0	1
22	0	0	0	0	0	0	0	0	0	0	0	0	1862	0	0	0	0	0
25	0	0	0	0	0	0	0	0	0	0	0	0	0	0	7439	0	0	0
29	0	0	0	0	0	0	0	0	0	0	0	0	0	0	0	1858	0	0
33	0	1	0	0	0	0	0	0	0	0	0	0	1	0	0	0	14846	0
34	0	0	0	0	0	0	0	0	0	0	0	0	0	0	0	0	0	1857

Table 6 Example of analytical measures computed from Random Sec 1 sub-division confusion matrix

TP	TN	FP	FN	AC	Precision	Sensitivity	Specificity	F- Score
216	131337	1	0	100.00	99.54	100.00	100.00	99.77
29742	107159	1182	1	99.14	96.18	100.00	98.91	98.05
41807	89451	7899	814	93.78	84.11	98.09	91.89	90.56
3709	461131	2	0	100.00	99.95	100.00	100.00	99.97
13964	117270	1624	3618	96.16	89.58	79.42	98.63	84.20
16718	123874	26	3686	97.43	99.84	81.93	99.98	90.01
3609	134856	1	1664	98.81	99.97	68.44	100.00	81.26
2793	128441	0	1865	98.60	100.00	59.96	100.00	74.97
3716	133191	0	0	100.00	100.00	100.00	100.00	100.00
6781	131005	1	862	99.38	99.99	88.72	100.00	94.02
610	136886	0	1836	98.68	100.00	24.94	100.00	39.92
5565	131335	1182	1	99.14	82.48	99.98	99.11	90.39
152	667462	2749	0	99.59	5.24	100.00	99.59	9.96
0	135366	0	320	99.76	0.00	0.00	100.00	0.00
1852	135048	0	0	100.00	100.00	100.00	100.00	100.00

Glossary

Agisoft:

a commercial based 3D reconstruction software that uses digital photos. The professional edition allows authoring of geographic information system (GIS) data to produce seamless imagery and 3D point clouds

ArcGIS:

a commercial based geographic information system (GIS) developed by Environmental Systems Research Institute

Autonomous:

operation of a UAV by onboard computer or ground based pilot by remote control

Diameter at Breast Height (DBH):

measurement location to obtain tree diameter usually at 4.5’ off the ground

Geodetic Control Point (GCP):

global positioning system (GPS) derived point that can be used to accurately position non-spatially referenced geographic data by serving as reference object that can be tied to its complimentary location in geographic data

Geographic Information System (GIS):

a computer based software that captures, manages, analyzes, edits and displays geographic data

Geotagging:

process of adding geographic metadata to photographs or imagery

Global Positioning System (GPS):

satellite based navigation system that provides locational information

Ground Control Station:

facilities and computer hardware that maintains human control over unmanned aerial vehicles during flight

Heads-Up-Digitizing:

GIS process for creating feature objects from data (i.e. imagery) displayed on a computer screen

Hyperspectral:

imaging technique that collects data by scanning objects across the electromagnetic spectrum using three techniques: scanning spatial images, sequential capture of full spectral data, or capture spatial and spectral data at the same time

Imagery:

images representing spatial objects on the earth's surface

Light Detection and Ranging (LiDAR):

remote sensing technique that uses a laser to measure distance by analyzing reflected light of a laser illuminated object on the earth

Mosaic:

process of creating a single image from a collection of images

Multi-Spectral:

process of capturing image data at specific frequencies of the electromagnetic spectrum

Near Infrared (NIR):

image data collected in the near infrared region of the electromagnetic spectrum this is closest to the radiation detected by the human eye

Orthomosaic:

combination of orthorectification and mosaicing to create a rectified image with limited distortion to form a single image from a collection of images

Orthorectification:

process of correcting imagery distortion by using based data such as elevation along with camera metadata to match map projection

Photogrammetry:

the scientific process(s) of developing measurements from photographs

Spatialtemporal:

term used to describe spatial data over a period of time

Urban Forest:

a collection of trees or forest stands within a city, town or suburb

Unmanned Aerial Vehicle (UAV):

term used to describe a remotely operated airborne vehicle that is flown in absence of a human pilot

Unmanned Aerial System (UAS):

ground control equipment, communication system and other support equipment including the unmanned aerial vehicle to maintain flight mission objectives

X, Y:

coordinate pair point representing values of a map projection that spatially locates an object on the earth's surface

Z-Value:

spatial value of a map projection that represents elevation of a located object

R Code for OBIA

```
#Import Libraries
library (raster)
library (rgdal)
library (randomForest)
library (caret)
library (randomcoloR)
library (xlsx)
library(xtable)
library(readxl)
library(ROCR)
library(pROC)
library(reprtree)
library (doParallel)
library(RColorBrewer)

# Load Data
trainSeg1 <- shapefile("Path to training data")
imgSeg1 <- brick("Path to segmented image")
colnames(trainSeg1)

# Attach Labels
roi_dataSeg1 <- extract(imgSeg1, trainSeg1, df= TRUE, na.exclude)
roi_dataSeg1$desc <- as.factor(trainSeg1$CID[roi_dataSeg1$ID])

# Set Seed Value for Reproducibility
set.seed(1234567890)
```

```
#Shorten Column Names
colnames(roi_dataSeg1)
colnames(roi_dataSeg1) <- c('ID', 'b1', 'b2','b3', 'desc')
colnames(roi_dataSeg1)

#Create Cluster to process random forest in parallel
cl <- makeCluster(detectCores())
registerDoParallel(cl)

# Clear out memory
gc()

# Run Random Forest Importance Matrix
beginCluster()
rfSeg1 <- randomForest(desc ~ b1 + b2 + b3, data= roi_dataSeg1, importance= TRUE,
mtry = 4, ntree= 200, trControl = rfSeg1Control, tuneGrid = rfSeg1Grid,metric =
"Kappa", maximize = true, na.action=na.exclude)
print(rfSeg1)
head(rfSeg1)
names(rfSeg1)
endCluster()

# Create Confusion Matrix Metrics and export
#Determine if levels and lengths are equal if not use code to make equal
identical(levels(rfSeg1$predicted),levels(roi_dataSeg1$desc))
identical(length(rfSeg1$predicted),length(roi_dataSeg1$desc))
length(rfSeg1$predicted)
length(roi_dataSeg1$desc)
```

```
#Code to make length and levels equal if needed
# noNA<-((is.na(roi_dataSeg1$desc)+is.na(roi_dataSeg1$Seg1))==0)
# n<-is.na(roi_dataSeg1$desc)
# o<-is.na(rfSeg1$predicted)
# noNA<- (o+n)==0
# conftbl <- confusionMatrix(rfSeg1$predicted,roi_dataSeg1$desc[noNA])

#Create Confusion Matrix
conftbl <- confusionMatrix(rfSeg1$predicted,roi_dataSeg1$desc)
print(conftbl)
n<- as.table(conftbl$byClass)
m<-as.matrix(conftbl$byClass)

# Write table to memory (if needed open Excel and select cell then Paste, Save excel file)
otherwise it will write it to an excel file

# write.table(m,'clipboard',sep='\t')
write.xlsx(m, "Path To File")

#Export Confusion Table
tbl <- (rfSeg1$confusion)
write.xlsx(tbl, "Path To File")
TBRSeg1 <- read_excel("Path To File")

# Read Table from Excel to make new data frame to Plot ROC
tblA<-read_excel("Path to File")
SS <- tblA[,2:3]
```

```
#Plot ROC
plot(SS$Specificity, SS$Sensitivity)
plot(roc(SS$Sensitivity,SS$Specificity, direction="<", col ="yellow"))

#Install tree library to create decision tree model
options(repos='http://cran.rstudio.org')
have.packages <- installed.packages()
cran.packages <- c('devtools','plotrix','randomForest','tree')
to.install <- setdiff(cran.packages, have.packages[,1])
if(length(to.install)>0) install.packages(to.install)
library(devtools)
if(!('reprtree' %in% installed.packages())){
  install_github('araastat/reprtree')
}
for(p in c(cran.packages, 'reprtree')) eval(substitute(library(pkg), list(pkg=p)))

# Plot decesion tree
tr<-getTree(rfSeg1, 1, labelVar="True")
print (tr)
reprtree:::plot.getTree(rfSeg1, cex=0.5)

# Plot err.rate with OOB
coll<-colorRampPallet(brewer.pal(8,"Dark2"))(100)
maxy <- max(rfSeg1$err.rate)
co_set<- rainbow(25)
layout(matrix(c(1,2),nrow=1),width=c(4,1))
par(mar=c(5,4,4,0)) #No margin on the right side
plot(rfSeg1, ylim=c(0,maxy), main="Class Error Rate Among N-Trees", col=co_set)
par(mar=c(5,0,4,2)) #No margin on the left side
```

```
plot(c(0,1),type="n", axes=F, xlab="", ylab="")
legend("top", colnames(rfSeg1$err.rate),cex=0.8,fill=co_set)
#cols<-rainbow(16)
#fill=1:16

#  Plot err rate
plot(rfSeg1$err.rate[,1], ylab="Error Rate")
layout(matrix(c(1,2),nrow=1),width=c(4,1))
par(mar=c(5,4,4,0)) #No margin on the right side
plot(rfSeg1, log="y")
par(mar=c(5,0,4,2)) #No margin on the left side
plot(c(0,1),type="n", axes=F, xlab="", ylab="")

# Model Accuracy
TPSeg1 <- sum(diag(rfSeg1$confusion))/sum(rfSeg1$confusion)
print (TPSeg1)
# Misclassification Rate
MRSeg1<- 1-sum(diag(rfSeg1$confusion))/sum(rfSeg1$confusion)
print(MRSeg1)

# Plot Variable Importance Measures
varImpPlot(rfSeg1)

# Classify
img_classSeg1 <- imgSeg1
names(img_classSeg1) <- c('b1','b2','b3')



# Predict
```

```
img_predSeg1 <- predict(img_classSeg1, model = rfSeg1, na.rm = T)

# Plot Classification
# Create color map
colors <- randomColor(100, hue = c(" ", "random", "red", "orange", "yellow","green",
"blue", "purple", "pink", "monochrome"), luminosity = c(" ","random", "light", "bright",
"dark"))
colors <- randomColor(100, hue = "random", luminosity = "random")
plotRGB(imgSeg1, r=1, g=2, b=3, stretch="lin")
plot(img_predSeg1, col=colors)
plot(rfSeg1$err.rate[]
```

CHAPTER FIVE

Conclusions: This research utilized recent advancements in UAV and photogrammetry software and was focused on determining if this combination of technologies could produce accurate field measurements for arboriculture and forestry. The use of UAVs provides high-resolution photos, but few studies have determined the efficacy of using UAV-derived products for forest management.

In chapter two, each 3D point cloud was compared to one another and to aerial LiDAR. Near analysis was used to compare point clouds and found spatial similarity between clouds (LiDAR, Leaf off and Leaf on). This trend was present for all points and when these points were stratified based on point classifications. Further comparison of elevations (generated from each point cloud) to survey grade GPS elevations demonstrated that point clouds (LiDAR, Leaf on, Leaf off) were nearly identical with differences of 0.21%, 0.34 % and 4.2% respectively. Building features showed some difference during spatial analysis and elevation comparisons. This may be because of miss-classification of points during the model processing. The miss-classification may have been caused because of classification parameters, detection algorithms, and or both. Further research is needed to determine the cause of these differences, but there is no indication that these errors limited the applicability of the UAV-point cloud for arboriculture and forestry applications.

Chapter three resulted in a model that can extract standard forest metrics (diameter at breast height (DBH), tree heights and crown metrics (radius, volume)) from point clouds. Using point cloud processing techniques discussed in chapter two, a model

was developed to measure tree heights and crown metrics from point clouds using third party applications developed for LiDAR. Tree heights from point clouds where compared to measured tree heights using hypothesis testing and found that pvalues (= 0.76) where not sufficient to reject the hypothesis that tree heights were equal at a level of significance of 0.05. These results show tree heights can be extracted from 3D and LiDAR point clouds with confidence that they will be representative of measured values. DBH could not be extracted directly in like manner to tree heights. A linear regression model was developed and resulted in an algorithm to estimate DBH from the point cloud model. The results show through hypothesis testing that the observed DBH of trees is equal to the measured DBH with, at the level of significance of 0.05, a pvalue = 0.94 was not able to reject the hypothesis. DEM creation from each point cloud show very little difference (UAV = ±0.123 m, LiDAR = ±0.114 m) between means. Further hypothesis testing of mean concludes at the level of significance ($\alpha = 0.05$) the means are equal ($p = 0.058$) (CI = (0.1695, 0.1750)). Chapter three shows that forest metric extraction and DEM creation from 3D and LiDAR point clouds can be successful.

Chapter four concludes this study with results that show species classification of trees at the genus/species level can be accomplished with UAV high resolution imagery. Traditional classification techniques could not be used with UAV imagery because of the high spatial resolution. A new model was successfully developed to utilize object-based image analysis along with supervised classification using random forest methodology. The resulting model was developed using RStudio and comparisons shows that the classification model had an overall accuracy of 94.3 % when identifying individual tree

species. Further research is needed to determine if modification of flight parameters and or temporal considerations would improve the model.

Forestry, both traditional and arboricultural, will benefit from this study. Field based tree measurements are both expensive and time consuming. Taking advantage of technological advances in remote sensing techniques and products allows the traditional data collection techniques to become more efficient saving time and reducing costs using UAV technology. This study represents opportunities for further application and research. The UAV has proven effective and further investigation and expansion of these results are warranted to extend and improve upon them to further test and examine applicability. This research does not represent the replacement of traditional methods but rather a new tool(s) in forest management.